

REGIONAL VARIATIONS IN BASEMENT STRUCTURE AND OVERLYING
SEDIMENTS OF THE SUBDUCTING PHILIPPINE SEA PLATE AND THEIR
EFFECT ON THE NANKAI ACCRETIONARY PRISM

A DISSERTATION SUBMITTED TO THE GRADUATE DIVISION OF THE
UNIVERSITY OF HAWAI'I IN PARTIAL FULFILLMENT OF THE REQUIREMENTS
FOR THE DEGREE OF

DOCTOR OF PHILOSOPHY

IN

GEOLOGY & GEOPHYSICS

AUGUST 2007

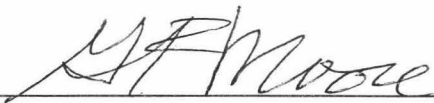
By
Toshihiro Ike

Dissertation Committee:

Gregory F. Moore, Chairperson
Brian Taylor
Garrett Ito
Jane Schoonmaker
Thomas A. Schroeder

We certify that we have read this dissertation and that, in our opinion, it is satisfactory in scope and quality as a dissertation for the degree of Doctor of Philosophy in Geology and Geophysics.

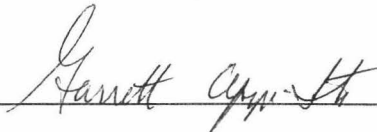
DISSERTATION COMMITTEE



Chairperson



Brian Taylor



ABSTRACT

We document regional and local variations in basement relief, sediment thickness, and sediment type on the northern Philippine Sea Plate using high-resolution seismic reflection survey. In this dissertation, I present results of three different projects, examining variations in the initial stage of the inputs to the Nankai Trough subduction zone and their effect on the toe structure of the overlying accretionary prism. Key geological parameters will include the distribution of turbidite depositional system in the Miocene and its facies architecture, diagenesis of mixed terrigenous and hemipelagic sediments overlying the basement relief. I defined three provinces (Western, Central, Eastern) on the northern Philippine Sea plate based on basement relief and examined their effect on sediment thickness and sediment type. Variations in the incoming sediment type comprise three major sedimentary units defined by ODP sites and four classes of seismic sequences along the Nankai Trough. Focusing this study on an isolated topographic high, Kashinosaki Knoll (KK), which influences sedimentation in the Eastern Province, seismic data demonstrate that the formation of KK and historical sedimentary succession differs over each basement slope. The lower portion of the sedimentary section is characterized by a package of high amplitude continuous

reflections (LSB-T subunit) that lap onto steep basement slopes ($\sim 20\text{-}30^\circ$) but are parallel to the gentle basement slopes ($\sim 5\text{-}10^\circ$). These results indicate that turbidite deposition in the Miocene occur over gentle basement slopes in the Eastern Province. Accretionary prism's morphology, deformation pattern, and taper angle are best explained by the initial condition of the accreted sediment thickness, underthrust sediment type, and local basement relief on the subducting plate. We use Coulomb wedge theory to relate the various structural styles, such as the geometry of imbricate thrusts, to the wedge taper angle and friction properties. The taper angle correlates with the thickness of accreted sediment, effective basal friction coefficient, and the underthrust sediment type. Variations in sediment classes characterizing the incoming sediment heterogeneity may be a strong cause for the variation in frictional properties along the base of the accretionary prism, and therefore the plate boundary.

ACKNOWLEDGEMENTS

I would like to acknowledge the support of my supervisor and chairperson, Gregory F. Moore, who contributed to all aspects of my development as a critical thinker, scientist and communicator. The results presented here would not be possible without the input from the dissertation committee; Brian Taylor, Garrett Ito, Jane Schoonmaker, and Thomas A. Schroeder.

I am indebted to Gregory F. Moore for the use of his excellent computer facilities, in Hawaii and in Japan, Brian Taylor for many stimulating discussions on a wide range of subjects. I benefited from the fruitful discussion with Garrett Ito on the interpretation of geophysical data along the subducting Philippine Sea Plate, with Jane Schoonmaker on the basic of clay mineralogy and sedimentation in particular. I also thank Thomas A. Schroeder for his contributions.

Seismic data was provided by the Japan Agency of Marine-Earth Science and Technology (JAMSTEC), and by a U.S.-Japan Collaborative Program.

Yoshiyuki Kaneda housed me in his lab, in JAMSTEC, for the last year of my tenure and gave me opportunities for feedback and support on a number of topics, for which I am grateful.

I thank Mike Underwood and Gaku Kimura for discussions and a critical review of an earlier review of this manuscript.

I would like to thank the School of Ocean and Earth Science and Technology (SOEST) at University of Hawai'i for all their support and help. My tenure in SOEST has been extremely enjoyable. Leona Anthony has consistently provided a very high standard of support in countless ways over the years, my work would have been impossible without her help, and it is an important component of the success of any graduate student in SOEST. Evelyn Norris has been very helpful on a diverse range of issues over the years.

Strong bonds with many members of the department have contributed to my positive experience. Specifically, I will never forget the meaningful friendships I have had over the past five years and the help that so many have selflessly provided when needed:

Adrienne J. Oakley, Eric Mittelstaedt, Todd Bianco, Kolja Rotzoll, Jonathan Weiss, Aisha R. Morris, Michael Chandler, Seung-Sep Kim, Masako Robb, Christopher Bochicchio, Andrew Delorey, B. Benjamin E. Studer, Melody A. Studer, Emily Chapp, Erin S. Diurba, Eva-Marie Nosal, Tom M. Fedenczuk, Christin Shacat, Joseph Shacat, Carrie Brugger, Jeff Perreault, Marcie Workman, Laurie Menviel-Hessler, Pierre Dutrieux, Patrick

Shamberger, Ayesha Siddiqi Genz, Stephen C. Leslie, Denise J. Hills, Nathan Charles

Becker, and Jim Jamshid Gharib.

My ability to go through difficult times, reach personal, and academic goals would not have been possible without the continuous support of my mother, father, brother, sisters, best friends, and to them I owe all I have and will potentially accomplish.

TABLE OF CONTENTS

ACKNOWLEDGEMENT.....	v
ABSTRACT.....	vi
TABLE OF TABLES	viii
TABLE OF CONTENTS.....	viii
LIST OF FIGURES	xi
CHAPTER I: Introduction	1
CHAPTER II: VARIATIONS IN SEDIMENT THICKNESS AND TYPE ALONG THE NORTHERN PHILIPPINE SEA PLATE AT THE NANKAI TROUGH	13
ABSTRACT.....	14
INTRODUCTION	15
GEOLOGICAL SETTING	17
DATA ACQUISITION AND PROCESSING.....	19
SEISMIC STRATIGRAPHY.....	22
BASEMENT TOPOGRAPHY AND PROVINCES.....	24
TOTAL SEDIMENT THICKNESS.....	27
LOCAL STRATIGRAPHIC VARIATIONS.....	28
Class I) Spatially uniform sediments over subdued basement relief	
Class II) Absence of LSB-T unit over relative basement highs	
Class III) Sediments in NW-trending basement lows along the Kinan Seamount Chain	
Class IV) Two turbidite units in the LSB-T unit	
The upper boundary of the LSB sequence	
DISCUSSION.....	34
CONCLUSIONS.....	44
ACKNOWLEDGEMENTS.....	45
CHAPTER III: TECTONICS AND SEDIMENTATION AROUND KASHINOSAKI KNOLL: A SUBDUCTING BASEMENT HIGH IN THE EASTERN NANKAI TROUGH.....	59
ABSTRACT.....	60

INTRODUCTION	61
GEOLOGICAL SETTING	63
DATA ACQUISITION AND PROCESSING SEISMIC	65
Seismic reflection data	
Bathymetry data	
STRUCTURAL CHARACTER OF KASHINOSAKI KNOLL	67
Ocean floor morphology	
Free-air gravity and magnetic anomalies	
SEISMIC STRATIGRAPHY	70
BASEMENT STRUCTURE OF KASHINOSAKI KNOLL AND ITS SURROUNDINGS	
.....	72
SEDIMENTATION PATTERNS OVER AND AROUND KASHINOSAKI KNOLL	
.....	70
DISCUSSION	82
CONCLUSIONS.....	90
ACKNOWLEDGEMENTS.....	91

**CHAPTER IV: THE INFLUENCE OF ALONG-STRIKE VARIATIONS IN
SUBDUCTING BASEMENT TOPOGRAPHY AND OVERLYING SEDIMENTS
ON THE TOE STRUCTURE OF THE NANKAI TROUGH ACCRETIONARY**

PRISM.....	109
ABSTRACT.....	110
INTRODUCTION	111
GEOLOGICAL SETTING AND PRISM GEOMETRY	115
INCOMING SEDIMENT SEQUENCES.....	117
SEISMIC REFLECTION DATA	121
COULOMB WEDGE MODEL	122
VARIATIONS IN STRUCTURE OF THE FRONTAL ACCRETIONARY PRISM	
.....	126
THE WESTERN PROVINCE: NORMAL PRISM.....	128
THE CENTRAL PROVINCE: MAJOR RIDGE SUBDUCTION.....	130
THE EASTERN PROVINCE: SEAMOUNT AND RIDGE SUBDUCTION.....	134
DISCUSSION	137
CONCLUSIONS.....	150

ACKNOWLEDGEMENTS..... 151

REFERENCE..... 173

LIST OF TABLES

<u>Table</u>	<u>Page</u>
2.1 Seismic Reflection Data Acquisition and Processing Parameters	46
4.1 Seismic Reflection Data Acquisition and Processing Parameters	152
4.2 Taper angle, thrust angles, friction properties, and sediment thickness.....	153

LIST OF FIGURES

<u>Table</u>	<u>Page</u>
Figure 1.1. Regional tectonic map showing the Philippine Sea Plate region	8
Figure 1.2. Tectonic map showing the plate motion velocities.....	9
Figure 1.3. Segmentation of the rupture zones along the Nankai Trough	10
Figure 1.4. Schematic illustration of smooth (a) and rough (b) plate interface	11
Figure 1.5. Results of pore pressure sensitivity analysis	12
Figure 2.1. Regional bathymetric map.....	47
Figure 2.2. Seismic stratigraphy of the Shikoku Basin sediments.....	48
Figure 2.3. Basement depth contour map	49
Figure 2.4. Total sediment isopach map along the northern Shikoku Basin.....	50
Figure 2.5. Total sediment thickness vs. Basement depth	51
Figure 2.6. Seismic depth section kr9904-01	52
Figure 2.7(a). Seismic depth section ODKM-102	53
Figure 2.7(b). Enlarged seismic depth section ODKM-102	54
Figure 2.7(c). Enlarged seismic depth section ODKM-102.....	55
Figure 2.8(a). Seismic depth section ODKM-103	56

Figure 2.8(b). Enlarged seismic depth section ODKM-103-2	57
Figure 2.8(c). Enlarged seismic depth section ODKM-103-2	58
Figure 3.1(a). Regional bathymetric map.....	92
Figure 3.1(b). Magnetic anomaly map of the northern Shikoku Basin	93
Figure 3.1(c). Free-air gravity anomaly map of the northern Shikoku Basin.....	94
Figure 3.2(a). Bathymetric map of Kashinosaki Knoll.....	95
Figure 3.2(b). Slope angle map with interpretation of the seafloor morphology	96
Figure 3.3(a). Seismic stratigraphy of the Shikoku Basin sediments.....	97
Figure 3.3(b). Basement topography map	98
Figure 3.4(a). Seismic depth section ODKM-22	99
Figure 3.4(b). Morphological comparison of seamounts with Kashinosaki Knoll ...	100
Figure 3.5. Seismic depth section ODKM-AB	101
Figure 3.6. Seismic depth section ODKM-AA	102
Figure 3.7. Seismic depth section ODKM-100.....	103
Figure 3.8. Seismic depth section ODKM-A9.....	104
Figure 3.9. Seismic depth section ODKM-104.....	105
Figure 3.10. Seismic depth section ODKM-ACA	106

Figure 3.11. Total sediment isopach map of Kashinosaki Knoll	107
Figure 3.12. Schematic view of turbidity currents migrated around the Knoll.....	108
Figure 4.1(a). Regional bathymetric map of the northern Philippine Sea Plate	154
Figure 4.1(b). Regional bathymetric map of the Nankai accretionary prism	156
Figure 4.2(a). Depth converted seismic reflection.....	157
Figure 4.2(b). Depth converted seismic reflection.....	159
Figure 4.2(c). Depth converted seismic reflection.....	161
Figure 4.3. Cartoon illustration of a critical wedge coordinate system	163
Figure 4.4(a). Seismic profiles focusing the toe structure of the prism.....	164
Figure 4.4(b). Seismic profiles focusing the toe structure of the prism.....	166
Figure 4.4(c). Seismic profiles focusing the toe structure of the prism.....	168
Figure 4.5. The relationship between the sediment thickness and taper angle.....	170
Figure 4.6. The relationship between the taper angle and friction properties.....	171
Figure 4.7. The relationship between the taper angle and friction ration (μ_i / μ_b')....	172

Chapter I

INTRODUCTION

Inputs to subduction zones have a direct impact on the structural diversity in convergent margins (*von Huene et al.*, 2000; *Moore et al.*, 2001; *Clift and Vannucchi*, 2004; *Taylor et al.*, 2005; *Underwood*, 2002, 2007). At convergent margins, the boundary between the overriding plate and the subducting plate periodically generate the world's largest and most destructive earthquakes, with the 2004 Indian Ocean earthquake being only the most recent example. Global comparison on the structure of convergent margins has been studied well, but the causes of these variations are much more difficult to demonstrate along each single subduction zone. Many authors have speculated that the subduction of seamounts should have enormous implications for the deformation of the overriding plate and the generation of large earthquakes (e.g., *Scholz and Small*, 1997; *Dominguez et al.*, 2000; *von Huene et al.*, 2000; *Bilek and Lay*, 2002; *Bilek et al.*, 2003), while others have suggested that the properties of subducting sediments control friction along the plate boundary, and therefore seismogenesis (e.g., *Ruff*, 1989; *Spinelli and Underwood*, 2003; *Underwood*, 2007). For instance, fluids are known to play a key role in faulting and earthquake mechanics (*Hickman et al.* 1995), as sediment compaction and

mineral dehydration reactions release large amount of water in response to increasing pressure and temperature, thus highlighting the importance of sediment type and thickness in this process (e.g., Safer and Bekins, 2006).

The international, multidisciplinary Seismogenic Zone Experiment (SEIZE) seeks to understand how subduction zone earthquakes are generated and what contributes to the variability of the Earth's convergent plate boundaries. The Nankai Trough subduction zone is especially favorable for the study of inputs along the plate boundaries because of its recognition as a critical end-member of subduction zones dominated by thick terrigenous sediments. The Nankai margin is located at the boundary between the subducting northern Philippine Sea plate (PSP) and the overriding Japanese Island Arc system (Figs. 1.1, 1.2). This margin has been extensively studied in recent years, yielding large amounts of data, such as seafloor bathymetry (Kaiko I Research Group, 1986; Ashi et al., 1989; Okino et al., 1994), seismic reflection (Aoki et al., 1986; Bangs et al., 1999; Park et al., 1999, 2000, 2002a, 2002b, 2003; Moore et al., 2001). There are nine major drill sites along the Nankai Trough tied with seismic reflection data. Three of the drill sites are located seaward of the prism, Deep Sea Drilling Program (DSDP) Site 582 (Shipboard Scientific Party, 1986) and Ocean Drilling Program (ODP) Sites

1173 and 1177 (Moore et al., 2001). These sites provide a reference for the geological characteristics of the incoming sedimentary section before deformation. Other sites sampled a landward progression of the prism's structure, such as incipient deformation, a major out-of-sequence thrust, and landward slope sediments.

Preexisting basement relief on the PSP igneous crust has been imaged (Yoshioka and Ito, 2001). This basement relief may affected the distribution of sediments, and therefore the fluid content of the sediment column should vary spatially. The presence or absence of turbidite facies, coupled with regional variations in smectite clay content may strongly affect the initial condition of sediment physical properties during subduction (Fig. 1.4).

Along-strike variations in frictional properties of material on the subduction plate interface are also believed to be important in controlling friction properties of the plate boundary (Song and Simons, 2003).

As part of the Nankai Trough Seismogenic Zone Experiment (NanTroSEIZE), I have had the opportunity to study the characteristics of the subducting PSP and its overlying sediment cover for this Ph.D. dissertation. The initial data set for my study was made available by the Japan Agency for Marine Earth Science and Technology (JAMSTEC), which conducted a series of marine multichannel seismic reflection and refraction

experiments in the Nankai Trough between 1997 and 2002. Because the focus of the JAMSTEC study was on the accretionary prism and seismogenic zone, little interest was focused on the portion of the data sets outboard of the trench. Thus, I was able to acquire approximately 20 regional seismic lines that extend out onto the northern part of the PSP for my study. A focused commercial seismic reflection survey was conducted by JAMSTEC in early 2003 in the Kumano Basin region of the Nankai Trough and I was also allowed to work on the portions of those lines that extended onto the PSP.

In late 2003, JAMSTEC was scheduled to conduct a high-resolution seismic reflection survey of potential drill sites on the PSP outboard of the Nankai Trough. I was asked to participate in this cruise and was ultimately able to specify the locations of many of the seismic track lines. I brought the data back to the University of Hawai'i, processed the lines and incorporated the new data into my study. The first result of this work has been the approval of several sites to be drilled during the up-coming IODP NanTroSEIZE drilling campaign in 2007/8.

In this dissertation, I present results of three different projects, examining variations in the initial stage of the inputs to the Nankai Trough subduction zone and variations in the overlying accretionary prism caused by these variables. Key geological parameters will

include the distribution of turbidite depositional system and its facies architecture, diagenesis of mixed terrigenous and hemipelagic sediments.

Chapter II presents an analysis of regional variations of large-scale basement topography and overlying sediment type and thickness. My co-authors and I show that basement topography has strong influence on the along-strike variations in sediment thickness and sediment type that enter the subduction zone and discuss these relationships associated with historical earthquakes. In the first phase of the analysis, we characterize the basement topography by its wavelength, amplitude, and lineation. Regional variations in basement depth lead to large thickness differences in the subducting sediment section. In the second phase of the analysis, we divide the seismic sediment sequences into four classes based on regional and sedimentary settings in relation to the basement relief. These classes have resulted in local changes in accommodation space, consequent sediment source location of depositional systems, and sediment pathways through time. In particular, most of the basement lows include Miocene turbidites in the deeper part of the stratigraphic column, but these turbidites are mostly absent over basement highs. A change from clay-rich to sand sediment increases permeability by 5 orders of magnitude (Saffer & Bekins 2006; Fig. 1.5). Therefore, these regional

variations in sediment sequences represent variations in the sediment property contrasts that may affect lateral migration of fluids expelled from sediments affected by progressive consolidation towards the subduction zone.

Chapter III presents local-scale basement topography around Kashinosaki Knoll (KK), which influences sedimentation in the eastern Nankai Trough through time. The data demonstrate a) the formation of KK and historical sedimentary succession that differs over each slope; b) the deposition of a Miocene turbidite unit that occurs not only in the basement lows but also on the gentle slopes of KK's basement high; and c) basement topography has an important control on changing sediment pathways as it reaches the accretionary prism. We discuss the formation of KK and the sedimentation associated with the subduction of topographic highs in the eastern Nankai Trough, and we describe the geological background obtained by geophysical data before the IODP drilling through the reference sites around KK (Tobin and Kinoshita, 2006).

We plan to submit chapters II and III to *Island Arc* as companion papers.

Chapter IV is the outgrowth of discussions with Dr. Gaku Kimura at University of Tokyo. It presents the influence of the along-strike variations in subducting basement topography and overlying sediment heterogeneity on the toe structure of the Nankai

Trough accretionary prism. We measure the angle of forward and backward thrusts with in the toe structure of the prism to estimate the along-strike variations in friction properties within the accretionary prism, and evaluate its relationship to incoming sediment heterogeneity within the accreted and underthrust sections. The major correlations with the friction properties are the accreted sediment thickness and the underthrust sediment type. We summarize the along-strike variations in frictional properties of material on the subduction plate interface and discuss future work.

We plan to submit Chapter IV to an international journal before NanTroSEIZE IODP drilling begins in fall, 2007.

FIGURES

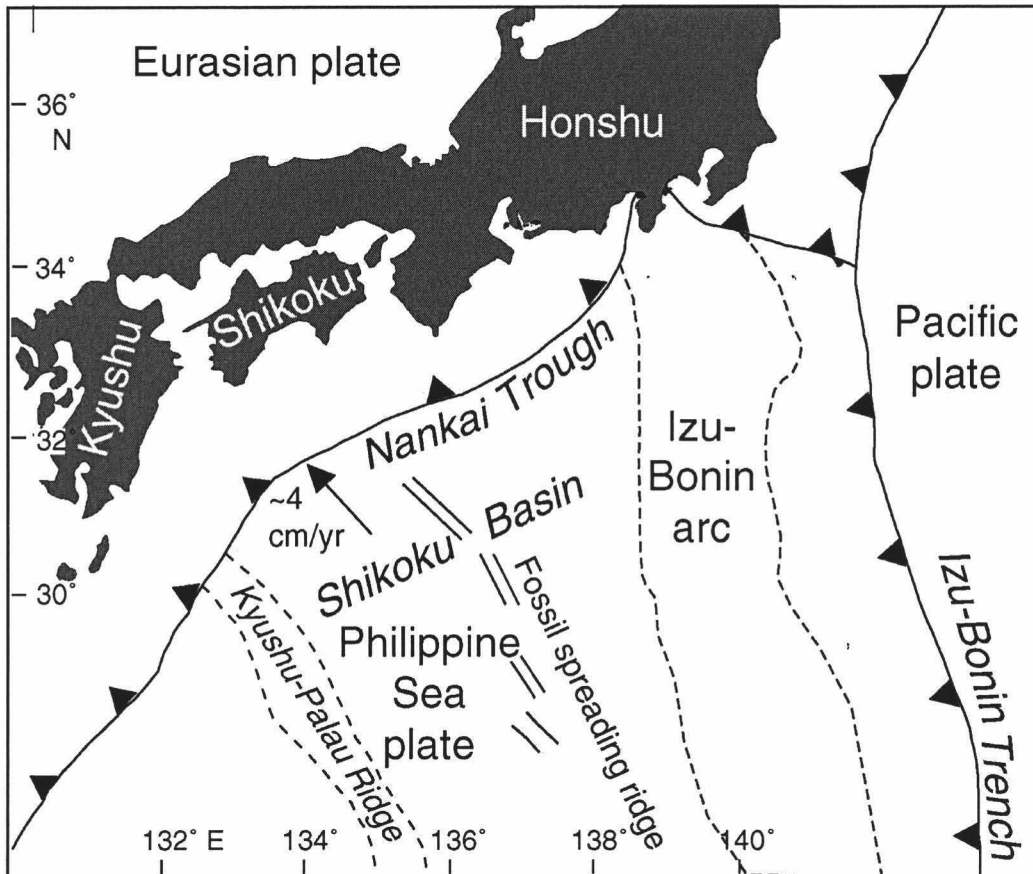


Fig. 1.1

Regional tectonic map showing the Philippine Sea region that includes the Nankai Trough. The arrow shows the convergence direction of the Shikoku Basin beneath Japan.

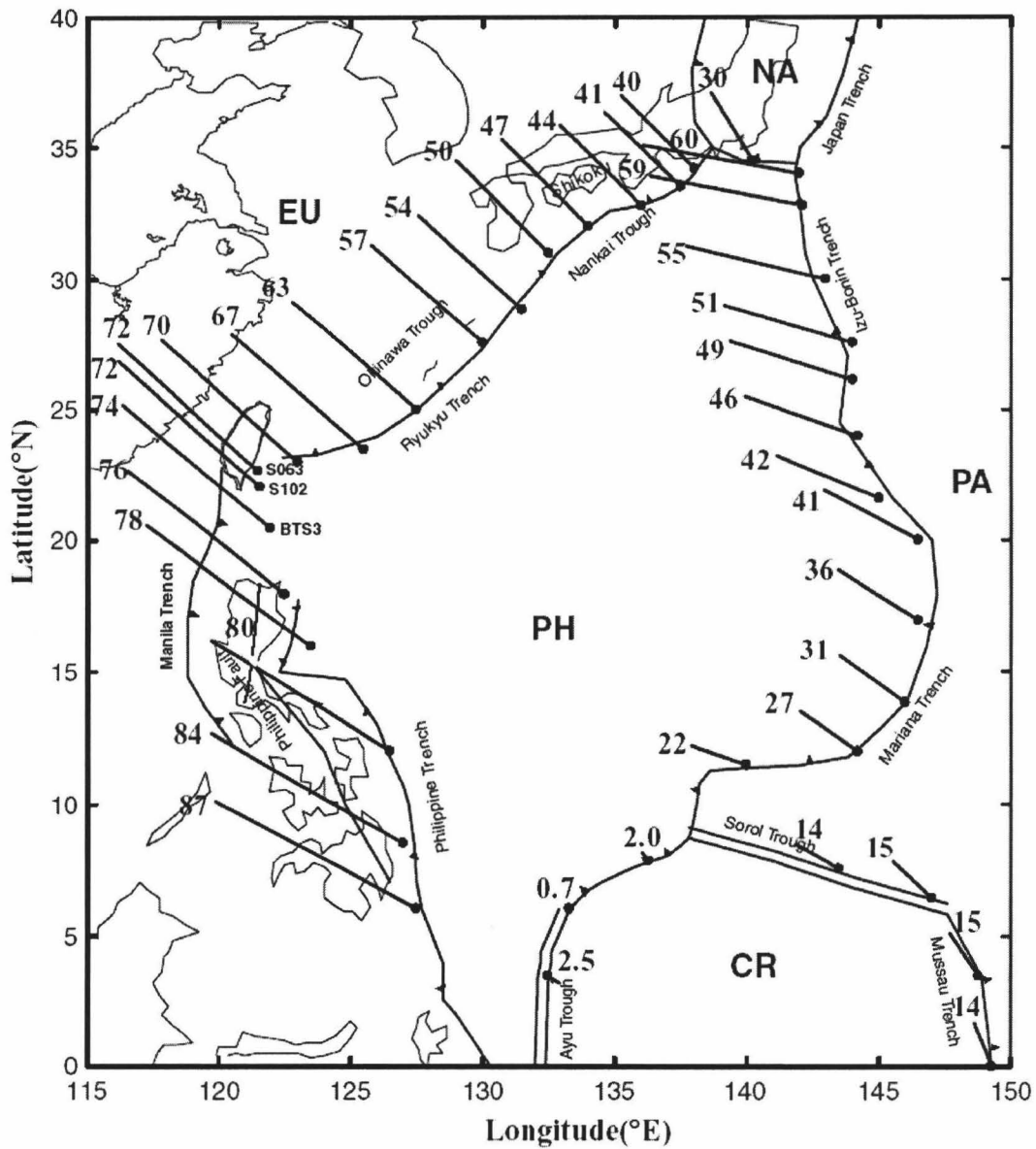


Fig. 1.2

Tectonic map showing the plate motion velocities (mm yr^{-1}) that includes the Philippine Sea (PH). Euler vector modeled from NUVEL-1A global plate motion. Azimuths are indicated by straight lines from circles. Plate name abbreviations are; EU, Eurasia; PA, Pacific; NA, North America; CR, Caroline. After Seno et al. (1993).

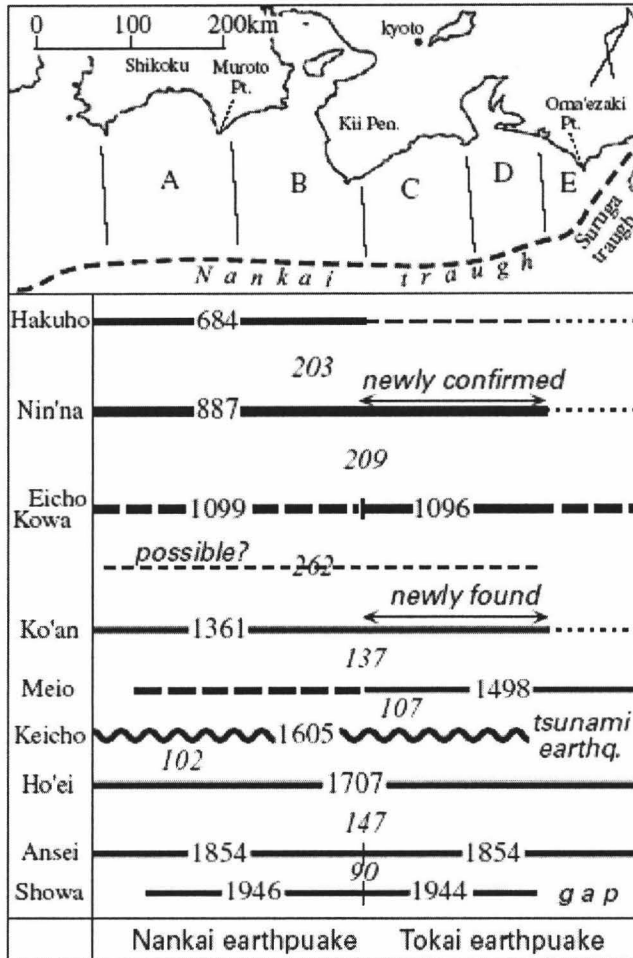


Fig. 1.3

Segmentation of the rupture zones deduced from seismological research and historic literature (Ando, 1975), associated with space-time distribution of great earthquakes along the Nankai Trough (Hori, 2006). Roman numbers indicate the year of earthquake's occurrence. Italic numbers indicate the interval between two earthquake successive series. Thick solid lines show certain rupture segment; whereas, thick and thin dashed lines show probable and possible rupture segment. Thin dotted lines show rupture segments that are unknown.

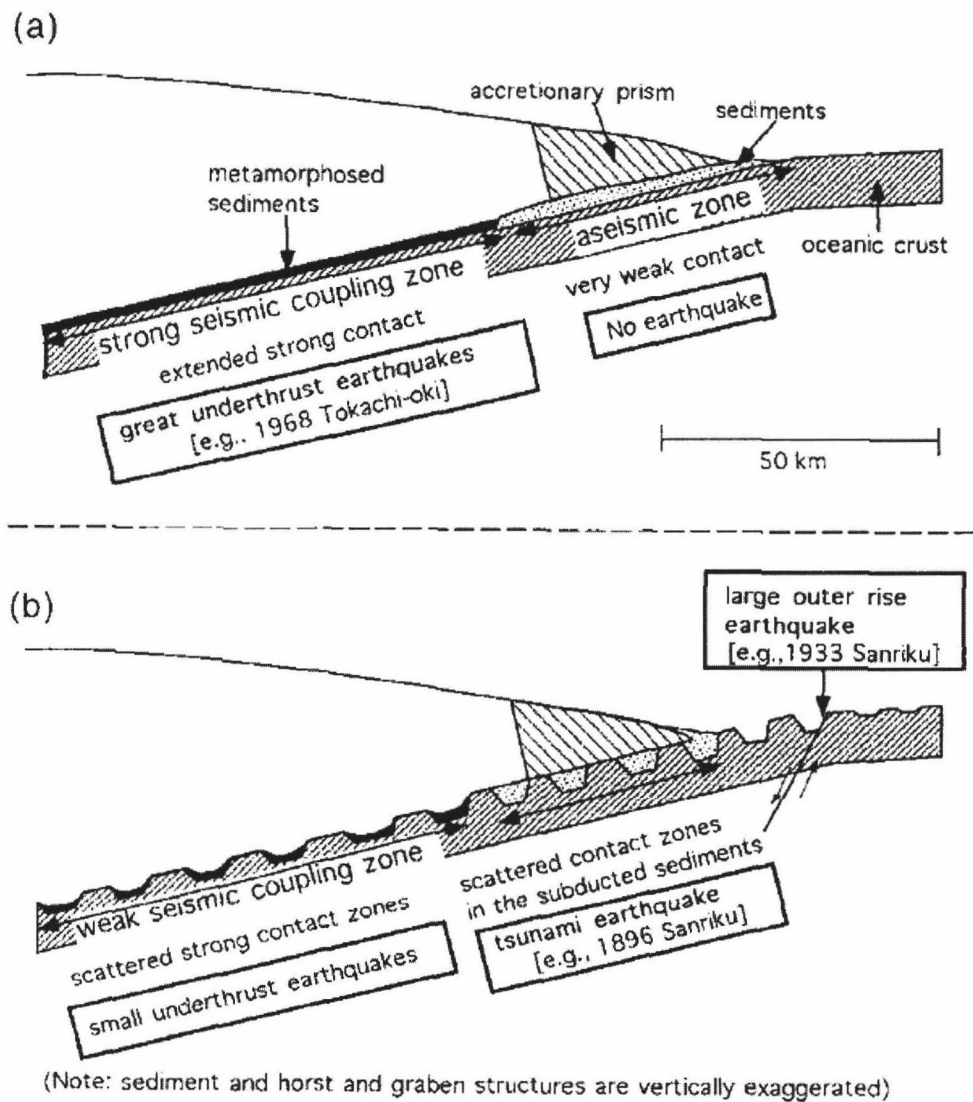


Fig. 1.4

Schematic illustration showing the relationship between smooth (a) and rough (b) plate interface with respect to the occurrence of great earthquakes. Sediment thickness and the structure of horst and graben are vertically exaggerated. From Tanioka et al., (1997).

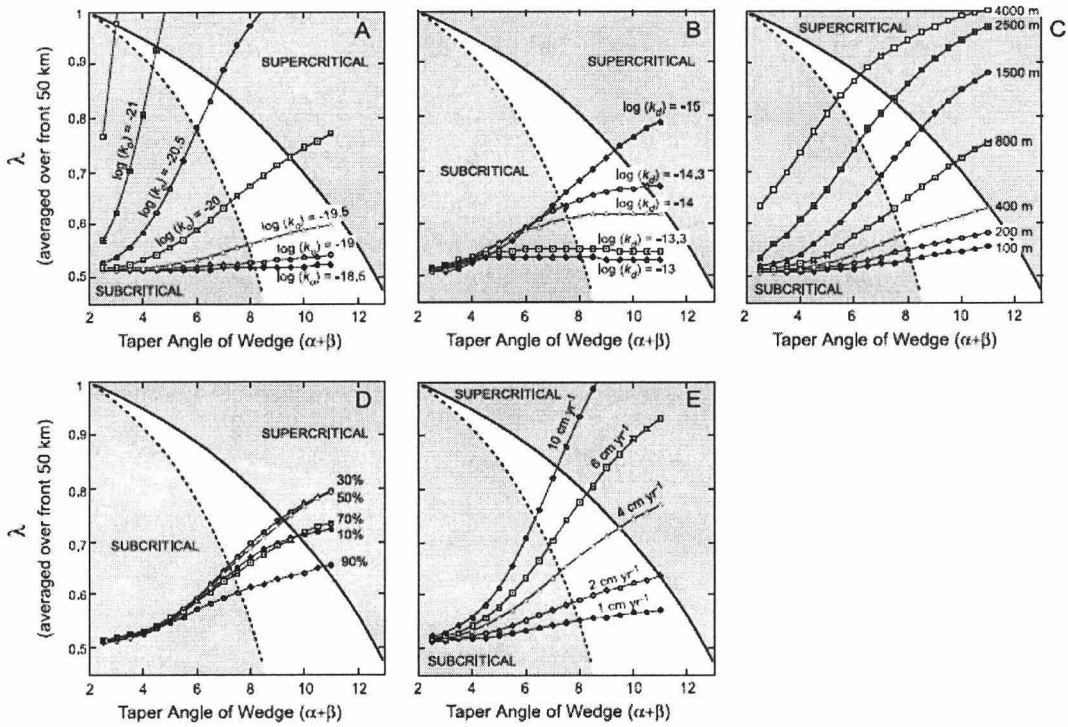


Fig. 1.5

Results of pore pressure sensitivity analysis, showing total taper angle of accretionary wedges ($\alpha + \beta$) versus modeled pore pressure ratio (λ) averaged over the front 50 km of the complex. Dots represent individual steady state model results. Model simulations are for the "base case" described in the text except for the individual parameter explored in each panel. Solid and dashed lines show critically tapered coulomb wedges for a strong ($\mu_b = \mu = 0.45$) and weak ($\mu_b = 0.3; \mu = 0.45$) décollement, respectively. Taper angle versus simulated λ is shown for varying (a) bulk permeability; (b) décollement permeability; (c) thickness of incoming sediment; (d) percentages of sediment accretion; and (e) plate convergence rate. From Saffer and Bekins (2006).

Chapter II

VARIATIONS IN SEDIMENT THICKNESS AND TYPE ALONG THE NORTHERN PHILIPPINE SEA PLATE AT THE NANKAI TROUGH

TOSHIHIRO. IKE^{1,*}, GREGORY.F. MOORE^{1,2}, SHIN'ICHI. KURAMOTO², JIN-OH.
PARK^{3,4}, YOSHIYUKI. KANEDA³, ASAHIKO. TAIRA²

¹ Department of Geology and Geophysics, University of Hawai'i, Honolulu, HI 96822,
USA

² Center for Deep Earth Exploration, JAMSTEC, Yokohama, Kanagawa, 236-0001, Japan

³ Institute for Frontier Research on Earth Evolution, JAMSTEC, Yokohama, Kanagawa
237-0001, Japan

⁴ Now at Ocean Research Institute, University of Tokyo, Nakano, Tokyo, 164-8639,
Japan

* Correspondence: IFREE, 3173-25 Showa-machi, Kanazawa-ku, Yokohama, Kanagawa,
236-0001, Japan

Email: tike@hawaii.edu

Phone: +81-45-778-5433

To be submitted to: Island Arc

Abstract

We document regional and local variations in basement relief, sediment thickness, and sediment type on the northern Philippine Sea Plate where it is subducting at the Nankai Trough. Seismic reflection data, tied with ODP drill cores, reveal that the variations in the incoming sediment sequences are correlated with basement topography. This study is based on detailed mapping of three-dimensional seismic facies distribution and measurements of representative seismic sequences and units. Trench-parallel seismic profiles show three regional provinces that are distinguished by the magnitude of the basement relief and sediment thickness in Shikoku Basin: western (< 200-400 m basement relief), central (> 1500 m), and eastern (< 600 m). The total thickness of the incoming sediment in basement lows is as much as 6 times greater than that over the basement highs. Turbidite sedimentation in the Shikoku Basin reflects the basement control on the heterogeneity of the incoming sediment in the lower Shikoku Basin (LSB) sequence, leading to the presence or absence of a turbidite unit (LSB-T unit) deposited during the middle Oligocene to the middle Miocene. Within the LSB-T unit, we classify two subunits (LSB-t1 & LSB-t2) that reflect regional variations in the pathways of turbidity currents through time. We propose that both regional and local variations in basement topography and sediment thickness/type cause lateral heterogeneities on the

underthrusting plate that in turn influence the lateral fluid flow along the toe of the accretionary prism.

INTRODUCTION

Basement topographic irregularities, such as aseismic ridges, seamounts and fracture zones have significant effects on trench landward slopes when they are subducted (e.g. Cadet *et al.* 1987; Kobayashi *et al.* 1987; McCann & Habermann, 1989; Dominguez *et al.* 2000; Kodaira *et al.* 2000; von Huene *et al.* 2000; Taylor *et al.* 2005) and specific examples offshore Costa Rica have been implicated as source regions for several large earthquakes during the past decade (Protti *et al.* 1995; Bilek *et al.* 2003). In thickly sedimented convergent margins, variations in sediment thickness and type entering the subduction zone also lead to regional along-strike differences in accretionary prism structure (e.g. Moore *et al.* 1980; Bekins & Dreiss 1992; Saffer & Bekins 2002; Spinelli & Underwood 2004). In addition, basement topography and the overlying sediments on the subducting oceanic plate control fluids entering the subduction zone. For instance, large contrasts in hydraulic impedance among different sediment types, such as the presence or absence of sandy/silty turbidites or hemipelagic mudstones, could affect

regional pressure gradient and fluid flow because sandy units are easier to dewater (Fisher *et al.* 1994; Giambalvo *et al.* 2000; Sibson 1996; Bourlange *et al.* 2003). The presence of thick sands deposited within isolated basement lows may create local compartments of excess pore pressure as they subduct if their dewatering pathways are restricted by surrounding impermeable units (Brown *et al.* 2003). Consequently, surface roughness of the subducting plate coupled with variations in fluid flux in the underthrusting sediment may affect the shallow dewatering processes that could, in turn, control interplate seismicity (e.g. Ruff 1989; Tanioka *et al.* 1997; Pritchard & Simons 2006).

The Nankai Trough, along the northern margin of the subducting Philippine Sea Plate (PSP) (Fig. 2.1), is known to be affected by destructive earthquakes and tsunamis every ~150 years (Ando *et al.* 1975). The trough is characterized by a thick terrigenous trench-sediment section entering the subduction zone. Studies of Ocean Drilling Program (ODP) drill cores across the northern PSP suggest that the Miocene turbidite unit identified within the lower Shikoku Basin facies in the western Nankai Trough (Ashizuri Transect, ODP site 1177), is missing in the central Nankai Trough (Muroto Transect, ODP site 1173) (Fig. 2.2). However, the regional variations in basement topography and sediment type have not yet been defined. Mapping the basement

topography and the distribution of Miocene turbidites along the northern PSP provides a better understanding of the local relationship between fluid reservoir and seal facies within the sediments deposited on the PSP outboard of the Nankai Trough.

In this paper, we document along-strike variations in basement topography on sediment thickness and sediment type deposited in the northern Shikoku Basin during the Neogene. We focus on characterizing the wavelength, amplitude, and lineation of the basement relief as they affect the overlying sediments. We use 40 high-resolution multi-channel seismic (MCS) lines tied to ODP drill core data to discuss the implications of the basement relief for controlling the deposition of turbidites derived from the Japanese Islands and fed out onto the PSP and the potential influence of these turbidites on the regional hydrostratigraphy on the PSP.

GEOLOGICAL SETTING

The PSP subducts beneath the Eurasian plate at a rate that varies along the Nankai Trough, from ~5 cm/year at N52°W in the west to ~4 cm/year at N48°W in the east (Seno *et al.* 1993). The latest phase of subduction is believed to have started at ~ 15 Ma (Taira 2001). Changes in volcanic activity in western Japan have been used to suggest that the

subduction either stopped or was very slow (less than 1 cm/yr) from 12-4 Ma, and increased to ~4-5 cm/yr at about 4 Ma (Taira 2001; Kimura *et al.* 2005). The marine sediments on the PSP have been sampled by ocean drilling in the western to central Nankai Trough off Shikoku Island (Karig *et al.* 1975; Taira *et al.* 1991; Moore *et al.* 2001a). The Nankai Trough extends northeastward about 700 km from the Kyushu-Palau Ridge to the Izu-Bonin Arc. A large amount of terrigenous sediment is presently being channeled down the trench axis from the Izu-Honshu collision zone along the Suruga Trough into the Nankai Trough (Taira & Niitsuma 1986; Aoike 1999). These trench strata overlie the hemipelagic strata deposited on the Shikoku Basin crust before it reached the trench.

The basement structure of the Shikoku Basin, the northern part of the PSP, was formed by the complex back-arc spreading history in the Izu-Bonin island arc (Kobayashi & Nakada 1978; Nakamura *et al.* 1984; Okino *et al.* 1994). The basement relief in the Shikoku Basin averages approximately 600 m (Hilde *et al.* 1969; Chamot-Rooke *et al.* 1987). Sediments fill in large basement lows that are interpreted to be fracture zones, probably formed by the last phase of seafloor spreading along Kinan Seamount chain (Le Pichon *et al.* 1987). Magnetic anomalies at the eastern and western sections of the basin

trend dominantly NNW-SSE, reflecting the early sea-floor spreading history (Okino *et al.* 1994; Kobayashi *et al.* 1995) that started ~27 Ma (mid-Oligocene), when the Kyushu-Palau arc was split by back-arc spreading. Lineated magnetic anomalies in the western half of Shikoku Basin clearly correlate with magnetic anomalies 6 to 7, but the anomalies in the eastern basin are less distinct and their correlations are less certain (Okino *et al.* 1999). Spreading proceeded at ~2.3-4.7 cm/yr until anomaly 6B (~20-23 Ma). Seafloor spreading anomalies 5B and 6 (~15-20 Ma) indicate that the spreading direction changed to NE-SW during this time. Seafloor spreading between chrons 5B and 5E was the last true spreading phase in the Shikoku Basin (Okino *et al.* 1994, 1999), but late-stage rifting may have continued until 7-10 Ma with associated volcanism that formed the Kinan Seamount Chain (Chamot-Rooke *et al.* 1987; Ishii *et al.* 2000). The estimate age of the youngest basalts dredged samples from Kii Seamount shows 10.1 ± 0.5 Ma, and 7.6 ± 0.5 Ma from Dai-ichi Kinan Seamount (Ishii *et al.* 2000).

DATA ACQUISITION AND PROCESSING

We used four seismic reflection data sets (Table 2.1), totaling 40 lines, collected by the Japan Agency of Marine-Earth Science and Technology (JAMSTEC) along the northern

PSP. The first data set was collected from 1997 to 2001 on the R/V *Kairei* using a variety of sound sources and multi-channel streamers. For data acquisition during the 1997 cruises, for example, an air-gun array of 3080 in³ (50 L) was used as the controlled-sound source and a 120-channel streamer (25 m group interval) was used as the sound receiver. During the 2001 cruises, a 360-channel streamer was used, with an untuned 196 L (~12,000 in³) airgun array as the sound source. Initial processing through stack was completed at JAMSTEC. We applied the second phase of data processing to this data set, including bandpass filters and post-stack time migration. The second data set was collected by a commercial contractor in the spring of 2003 using a 480-channel streamer and a tuned 70 L (4240 in³) airgun array as the sound source (Taira *et al.* 2005). We processed several of these lines through stack and post-stack time migration, and performed Pre-stack Depth Migration (PSDM). The third data set was collected from 2003-2004 on the R/V *Kaiyo* in December 2003 – January 2004 using an 18-channel streamer and a single 5 L (total 355 in³) generator-injector (GI) gun as the sound source. We have also processed these lines through filter, stack, and post-stack time migration. We also used a 3-D seismic data set that was collected by a U.S.-Japan Collaborative Program off Muroto in 1999 using the R/V *Maurice Ewing* (Moore *et al.*

2001b). The acquisition parameters include a single 6 km streamer with 240 channels and a tuned 70 L (4270 in³) airgun array, and the resultant survey covered a region ~8 km wide and 80 km long.

We developed a velocity model based on the PSDM velocity analyses from lines ODKM-22 and ODKM-B, from the eastern part of the Shikoku Basin (*P. Costa Pisani*, unpublished data, 2006), and Muroto-3D-284 (from the central Shikoku Basin) and used these velocities for depth conversion of the other seismic lines. In the Kumano area, where the topography is relatively flat, the velocity model has values of 1510 m/sec at the seafloor followed by a gradient of 650 m/sec² with increasing two-way travel time. The velocities over Kashinosaki Knoll have a smaller gradient of 550 m/sec². In the Muroto area, the velocity model has values of 1510 m/sec at the seafloor followed by a gradient of 900 m/sec² for the trench wedge turbidites within the trench axis, whereas the gradient is 550 m/sec² seaward of the trench axis. These velocities are accurate enough to identify regional sediment thickness trends, so we extend this velocity model throughout the data set along the Nankai Trough.

To supplement the digital seismic reflection lines, we also digitized the basement depth from the seismic lines collected by the Kaiko Project (Kaiko I Research Group,

1986). We used the lines that are located off Cape Muroto. We developed a constant velocity model, for the sediment column (1900 m/sec), that correlates the basement depth well with the other seismic data. The miss fit of the basement depth measured from the Kaiko Project to the other seismic data is approximately 150 m which increases as the basement deepens. In this digitized data set, we focus on describing the basement depth and total sediment thickness but not the sediment sequences.

SEISMIC STRATIGRAPHY

We interpret and define four major seismic stratigraphic sequences that are correlated with the key lithostratigraphic units defined at the ODP Leg 131 and 190 drill sites (Taira *et al.* 1991; Moore *et al.* 2001a) (Fig. 2.2). The base of the stratigraphic sequence is a thin volcanoclastic unit that overlies oceanic crust (Moore *et al.* 2001a). The oldest mapped sediment unit is the lower Shikoku Basin (LSB) sequence that overlies the volcanoclastics. This sequence is characterized by discontinuous to moderately-continuous, hummocky reflections at the upper boundary, with very low-amplitude and very few coherent internal reflections in the lower portion. The LSB sequence is correlated with the middle Miocene to lower Pliocene hemipelagic mudstone

sampled at the ODP drill sites (Moore *et al.* 2001a). Within this sequence, there are laterally continuous, high-amplitude reflections correlated with Miocene turbidites (LSB-T unit) cored at ODP Site 1177. This unit has a terrestrial component characterized by plant detritus, pieces of wood, and 25-55 percent of smectite content of the bulk mudstone (Moore *et al.* 2001a). The probable source of the sands within lower Shikoku turbidite facies, early to late Miocene age (~6-16 Ma) at ODP Site 1177 (Moore *et al.* 2001a), is suggested to be the inner zone of southwest Japan (Fergusson 2003). Hemipelagic clay that interbed the Miocene turbidites shows a strong volcanic component of suspended-sediment input from Izu-Bonin arc (Underwood & Fergusson 2005). In the eastern part of Shikoku Basin, we identify two high-amplitude seismic facies within the LSB-T unit, which we interpret as turbidite sections separated by a thick section of low amplitude reflections (hemipelagic sediments). Where these two turbidite facies occur, we divide the LSB-T unit into two subunits (LSB-t1 & LSB-t2). The LSB-t1 subunit is characterized by low-amplitude reflections in the upper part of the LSB-T unit, whereas the LSB-t2 subunit is characterized by high-amplitude laterally-continuous reflections in lower part of the LSB-T unit.

The boundary between the LSB and the overlying upper Shikoku Basin (USB)

sequence is diagenetically controlled, at least partially, by the breakdown of sparse ash layers and opal reaction in the lower unit (Taira *et al.* 1991; Moore *et al.* 2001a). The USB sequence, characterized by low amplitude seismic reflections in the upper part of the sequence and few coherent reflections in the lower part, is correlated with a hemipelagic mudstone and an abundant ash and tuff unit that is Quaternary to Pliocene in age at ODP Site 1173. Sediment properties in the USB sequence at ODP Site 1173 do not follow a typical compaction profile in which porosity decreases uniformly with depth. Instead, porosity is nearly constant, ~55-65%, over a depth range of approximately 240 m (Moore *et al.* 2001a). A change in physical properties associated with the phase transition from cristobalite to quartz or dissolution of a weak opal cement may also be responsible for the reflections within the lower section of the USB sequence (Moore *et al.* 2001a; Spinelli *et al.* 2007). Note that the hummocky reflections at the top of LSB sequence in Muroto (Site 1173) and off Kumano Basin are not present off Ashizuri (Site 1177).

BASEMENT TOPOGRAPHY AND PROVINCES

Seismic reflection profiles across the northern PSP demonstrate large variations in

basement relief that are not reflected in the regional bathymetry (Fig. 2.3) because of the thick sediment blanket. We classified the Shikoku Basin into three provinces based on its basement relief and associated sediment cover. Our boundaries follow closely those proposed by Kido and Fujiwara (2004) based on regional magnetic anomaly correlations, thus indicating that the primary basement character is controlled by the seafloor spreading history.

The Eastern Province of Shikoku Basin is characterized by relatively rough basement relief, both lineated and isolated, associated with Kashinosaki Knoll (basement amplitude < 1500 m) and other unnamed topographic highs (< 600 m). The half-wavelength of the basement highs, parallel to the trench, ranges from ~10 to 20 km. The basement highs are generally about 1/2 to 1/3 as wide as the intervening basement lows. The Central Province has ~10-20 km wide, NW-trending basement lows that are ~1-2 km deeper than adjacent horst blocks along the Kinan Seamount chain (Fig. 2.3). In most cases, the amplitude of the basement highs is ~6 times greater than that of the overlying seafloor topographic relief. The basement relief is not easily recognized in the seafloor bathymetry because thick sediments burry the basement relief. Sdrolias *et al.* (2004) indicates that the late stage seafloor spreading of Shikoku Basin (~18 Ma) has a half

spreading rate of ~ 2.0 cm/year that is more than 1.0 cm/year lower than the major spreading rate of the Shikoku Basin. The formation of large basement relief in the Central Province may relate to the rotation of seafloor spreading associated with a low spreading activity, and young seamount eruption (Le Pichon *et al.* 1987). These basement lows in the Central Province have 3-5 times larger relief than those in the Western Province, which is characterized by relatively smooth basement relief (< 200 - 400 m). The basement relief is the smoothest along the trench-perpendicular seismic lines. In detail, the majority of the basement in this zone has relief of ~ 170 m perpendicular to the trench and 200 - 400 m parallel to the trench. Moreover, there are lack of isolated basement relief and seamounts and ridges in the Western Province. These observations imply that the relief of the abyssal plain may be parallel to the trend of the seafloor spreading axis. In addition, oceanic crust in the Western Province may formed by seafloor spreading without additional volcanic intrusions from the spreading axis or the nearby volcanic arc, such as Kyushu-Palau ridge and Izu-Bonin arc. Although the data coverage is less in the western part of Shikoku Basin compared with other areas, the trench-perpendicular basement relief on the Western Province has lower amplitude than the Eastern Province. The basement relief in the Eastern Province has a

degree of roughness in between the Western and Central Provinces. There are abyssal plain that relief is < 600 m, and seamounts. The basement depth is shallower than the Western Province that has a similar crustal age. Oceanic crust in the Eastern Province may formed by seafloor spreading associated with volcanic intrusions from the spreading axis or the nearby volcanic arc.

TOTAL SEDIMENT THICKNESS

Isopachs of sediment sequences, determined by subtracting the depth of the seismic sequence's upper boundary from the lower boundary on the seismic lines and extrapolated between lines, are shown in Figure 2.4. The incoming sediment blanketing the basement relief shows local variations in total thickness. For instance, the maximum sediment thickness seaward of the deformation front is approximately 2000-2200 m in the central Shikoku Basin. The minimum thickness is less than 300 m over the topographic highs, such as Kashinosaki Knoll and near the Kinan Seamount Chain. The total sediment thickness in the Western Province ranges mostly between 500 and 750 m, in the basement lows seaward of the Nankai Trough, without much variation parallel to the trough. On the other hand, the total sediment thickness in the Central and Eastern

Provinces exceeds 1000 m in the basement lows seaward of Nankai Trough.

Previous studies indicated that the total sediment thickness generally increases towards the trench and the Izu-Bonin arc (Ludwig & Houtz 1979; Nemoto *et al.* 1995).

Our observations generally follow the same trend. A plot of basement depth versus total sediment thickness shows that the two parameters are linearly related with a slope of 0.83 (Fig. 2.5), indicating that turbidites are channeled into the basement lows. We note that there is a significant variation in sediment thickness (600-800 m) for a given basement depth (Fig. 2.5).

LOCAL STRATIGRAPHIC VARIATIONS

We divided the seismic sequences into four classes based on regional and sedimentary settings. The first-order defining stratigraphic feature of the incoming section is the presence or absence of the LSB-T unit in the LSB sequence.

Class I) Spatially uniform sediments over subdued basement relief

Class I is characterized by the presence of the LSB-T unit associated with relatively smooth basement lows in the Western Province of Shikoku Basin (Fig. 2.6). The sediment sequences in this class are correlated with those at ODP site 1177 (Fig. 2.2).

The LSB-T unit, in general, has high-amplitude continuous reflections and is generally sub-parallel to the basement (Fig. 2.7a, S.P. 7000-8200), although in some areas, the LSB-T unit shows low-amplitude reflections in the lower section. The thickness of the high-amplitude reflection section, LSB-T unit, ranges from ~200 to 350 m (Fig. 2.7b).

The LSB-T unit mostly laps onto basement highs whose summits exceed 400 m above the adjacent basement lows seaward of the Nankai Trough. Class I is restricted to the Western Province of Shikoku Basin (Fig. 2.6) and part of the Central Province (Fig. 2.7a). The sediment sequence in the Eastern Province (Fig. 2.7c) partially has similar characteristics with Class I; however, they are distinct in detail.

Class II) Absence of LSB-T unit over relative basement highs

Class II is characterized by basement highs associated with the absence of the LSB-T unit. A region characteristic of Class II is the Muroto area in the central part of Shikoku Basin, where the sediment sequences were drilled at ODP site 1173 (Fig. 2.2). The total sediment thickness in this class ranges from ~500 to 800 m, a value that represents the minimum thickness in the northern Shikoku Basin.

In this class, the basement highs have three characteristics in common: they are at least ~400-600 m higher than the adjacent basement lows; their maximum slope angle is

~20-25 degrees, and their width is ~5-10 km parallel to the trench. Major basement highs are located off Cape Muroto, off Kii peninsula (Fig. 2.7a), and a few in the western part of Shikoku Basin (Fig. 2.6).

Class III) Sediments in NW-trending basement lows along the Kinan Seamount Chain

Class III is characterized by a thick section of the LSB-T unit within large basement lows. This class occurs mostly near the Kinan Seamount Chain, along the extinct spreading center of the Shikoku Basin (Fig. 2.7a, 2.8a). In this class, a section of low-amplitude reflections characterizes the bottom portion of the LSB sequence (e.g. Fig. 2.8a, S.P. 3200-4000). This unit thins from approximately ~500 m thick in the deepest parts of the basins to less than seismic resolution on the basin flanks (e.g. Fig. 2.8b, S.P. 3200-4000). This distinct "transparent" character is indicative of a homogeneous section containing no significant acoustic impedance contrasts that were probably formed mostly of hemipelagic sediments that were originally deposited on the adjacent topographic highs then slumped into the intervening lows. Overlying the transparent layer, the LSB-T unit is ~450-800 m thick and exhibits high-amplitude, continuous reflections. On the flanks of the basins, where the underlying hemipelagics become very thin, the LSB-T unit onlaps the basement of the adjacent topographic highs. The

LSB-T unit is folded in some of the basins due to differential compaction of the underlying hemipelagic strata (e.g. Fig. 2.7a, SP 6200-6600 and Fig. 2.8a, S.P. 1250-1750, 3200-4000). Thus, Class III is characterized by thick (> 1000m) hemipelagic and terrigenous sediments within deep basement lows.

Class IV) Two turbidite units in the LSB-T unit

Class IV is restricted to the Eastern Province and is characterized by two high-amplitude seismic facies within the LSB-T unit, LSB-t1 and -t2 subunits. LSB-t2 occurs in the lower half section of the LSB-T unit and has high-amplitude laterally-continuous reflections that lap onto the basement highs, similar to the LSB-T unit in Class I (Fig. 2.7c). The thickness of the LSB-t2 subunit ranges from ~100 to 350 m, depending on the basement relief. Locally, the LSB-t2 subunit is characterized by very low-amplitude discontinuous reflections that are no different from the transparent character found in Class III (Fig. 2.8a, S.P. 4000-6300). These very low-amplitude reflections are geographically restricted to the region south of the Kii peninsula (e.g. Fig. 2.8c).

The upper half section of the LSB-T unit has low-amplitude discontinuous reflections (LSB-t1 subunit). The thickness of the LSB-t1 subunit ranges from ~100 to 380 m (Fig. 2.7a). The upper boundary of the LSB-T unit (also LSB-t1 subunit) is characterized by

a thin section (< 100 m) of high-amplitude continuous reflections, gradually dipping towards the northwest (Fig. 2.7a). These high-amplitude reflections are tied with the upper boundary of the LSB-T unit in Class I and III. In addition, these reflections onlap the underlying hemipelagic sediment section above the basement highs (Fig. 2.8c). This boundary is concave-up in the basement lows.

The seismic character of the LSB-T unit changes over Kashinosaki Knoll. The upper boundary of the LSB-T unit shows two to three high-amplitude hummocky reflections. These hummocky reflections lap onto the basement on the northwest of Kashinosaki Knoll (Fig. 2.7c). Although the local basement highs, associated with steep slopes over Kashinosaki Knoll, exceed 400-600 m adjacent to the surrounding basement lows, the LSB-T unit occurs over the basement associated with a relatively shallow dip on its landward margin. We define the eastern boundary of Class IV at the eastern edge of Kashinosaki Knoll because the sediment sequence is affected by Quaternary turbidites and debris flows that are not common to other Classes towards the west.

The upper boundary of the LSB sequence

The second-order heterogeneity in the incoming sediment can be made based on the change in the seismic character along the upper boundary of the LSB sequence. The

acoustic response from the boundary between the LSB and USB sequences is diagenetically controlled, such as the breakdown of sparse ash layers (Taira *et al.* 1991; Moore *et al.* 2001a). The hummocky reflection that is the classic characteristic of this boundary is not clearly shown in the Western Province (Fig. 2.6). To the east, the hummocky reflections clearly appear near ODP drill Site 1173 (344 m below seafloor), in the Central Province (Fig. 2.7a). The lateral continuation of these reflections shows two seismic characteristics: 1) they are parallel to the basement relief or 2) they are parallel to the upper boundary of the LSB-T unit. The first case appears in the central Shikoku Basin (Fig. 2.8a, S.P. 2000-3000). The upper boundary of the LSB sequence shows concave-up morphology over the basement lows (Fig. 2.8b, S.P. 3200-4000). Its relief is more parallel with the reflections in the LSB-T unit than the seafloor relief. The second case appears in the Eastern Province (Fig. 2.8a, S.P. 4300-5200). In this area the upper boundary of the LSB sequence is located approximately ~290-380 m beneath the seafloor. Therefore, the acoustic response from the boundary between LSB and USB sequence vary along the Nankai Trough, and this boundary may not solely controlled by diagenesis but with other lithofacies transitions.

DISCUSSION

Our high resolution seismic data illustrate a complex interaction between the Shikoku Basin basement relief and sedimentation that produces regionally variable sediment thickness and facies that, in turn, likely affect the physical properties of the subducting section along the northern PSP. Comparisons of basement relief, sediment thickness, sediment type, and extent of diagenesis lead us to divide the northern Shikoku Basin into three distinct provinces. Variations in the above factors could contribute to regional variations in the rupture process of earthquakes, seismic segmentation, and the frictional properties along the subducting plate interface (Sibson 1986; Prawirodirdjo *et al.* 1997; Liu-Zeng 2005).

TECTONIC AND BASEMENT CONTROLS ON SHIKOKU BASIN SEDIMENTATION

We have shown that the basement morphology in each province is correlated with the sediment Classes. It is apparent from the seismic profiles that lateral variations in the basement relief had significant control on the deposition of turbidites within the LSB sequence. The present distribution of the LSB-T unit is highly variable, with most occurrences being within topographic lows, and locally over relative basement highs

associated with gentle slopes, thus suggesting that turbidity currents flowing from the Japanese islands were deflected around topographic highs and flowed into the topographic lows in the Shikoku Basin. This led to significant variations in sediment thickness and type across the width of the Shikoku Basin in the LSB section. Here, we examine the effect of basement relief on the formation of LSB-T unit. We focus on the presence or absence of LST-T unit (Miocene turbidites) because this could affect physical properties along underthrust sediments in the subduction zone.

The presence of turbidite units within the early to late Miocene deposits of Shikoku Basin (LSB-T unit) and the absence of turbidite units in the late Miocene to Pliocene deposits (the upper portion of LSB sequence and USB sequence) implies a major change in sedimentation in Shikoku Basin at the end of the late Miocene. Turbidites coming from the Japanese Islands are not currently able to flow out into the Shikoku Basin, except for the region around Kashinosaki Knoll and Zenisu Ridge, because they are trapped in either the forearc basins, in basins on the accretionary prism, or in the trench. The most likely significant difference was the lack of a bathymetric trench and basins along the base of the continental slope and a bathymetric trench to trap sediments derived from the Japanese Islands, thus allowing the sediments to flow out onto Shikoku Basin in

the early Miocene. This is consistent with the inference of extremely low subduction rates during this time (Kimura *et al.* 2005), which would have meant that the rate of growth of any accretionary prism must have been very slow, even though there were thick sediments at the base of the continental slope that could have been accreted. For another scenario, the young age of Shikoku Basin crust may not have significant flexure, similar to Cascadia Basin (Underwood *et al.* 2005), so the plate may be relatively flat without a large trench. At the end of the early Miocene, rejuvenated subduction and a possibly steeper subduction angle led to rapid building of the present accretionary prism, thus forming accommodation space within and seaward of the prism and cutting off the supply of turbidites to the Shikoku Basin.

In addition, the difference in the seismic character of the LSB-T unit, between Class I (Western Province) and IV (Eastern Province), indicates a local change in hemipelagic sedimentation during the formation of the LSB sequence. The appearance of the LSB-t1 subunit, characteristic of low-amplitude reflection representing hemipelagic sedimentation in Class IV, is limited to the Eastern Province of Shikoku Basin. In this province, a high rate of hemipelagic sedimentation should have occurred in the lower Miocene to mid-Miocene. The probable source of clay could be the proximal Izu-Bonin

island arc which, after a volcanic minimum in the early Miocene, increased production of volcanoclastic sediments in the middle Miocene (~17 Ma, Taylor 1992). These clay dispersal is controlled by bottom currents (Underwood & Fergusson 2005); therefore, the appearance of low amplitude reflections characterizing the LSB-t1 subunit in Class IV, but not in Class I, may be explained by bottom currents flowing counter clockwise on the Shikoku Basin.

IMPLICATION FOR THE PHYSICAL PROPERTIES ALONG THE PLATE BOUNDARY

We have shown the morphology of basement and its effect on the formation of LSB-T unit in each province. Here, we discuss the possible effect of basement relief and incoming sediment properties on the plate boundary. We focus on sediment classes because each class should have a distinct character in the dewatering system that could also affect friction properties as the sediments subduct. Several researchers have suggested that sediments may play an important role in the locking and rupturing at the plate boundary as well as tsunamigenic earthquakes (Okal 1988; Tanioka et al., 1997; Wang & Hu, 2006). No interplate earthquakes can nucleate in the trench landwards

slope as a consequence of the presence of unconsolidated sediments that form a stable sliding (velocity strengthening) zone. If earthquake propagates into this stable region, a negative stress drop will occur, resulting in a rapid stop to the rupture propagation (Scholz 1998). Different sediment types, such as turbidites and hemipelagic clay, could cause regional variations in permeability for several orders of magnitude (Giambalvo *et al.* 2000). In the Western Province of the Shikoku Basin, mudstones in the lower Shikoku Basin turbidite facies and volcanoclastic-rich facies, at ODP site 1177, are enriched by much higher percentages of smectite in the basement lows (Steurer *et al.* 2003), which could also affect the generation of fluids and the pore fluid pressure (Moore & Vrolijk 1992). The well-connected basement lows associated with sediment Class III contain the thickest sediment sections and contain the thickest turbidite sequences that may represent an area of higher drainage; therefore, generate regions of high effective stress compared with the other classes. On the other hand, isolated basement lows may create local compartments of excess pore pressure as they subduct because the turbidites contain more pore fluids than the sections dominated by hemipelagics and their fluid flow pathways are likely restricted where they pinch out against the highs (e.g., Brown *et al.* 2003; Underwood, 2007), which could generate regions of lowered effective stress,

perhaps facilitating rupture over these areas (Scholz 1990). In addition, the amount of hemipelagic clay may also affect the dewatering system because thick accumulation of clay and its dehydration may represent an area of high fluid source. Sediment Class III may create large amount of fluids due to clay dehydration in the Central Province that is associated with high heat flow (Yamano *et al.* 2003). Therefore, the Central Province, along the extinct spreading center of the Shikoku Basin, may have higher degree of pore pressure build up, in the early stage of consolidation, due to clay dehydration than the Western and Eastern Provinces. In addition, the top of the LSB-T may be overpressured because the overlain hemipelagic sequence could cap and inhibit upward escape of water.

The significant variations in the sediment thickness and type along the subducting northern Shikoku Basin will likely have associated major effects on the shallow levels of the subduction zone. The décollement in the central and western Nankai Trough apparently localizes at nearly the same stratigraphic level within the upper part of the LSB sequence (Moore *et al.* 2001a). Thus, most of the LSB sequence is subducted beyond the toe of the accretionary prism and this is the section that has the most variability in thickness and sediment type across the Shikoku Basin. We suggest that the rupture propagation of the 1946 earthquake might be disturbed by the thick sediments in

Class I and III. On the Eastern Province, the ridge subduction in the Kumano Basin (Park et al., 2003) where embayment structure is absent, thick accumulation of sediments detached from the basement high may have caused the accretionary prism to rebuild quickly after the ridge subduction. Therefore, the ridge has enough contact to the overriding plate for longer rupture propagation.

These phenomena may be commonplace wherever seafloor topography with linear ridges, horst-graben structures, and a high rate of terrigenous sedimentation intersects a margin. For example, off northern Chile subduction of a thick sediment section appears to increase the maximum depth of seismicity (Zhang & Schwartz 1992; Pritchard & Simons 2006). In the Cascadia margin, the deep grabens of the Juan de Fuca spreading system channel turbidites from western North America, leading to highly variable sediment sections entering the subduction zone (Underwood 2002; Underwood *et al.* 2005). These variable sediments may also be applied to the lineated basement relief associated with sediment Class II and III in the Central Province. The lineated relief in this province may create variations in effective hydrologic seal and drainage or hydrogeologic conversion of basement and sediment seal.

REGIONAL VARIATIONS IN BASEMENT TOPOGRAPHY AS A CAUSE FOR PLATE BOUNDARY EARTHQUAKE RUPTURE VARIATIONS

We have shown that the morphology of basement and sediment thickness and type in each province may have distinct physical properties along the plate boundary. Here, we discuss the possible effect of plate boundary properties on rupture propagation.

Most large earthquakes occur at the plate boundary subject to tectonic stress and rapid shear faulting. The rupture propagation is usually irregular, and the slip motion is rather heterogeneous over the fault plane. A large slip area is called an asperity that is characterized by the interface strongly sticks during the inter-seismic period, and then abruptly slips to generate seismic waves. These asperities have often been compared with seafloor bathymetry. For example, the dislocation distribution (asperity) is well correlated with subducted seamounts (Cloos, 1992; Kodaira et al, 2000; Bilek et al., 2003). Although the specific mechanism for bathymetry to asperity has yet to be identified, it is very likely that the repetition of the fault motions in the same area has built up by bathymetric features. In addition, Wells et al. (2003) summarized that there is strong correlation between the asperities of megathrust earthquakes and the forearc basins.

Our study has demonstrated that regional variations in both basement structure and sediment thickness/type on the subducting PSP occur on both regional (100-200 km) and local (~5-20 km) scales. The Nankai Trough plate boundary has been shown to rupture in regional segments (e.g., Ando, 1975) and local variations in earthquake characteristics have been correlated with similar magnitudes of basement relief in other subduction zones (e.g., Bilek & Lay 2002; Bilek *et al.* 2003). In addition, the rupture area of tsunami generation for the 1944 and 1946 events are reasonably well understood (Baba and Cummins, 2005). Regional variations in earthquakes along northern Honshu, Japan, are correlated with variations in subducting topography in the Japan Trench by Tanioka *et al.* (1997), who propose that large earthquakes occur in the shallow part of the plate boundary in the smooth surface region because of the large amount of subducted sediments and that tsunami earthquakes occur in the rough surface region because the topographic highs form strong contacts along the shallow part of the plate boundary. The Western Province of Shikoku Basin has the smoothest basement relief (< 200-400 m). It correlates with the low irregularities in the sediment thickness that range from ~500-1300 m (Nemoto *et al.* 1995; Yoshioka & Ito 2001). This area may represent geologic candidates for asperities as smooth surfaces created by subducted sediment

(Ruff, 1989). The fault plane in the western part of Shikoku Basin overlaps Zones A defined by Ando (1975); however, the eastern portion of Zone A may overlap with the Central Province. The Central Province of the Shikoku Basin has the largest basement relief ($> \sim 1200\text{-}1500$ m). The NW-trending basement low that is characterized by sediment Class III has strong correlation with the negative gravity anomaly as the asperities of megathrust earthquakes proposed by Wells et al. (2003). The rupture propagation presented by Baba et al., (2005) may indicate that the large amount of sediment could prevent the rupture in the Central Province. Adjacent to the basement low, the lineated basement high should form strong contacts along the shallow part of the plate boundary compared with the Western Province. The Central Province is offshore of the central part of Zone B defined by Ando (1975); however, the eastern portion of Zone B overlaps with the Eastern Province. These results indicate that the Central Province associated with subduction of large basement relief may relate to shorter rupture propagation. The Eastern Province of the Shikoku Basin is also correlated with relatively large basement relief (< 600 m) associated with local topographic highs, such as Kashinosaki Knoll and other large bathymetric features. The basement relief, both isolated and lineated features, correlates with the eastern part of Zone B and C defined by

Ando (1975).

CONCLUSIONS

Our seismic reflection data sets across the northern Philippine Sea plate (PSP) suggest the following conclusions:

- 1) The subducting Shikoku Basin crust can be classified into three provinces depending on the morphology of the basement relief and tectonic settings. Irregularities in the basement relief (> 1500 m) of the Central Province are 3-5 times larger than those in the Western and Eastern Provinces. The basement topography in the Eastern Province is characterized by relatively rough geometry (< 600 m in average), more than the Western Province (< 200 - 400 m). The Western Province represents a wide area of smooth basement relief associated with low-amplitude, less lineation, and long wavelength that leads to low variations in the incoming sediment heterogeneity.
- 2) The basement depth and total sediment thickness are linearly related because turbidites are channeled into basement lows, thus increasing sediment thickness in the lows at the expense of the basement highs.
- 3) Four distinct classes of sediments are recognized on the subducting Shikoku Basin

crust. The classes, distinguished on the basis of the sediment thickness and type within the LSB sequence, allow us to delineate local (~5-20 km) sediment variations. Within the LSB sequence, we classify two subunits (LSB-t1 & LSB-t2) that reflect regional variations in the pathways of turbidity currents. Locations of onlap are likely overpressured at the top of the LSB-T unit. The turbidites are generally absent where the basement highs have relief exceeding 500-600 m, except over Kashinosaki Knoll, which has a relatively shallow dip on its landward margin, allowing the turbidites to climb up towards its flank.

ACKNOWLEDGEMENTS

We thank the Captain and crew of the R/V Kaiyo for assistance in obtaining the seismic reflection data presented in this paper. We thank Mike Underwood for discussions and a critical review of an earlier review of this manuscript. We greatly appreciate JAMSTEC for providing seismic data. This work was supported by the US National Science Foundation through grants OCE-0137224 and EAR-0505789

TABLE

Table 2.1 Seismic Reflection Data Acquisition and Processing Parameters

Acquisition Parameters

Survey initial	ODKM	ODKM	KR
Survey vessel	R/V <i>Kaiyo</i>	M/V <i>Polar Princess</i>	R/V <i>Kairei</i>
Recording year	2003-2004	2003	~2001
Seismic source	One GI gun	Tuned air-gun array	Non-tuned air-gun array
Gun volume, l, in ³	5.7, 350	70, 4240	~196, ~12,000
Shot interval, m	25	50	50
Number of channels	18	480	~156
Channel interval, m	25	12.5	25

Processing sequence

Bandpass Filter (12-24-100-150Hz)	Spiking Deconvolution	Bandpass Filter (3-5-100-120Hz)
Spiking/Predictive deconvolution	Bandpass Filter (8-12-72-80Hz)	Deconvolution
Spike & Noise Edit	Velocity analysis	Velocity analysis
Velocity analysis	Dip moveout correction (DMO)	Normal moveout correction (NMO)
NMO	NMO	Mute
Mute	Mute	Stack (by JAMSTEC)
Stack	Stack	F-K time migration
F-K time migration	F-K time migration	Depth conversion
Depth conversion	Depth conversion	

FIGURES

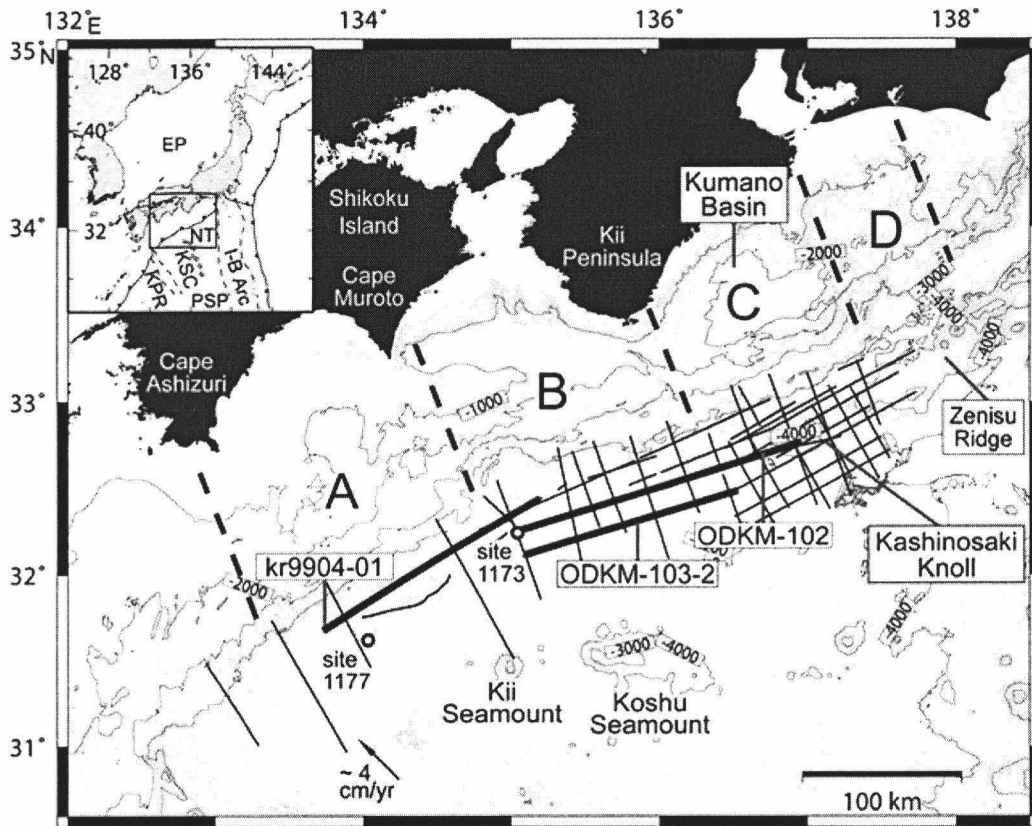


Fig. 2.1

Regional bathymetric map showing the location of the seismic lines (solid lines) used in this study. Solid bold lines are the track of the seismic sections presented in this paper (Fig. 6-8). Contour intervals are 1000 m (bold) and 200 m (fine). The heavy dashed lines are the boundaries between earthquake segments A-D defined by Ando (1975), indicating the units of megathrust rupture along the Nankai Trough. Insert box is showing the tectonic map of the Philippine Sea Plate (PSP), and Japan Arcs. EP: Eurasian Plate, I-B Arc: Izu-Bonin Arc, KSC: Kinan Seamount Chain, KPR: Kyushu-Palau Ridge.

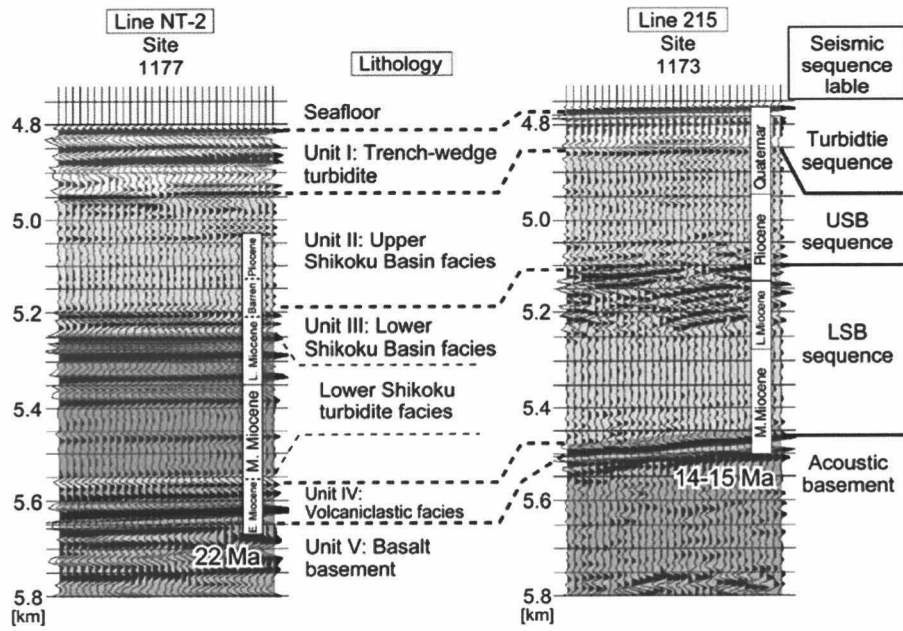


Fig. 2.2

Seismic stratigraphy of the Shikoku Basin sediments (scale in km) correlated with stratigraphy at ODP sites 1173 and 1177.

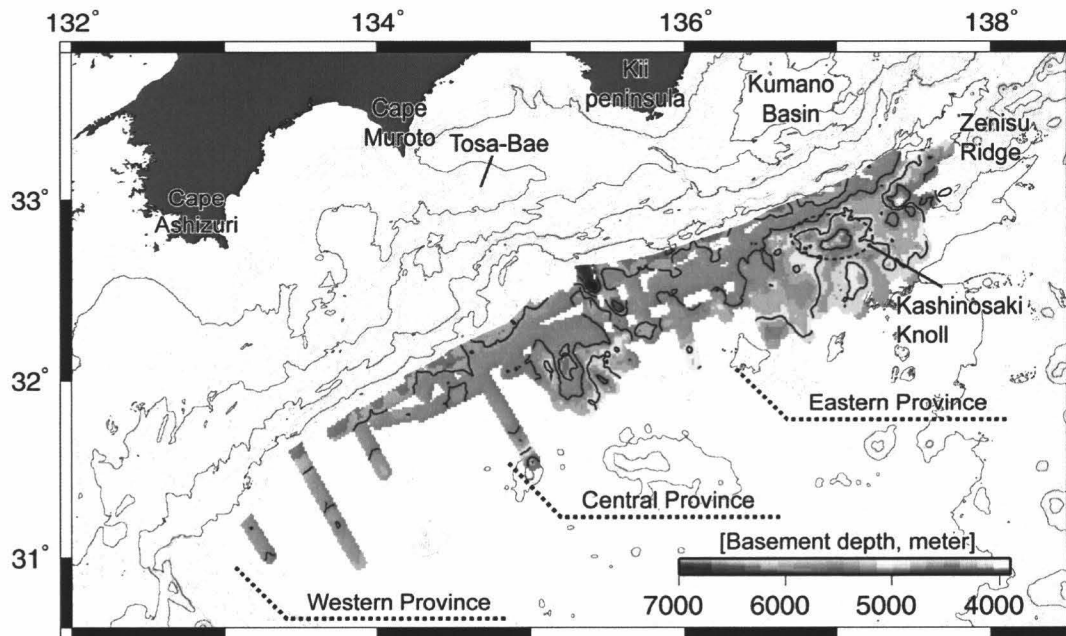


Fig. 2.3

Basement depth contour map based on the interpretation of seismic reflection data shown in Fig.1. A color scale for each isopach is shown at the bottom right of the figure. Within the colored isopach, solid lines are the thickness contour with 500 m interval.

Bathymetric map shown in the background has contour intervals of 1000 m (bold) and 200 m (fine). Regional basement/sediment provinces also shown. KK: Kashinosaki Knoll, ZR: Zenisu Ridge

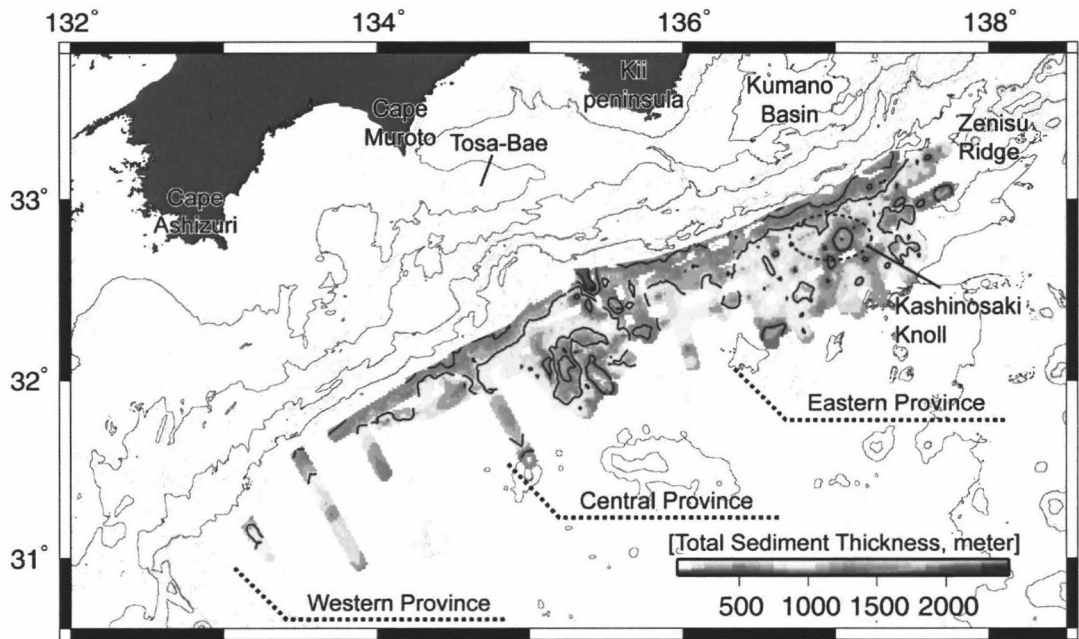


Fig. 2.4

Total sediment isopach map along the northern Shikoku Basin. A color scale for each isopach is shown at the bottom right of the figure. Within the colored isopach, solid lines are the thickness contour with 500 m interval. Bathymetric map shown in the background has a 200 m contour interval. KK: Kashinosaki Knoll, ZR: Zenisu Ridge.

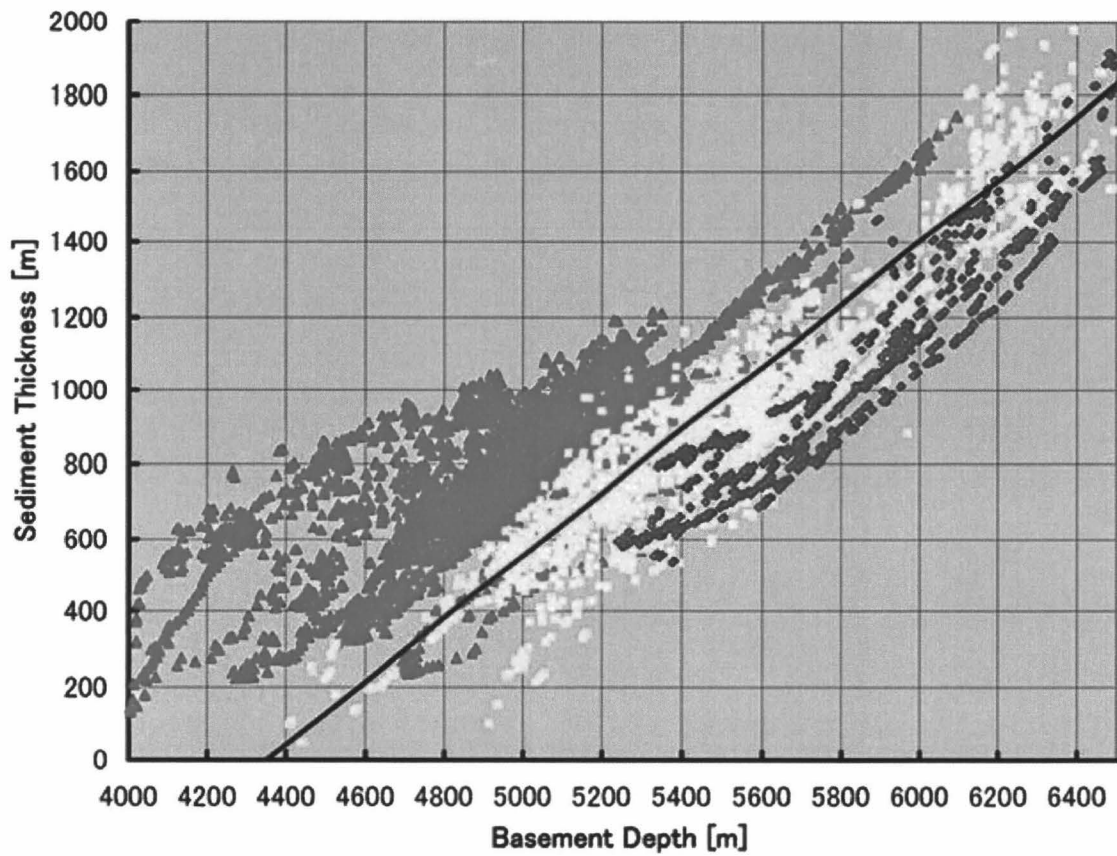


Fig. 2.5

Total sediment thickness vs. Basement depth, in the Western (blue), Central (yellow), and Eastern (red) Provinces of the Shikoku Basin. The black line indicates the best fit for the central (yellow) part.

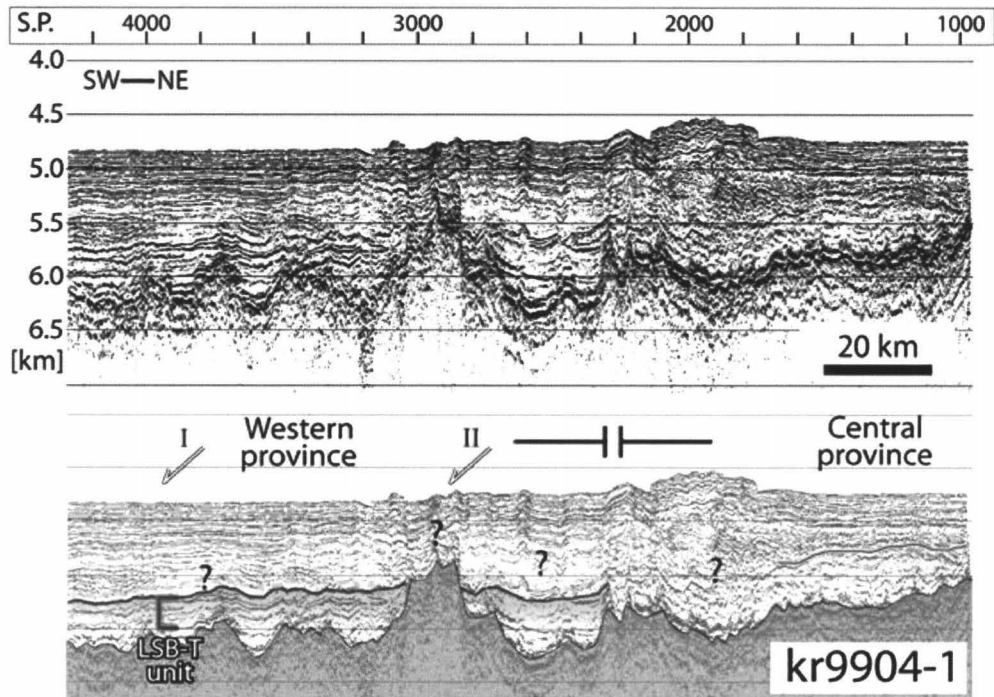


Fig. 2.6

Upper: Seismic depth section kr9904-01. Lower: Interpreted seismic stratigraphy. Vertical axis is depth in km. S.P = Shot Point, interval = 50 m. Vertical exaggeration is ~20 x.

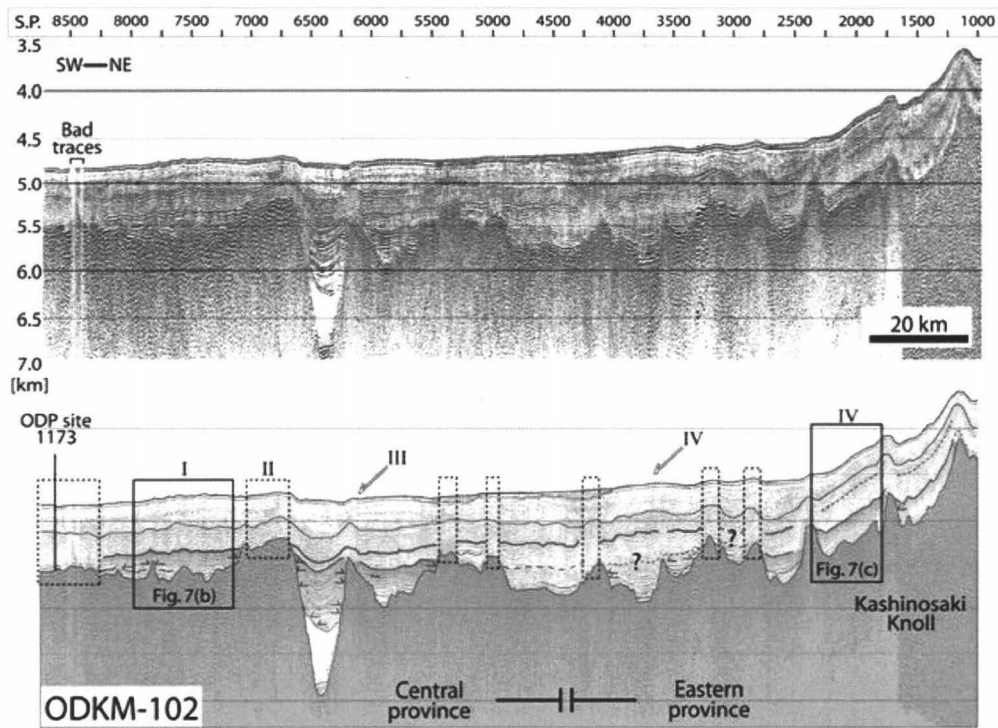


Fig. 2.7(a)

Upper: Seismic depth section ODKM-102 that crosses through site 1173 and Kashinosaki Knoll showing along strike variations of basement topography associated with sediment thickness and type. Lower: Interpretation showing stratigraphic boundaries. Small black-colored arrows indicate onlap structure. Arabic numbers correlate with the sediment sequence classes. Vertical axis is depth (km). S.P = Shot Point, interval = 25 m. Vertical exaggeration is ~20 x.

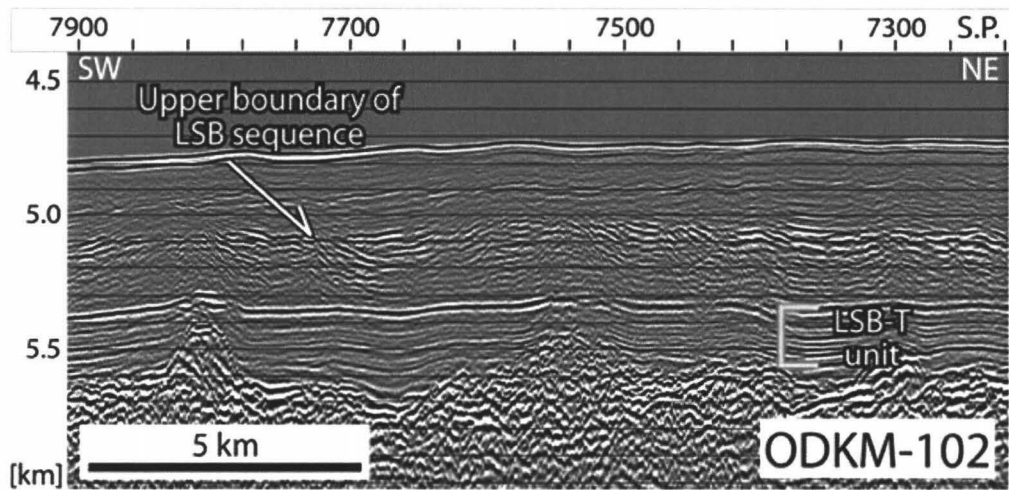


Fig. 2.7(b)

Enlarged seismic depth section ODKM-102 between S.P. 7220-7900 showing the relationship between the relative basement low and sediment sequences of Class I. Vertical exaggeration is 5 x.

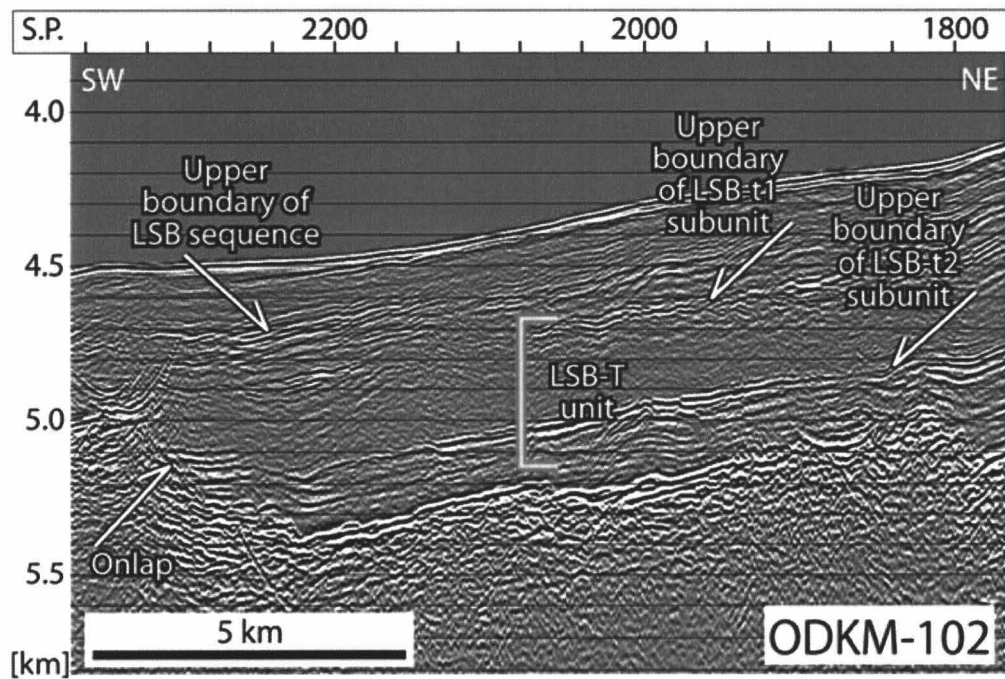


Fig. 2.7(c)

Enlarged seismic depth section ODKM-102 between S.P. 1800-2360 showing the relationship between the basement relief and sediment sequence of Class IV. Vertical exaggeration is ~5 x.

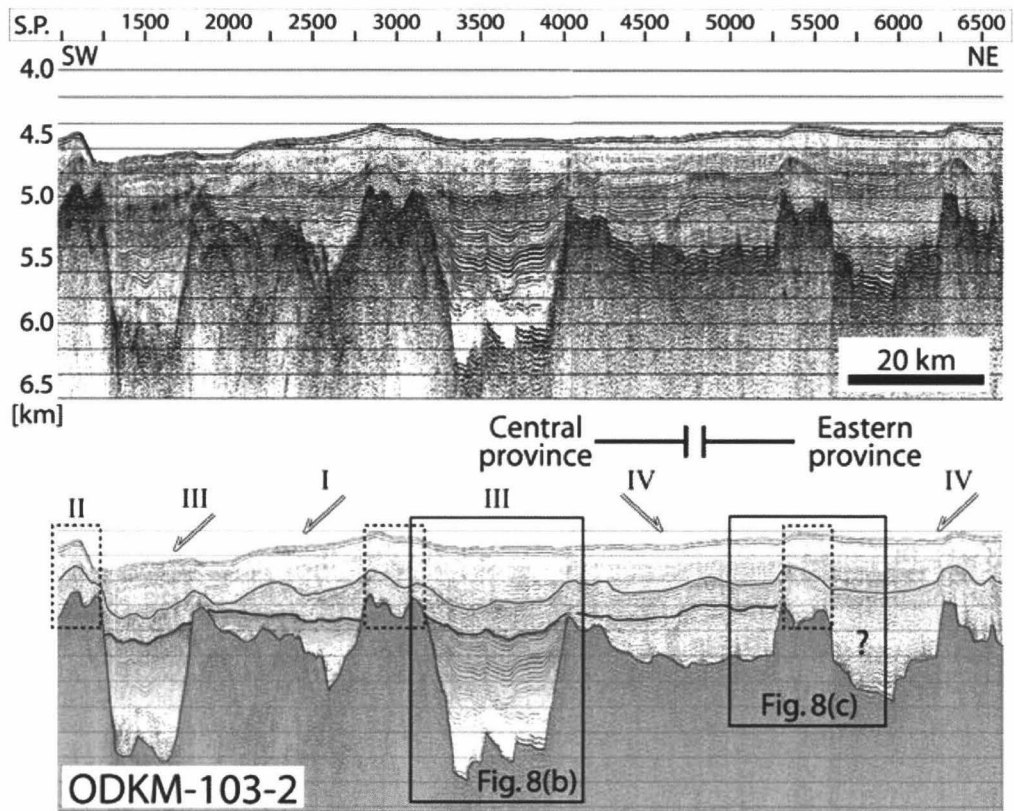


Fig. 2.8(a)

Upper: Seismic depth section ODKM-103 that runs near ODP site 1177 in the Western Province of Shikoku Basin, along the Nankai Trough. Lower: Interpretation showing regional stratigraphic boundaries. Vertical axis is depth in km. S.P = Shot Point, interval = 25 m. Vertical exaggeration is ~20 x. Arabic numbers correlate with the sediment sequence classes.

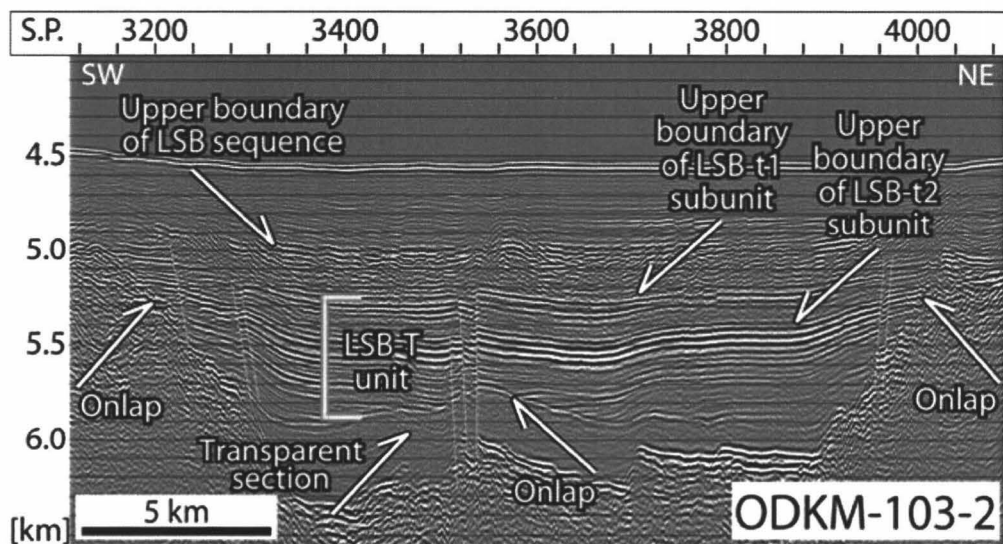


Fig. 2.8(b)

Enlarged seismic depth section ODKM-103-2 between S.P. 3120-4080 showing the relationship between the basement low and sediment sequences of Class III. Vertical exaggeration is ~5 x.

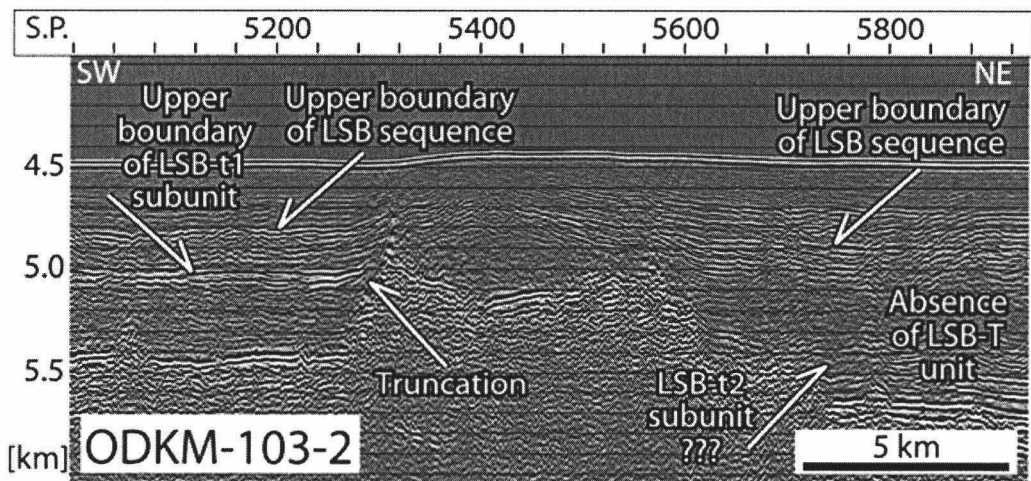


Fig. 2.8(c)

Enlarged seismic depth section ODKM-103-2 between S.P. 5000-5920 showing the relationship between the basement relief and sediment sequence of Class II & IV. Vertical exaggeration is ~5 x.

Chapter III

TECTONICS AND SEDIMENTATION AROUND KASHINOSAKI KNOLL:

A SUBDUCTING BASEMENT HIGH IN THE EASTERN NANKAI TROUGH

TOSHIHIRO. IKE^{1,*}, GREGORY.F. MOORE^{1,2}, TADASHI. OKANO², SHIN'ICHI.
KURAMOTO², JIN-OH. PARK^{3,4}, YOSHIYUKI. KANEDA³, ASAHIKO. TAIRA²

¹ Department of Geology and Geophysics, University of Hawai'i, Honolulu, HI 96822,
USA

² Center for Deep Earth Exploration, JAMSTEC, Yokohama, Kanagawa, 236-0001, Japan

³ Institute for Frontier Research on Earth Evolution, JAMSTEC, Yokohama, Kanagawa
237-0001, Japan

⁴ Now at Ocean Research Institute, University of Tokyo, Nakano, Tokyo, 164-8639,
Japan

* Correspondence: IFREE, 3173-25 Showa-machi, Kanazawa-ku, Yokohama, Kanagawa,
236-0001, Japan

Email: tike@hawaii.edu

Phone: +81-45-778-5433

To be Submitted to Island Arc

Abstract

When seamounts and other topographic highs on an oceanic plate are subducted, they can cause significant deformation of the overriding plate and may act as asperities when carried into the seismogenic zone. Kashinosaki Knoll (KK) is an isolated basement high of volcanic origin on the subducting Philippine Sea plate that will soon be carried into the eastern Nankai Trough. Multi-channel seismic imaging reveals a thick accumulation of sediments, up to 1200 m, over the knoll. The lower portion of the sedimentary section is characterized by a package of high amplitude continuous reflections (LSB-T subunit) that lap onto steep basement slopes ($\sim 20\text{-}30^\circ$) but are parallel to the gentle basement slopes ($\sim 5\text{-}10^\circ$). Total sediment thickness on the western and northern slopes is approximately 40-50 % more than on the summit and southeastern slopes of KK. These characteristics imply that the basal sedimentary section northwest of KK was deposited by infrequent high-energy turbidity currents in the Miocene, whereas the area southeast of KK was dominated by hemi-pelagic sedimentation over asymmetric basement relief. From the sediment structure and magnetic anomalies, we estimate that the knoll likely formed near the spreading center of the Shikoku Basin in the early Miocene. Its origin differs from that of the nearby Zenisu Ridge, which is an echelon seamount chain related

to Izu-Bonin back-arc volcanism. As KK is carried into the Nankai Trough, it is deflecting Quaternary trench turbidites towards the southern side of the knoll. When KK is carried into contact with the accretionary prism in a million years, it will strongly deform the prism, likely causing a large slope failure and leaving a large embayment in the prism, similar to the Tosa-bae embayment just to the west. The thick sediment deposited on KK may be detached and contribute to a quick rebuilt of the accretionary prism. The rough topography of the knoll may affect the seismogenic zone as an asperity as it is subducted deeper beneath the prism.

INTRODUCTION

The subduction of seamounts, fracture zones and aseismic ridges at convergent margins causes significant deformation of the overriding plate (Cadet *et al.* 1987; Kobayashi *et al.* 1987; McCann & Habermann 1989; Dominguez *et al.* 2000; Kodaira *et al.* 2000; von Huene *et al.* 2000; Taylor *et al.* 2005). At margins with voluminous trench sediment supply, the introduction of these topographic highs into the trench disrupts the normal flow of trench turbidites, causing significant along-strike variations in sediment thickness and type entering the subduction zone (Underwood *et al.* 1993; Alexander & Morris

1994). This in turn leads to potential lateral variations in pore fluid pressure that can further affect accretionary processes (e.g. Saffer & Bekins 2002; Spinelli & Underwood 2004). Moreover, these bathymetric features are likely to act as asperities when they are carried to deeper levels of the subduction zone (Cloos & Shreve 1996; Scholz & Small 1997).

The Nankai Trough, south of Japan, is the site of on-going seamount subduction, as evidenced by several large and small embayments in the fore-arc (Okino & Kato 1995). The largest of these, the Tosa-bae embayment is directly in line with the Kinan Seamount chain on the subducting Philippine Sea plate (PSP; Yamazaki & Okamura 1989), and a subducted seamount in this region has been identified (Kodaira *et al.* 2000). Collision of the Zenisu Ridge (ZR) and paleo-Zenisu Ridge has caused massive modification to the Nankai accretionary prism, farther to the NE (Le Pichon *et al.* 1987). South of Kumano Basin, there is a large seamount, Kashino Knoll (KK) that is just about to enter the subduction zone. This seamount has been interpreted to be part of the ZR complex farther to the northeast (Aoki *et al.* 1982; Lallemand *et al.* 1989), but it may be an isolated seamount not connected to any other ridges.

As part of the Nankai Trough Seismogenic Zone Experiment (NanTroSEIZE), we

recently collected many new seismic reflection lines and swath bathymetric data to formulate a better understanding of the structures in the initial stages of subduction offshore Kumano Basin. Here we present an analysis of those data sets aimed at defining the structure of KK and its sediment cover. We have also utilized free-air gravity and magnetic anomaly data that supply important constraints on basement structure and its age of formation (Geological Survey of Japan 2000). Our main objectives are to document the tectonic history, structural characteristics and associated sedimentary facies of KK, a subducting bathymetric high that will soon strongly deform the Nankai accretionary prism as it is subducted.

GEOLOGIC SETTING

The Nankai Trough is the convergent boundary between the subducting PSP and the overriding Eurasian plate (Fig. 3.1a). The subduction rate varies along the Nankai Trough, from ~5 cm/year in the western part of the study area (52°W) to ~4 cm/year in the east (48°W; Seno *et al.* 1993). Changes in volcanic activity in western Japan have been used to suggest that subduction was very slow (less than 1 cm/yr) from 12-4 Ma, and increased to ~4-5 cm/yr at about 4 Ma (Taira 2001; Kimura *et al.* 2005). Large

amounts of terrigenous sediments are presently being channeled down the trench axis from the Izu-Bonin collision zone along the Suruga Trough into the Nankai Trough (De Rosa *et al.* 1986; Taira & Niitsuma 1986; Aoike 1999).

The basement structure of Shikoku Basin, the northern part of the PSP, was formed by complex back-arc spreading in the Izu-Bonin island arc (Kobayashi & Nakada 1978; Nakamura *et al.* 1984; Hibbard & Karig 1990; Okino *et al.* 1994). Major spreading stopped around 15 Ma (Okino *et al.* 1994; 1999), but late-stage rifting may have continued until 7-10 Ma with associated volcanism that formed the Kinan Seamount Chain (Chamot-Rooke *et al.* 1987; Ishii *et al.* 2000).

Magnetic anomalies in the northern Shikoku Basin trend dominantly N to NNW (Fig. 3.1b), reflecting the sea-floor spreading history (Kobayashi *et al.* 1995). Lineated magnetic anomalies in the western half of Shikoku Basin clearly correlate with magnetic anomalies 6 to 7, but the anomalies in the eastern basin are less distinct and their correlations less certain (Okino *et al.* 1999). An axial zone of NW-trending magnetic anomaly 5b-5d reflects the late Miocene reorientation of the back-arc spreading center (Okino *et al.* 1994).

The free-air gravity anomalies generally trend parallel to the trench (Fig. 3.1c).

Positive anomalies are centered over the SW Japan arc and the fore-arc ridge, whereas negative anomalies are centered along the fore-arc basin and the trench. The free-air anomalies seaward of the Nankai Trough are generally low (Fig. 3.1c), with the exception of positive anomalies over bathymetric highs such as KK, ZR and NE-trending volcanic cross-chains of the Izu-Bonin arc system (Kaizuka, 1975). We note that a negative gravity anomaly separates KK from ZR.

DATA ACQUISITION AND PROCESSING

SEISMIC REFLECTION DATA

We used three multi-channel seismic reflection data sets (Table 2.1) collected by the Japan Agency for Marine-Earth Science and Technology (JAMSTEC) over the eastern Nankai Trough and NE Shikoku Basin. The first data set was collected from 1997 to 2001 on R/V *Kairei* using a variety of sound sources and multi-channel streamers. For data acquisition during the 1997 cruises, an air-gun array of 50 L (3080 in³) was used as the sound source and a 120-channel streamer (25 m group interval) was used as the receiver. During the 2001 cruises, a 156-channel steamer and an untuned 196 L (~12,000 in³) airgun array was used as the sound source. Initial processing through

stack for these lines was completed by JAMSTEC. We applied a second phase of advanced processing, including post-stack time migration and depth conversion. The second data set was collected by a commercial contractor in the spring of 2003 using a 480-channel steamer and a tuned 70 L (4240 in³) airgun array as the sound source (Taira *et al.* 2005). We processed several of these lines through stack and post-stack time migration, and performed Pre-stack Depth Migration (PSDM) on lines ODKM-22 and ODKM-B. The third data set was collected on the R/V *Kaiyo* in December 2003 - January 2004 using an 18-channel streamer and a single 5 L (355 in³) generator-injector (GI) gun as the sound source. We have also processed these lines through stack and post-stack time migration. We developed a velocity model based on the PSDM velocity field from ODKM-22 and ODKM-B and used these velocities for depth conversion of the other seismic lines. In areas where topography is relatively flat, we used a sediment velocity model of 1510 m/sec at the seafloor with a gradient of 0.65 km/sec² with increasing two-way travel time. We used a lower velocity gradient over KK (0.55 km/sec²).

BATHYMETRY DATA

Multibeam bathymetry data were collected with the SeaBeam 2112 systems on the JAMSTEC vessels *Kairei* and *Yokosuka* (Fig. 3.2a). Post-processing consisted of editing the cross track and navigation data and gridding using the MB-System software (Caress & Chayes, 1996). The data were gridded with 100 x 100 m grid size and were merged with the regional satellite bathymetry data set of Sandwell and Smith (1997). We used the GMT function called 'grdgradient' to emphasize the knoll's slope structures (Wessel & Smith 1995). This function outputs the scalar magnitude of gradient vectors for each slope obtained from bathymetric data. Subsequently, we converted the outputs of slope angle from radians to degrees and then used 'grdimage' to create a color-coded image of the slope angle along with the bathymetric contours (Fig. 3.2b).

STRUCTURAL CHARACTER OF KASHINOSAKI KNOLL

OCEAN FLOOR MORPHOLOGY

Kashinosaki Knoll is approximately 30 x 40 km, forming a rectangular body that is elongated to the NNE (Fig. 3.2a). The knoll is bathymetrically separated from ZR by a 25 km wide flat plain (Fig. 3.1a). The knoll's summit, approximately 40 km south from the trench landward slope, is characterized by four ridges separated by narrow valleys: an

ENE-trending ridge located on the northwest side of the knoll, with depth ranging from 3.9-4.5 km; a pair of NW-trending ridges on the southwest side, with depth ranging from 4.0-4.5 km; and a crescent-shaped ridge, forming the summit of KK that is ~600 m higher than the adjacent flat seafloor (Fig. 3.2b). Each ridge is undissected and lacks volcanic morphologies such as craters or cones.

The gentle north-dipping bathymetric slope on the eastern side of the crescent ridge is cut by two major NE-trending scarps. The southern slope of the crescent-shaped ridge has a steep landslide scarp that dips ~10-20° south, and has a slump block at its flank. The pair of NW-trending ridges has smooth western slopes of ~7°. The northern slope of KK is ~12° on the western half along the ENE-trending ridge, and ~3° on the eastern half. North of KK, there is a narrow trench ridge ~18 km long, ~1 km wide and ~50 m high, located at the edge of the trench. It trends roughly east-west, and its western edge terminates near the trench axial channel.

FREE-AIR GRAVITY AND MAGNETIC ANOMALIES

Magnetic anomalies trend NNW-SSE across the western flank of KK, and magnetic anomaly 6 (19-20.5 Ma) is parallel to the knoll just to the west (Kido & Fujiwara, 2004)

(Fig. 3.1b). Over the summit, there is a dipolar anomaly that is positive (~ 100 nT) on the SW and negative (~ -200 nT) on the NE (Fig. 3.1b). The orientation and intensity of the magnetic anomaly on the knoll are distinct from that observed over ZR. The positive amplitude of the anomaly over ZR is more than ~ 50 nT higher than over KK. Along ZR, the trend of magnetic anomalies is dominantly NE-SW on its east, with positive on the SSE and negative on the NNW. The anomalies extend towards the SW, likely overprinting the anomalies related to the back-arc spreading of the northern Shikoku Basin (Chamot-Rooke *et al.* 1987). Seafloor spreading magnetic anomalies indicate that the crustal age across the south part of ZR is 22 to 24 Ma (anomalies 6B and 6C) (Lallemant *et al.* 1989). We interpret magnetic anomaly 6A (20.55 Ma) crossing Kashinosaki Knoll (Brian Taylor, personal communication, 2006).

The free-air gravity anomaly also indicates differences between KK and ZR (Fig. 3.1c). KK and ZR both have positive anomalies; however, these two features are separated by an area of negative anomaly. The positive anomaly over KK is circular and 30-80 mGal lower than that over ZR that is more elliptical. The positive anomaly over ZR is surrounded by negative anomalies (~ -50 mGal) on its north and south. The anomaly increases to about -20 mGal north of KK and it decreases towards the southwest.

The lineation of the negative anomaly south of ZR does not extend south of KK. The high amplitude negative anomaly separates KK and ZR, indicating a significant separating on volcanic structure. The high amplitude negative anomaly on the southern side of KK is missing.

SEISMIC STRATIGRAPHY

Seismic stratigraphic sequences, defined in the western and central Nankai Trough off Shikoku Island, have been sampled by ocean drilling (Karig *et al.* 1975; Taira *et al.* 1991; Moore *et al.* 2001). We define three major seismic stratigraphic sequences above the acoustic basement: 1) lower Shikoku Basin (LSB) sequence and its subunit (Miocene turbidites; LSB-T); 2) upper Shikoku Basin (USB) sequence; and 3) Quaternary turbidite sequences. These sequences are correlated with the key lithostratigraphic units defined at the ODP Legs 131 and 190 drill sites (Fig. 3.3a). Seismic line ODKM-102 crosses over ODP Site 1173 and runs parallel to the Nankai Trough axis, allowing us to extrapolate the seismic sequences defined at the drill site into our study area south of Kumano Basin (Ike *et al. in prep.*).

The oldest unit, the LSB sequence, overlies a thin drape of volcanoclastic sediments

above the basement. It is characterized by low amplitude reflections in the lower section, and relatively high amplitude, discontinuous to moderately-continuous hummocky reflections at its upper boundary (Fig. 3.3a). This sequence is correlated with the middle Miocene to lower Pliocene hemipelagic mudstones sampled at the ODP drill sites. We interpret high amplitude, laterally continuous reflections within the LSB sequence as a subunit (LSB-T) that correlates with turbidite sands recovered at ODP site 1177 (Moore *et al.* 2001). In some areas, this subunit also shows relatively low amplitude discontinuous reflections. The probable source of these turbidites is suggested to be southwestern Japan, the inner zone of Shikoku Island, with delivery of sediment across the trench and out onto the Shikoku Basin floor (Fergusson, 2003).

The second sequence, the USB sequence is characterized by low amplitude, moderately-continuous reflections, and abundance of ash layers. Its lower boundary is controlled in part by the diagenetic breakdown of ash layers in the lower unit (Taira *et al.* 1991; Moore *et al.* 2001). The third and youngest seismic sequence, another turbidite unit, exhibits laterally continuous and high amplitude reflections that lap onto the USB sequence. It is correlated with the “trench facies” at the ODP sites, although the distribution of Quaternary turbidites in our study area is not restricted to the morphologic

trench.

BASEMENT STRUCTURE OF KASHINOSAKI KNOLL AND ITS SURROUNDINGS

Seismic profiles reveal that the basement summit of KK does not directly underlie the seafloor summit (Fig. 3.3b, 3.4a). Comparing the morphology of this basement with seamounts that are located close to active margins, KK is as high as the conical seamounts and as wide as the flat topped seamounts studied by Dominguez et al., 1998 (Fig. 3.4b). At the seafloor summit of KK's Crescent Ridge, there is a basement peak that is 4 km below sea level, but the basement summit is approximately 8 km to the east from the knoll's bathymetric peak (Fig. 3.4a, 3.5). Between these two basement peaks towards the northern slope of KK, there is a NS-trending basement depression that is not present in the bathymetry. The maximum depth of this depression is ~250-300 m near the summit of KK, and it decreases towards the north. The basement slope landward of KK is ~5-15°, while the seaward slope of the knoll is ~20-30° (Fig. 3.5).

At a local scale, there are two isolated basement highs (IBH) with little or no bathymetric expression, one on the western flank of KK (Fig. 3.3b, 3.4a), and another on the southwestern flank (Fig. 3.3b, 3.6). These basement highs have three characteristics

in common: a diameter that is approximately 5 km at their base; a peak ~600 m higher than the adjacent basement, and a basement slope up to 20°. The overlying sediment thickness ranges from ~200-400 m over the peaks, and increases away from the peaks.

We note that the IBHs are too small to overprint the NS-trending magnetic anomalies that cross KK.

In other parts of KK, there are basement structures that are present in the bathymetric trends. The basement structure on the eastern side of KK is generally parallel to the bathymetry except over the two NE-trending scarps (Fig. 3.4a, S.P. 1860 and 2000). For instance, over the basement summit, the total sediment thickness decreases from ~550 m near the bathymetric summit of KK to ~200 m above the basement summit (Fig. 3.4a, S.P. 1860). Towards the east, the sediment thickness between S.P. 1860-2000 is ~500 m, and it decreases to ~200 m at the scarp. To the west from the summit of KK, the basement structure beneath the pair of NW-trending ridges is relatively planar, with a ~5° slope that generally dips towards the west (Fig. 3.3b).

Basement relief around KK is also very complicated. The basement highs trend roughly perpendicular to the trench; seismic lines parallel to the trench axis show long wavelength and high amplitude basement features (Fig. 3.7), whereas lines perpendicular

to the trench do not show high amplitude basement relief (Fig. 3.8). The amplitude of the short-wavelength basement relief parallel to the trench between KK and the trench is 200 m to the northwest of KK, and increases to 500 m northeast of the knoll (Fig. 3.7).

Along the west side of KK, there are several short-wavelength and low-amplitude basement highs (Fig. 3.8). The basement relief in this area is generally subdued compared with other areas. The basement relief on the south side of KK has a wavelength of ~25-30 km (Fig. 3.9). The amplitude of the basement relief (~500 m) in this area is similar to that north of the knoll.

The trench-perpendicular line shows undulation in the basement relief between KK and ZR. The relief is lineated parallel to the trench axis with a wavelength of ~5 km and amplitude of ~400 m on the northern half, and a wavelength of ~10 km and amplitude of ~250 m on the southern half (Fig. 3.10).

SEDIMENTATION PATTERNS OVER AND AROUND KASHINOSAKI KNOLL

Our seismic profiles clearly image variations in sediment thickness and type that are controlled by the basement structure of KK (Fig. 3.11). The total sediment thickness around KK ranges from ~300 to 1600 m. The maximum thickness occurs along the

trench axis and between KK and ZR (Fig. 3.10). The minimum thickness, less than 300 m, occurs over the basement summit of KK (Fig. 3.4a). Within our study area, the average total sediment thickness over KK is approximately 40-50 % more on the western and northern slopes than that at the summit, southeastern slopes and over IBHs where the basement slope is steep ($\sim 20^\circ$) (Fig. 3.11). At a local scale, the total sediment thickness along the western slope of KK ranges from 850 to 1000 m, and is nearly constant along the gentle basement slope and towards the west (Fig. 3.4a, 3.6). Northwest of KK, the graben along the NW-trending ridge has 15-20 % more sediments than the adjacent horst (Fig. 3.6). At the summit of KK, the total sediment thickness is approximately 590 m and it decreases towards the eastern slope. To the south, the southern flank of KK has sediment thickness similar to that over the summit (Fig. 3.5). Sediment thickness increases in parallel with the increase of the basement depth towards the south (Fig. 3.5, 9). In this area, the reflections within each seismic sequence show similar patterns with the west side of KK, such as the continuous and discontinuous reflections within the LSB-T subunit (Fig. 3.5, S.P. 1210-1650).

LSB Sequence

The depth variation in the upper boundary of the LSB sequence shows a positive correlation with seafloor depth, i.e., the LSB sequence is thicker in the basement lows than over the basement highs. The thickness of the LSB sequence is roughly 60 % of the total sediment thickness; however, this does not apply where the LSB-T subunit is absent, and where the deposition of the Quaternary turbidite occurs. The thickness of the LSB sequence is more than 500-600 m where the LSB-T subunit appears in the sediment sequence, whereas it is less than ~400 m where the LSB-T subunit is absent or poorly defined. In detail, the thickness of the LSB sequence is approximately 350 m at the bathymetric summit of KK, and it is less than 200 m over its basement summit to the east (Fig. 3.4a). To the southwest, over the pair of NW-trending ridges, its thickness is approximately 500 m except for the areas over IBH where its thickness is less than ~250 m (Fig. 3.6). To the northwest, over the ENE-trending ridge, its thickness is ~600 m over the horst and ~800-850 m within the graben (Fig. 3.5, 3.6).

LSB-T Subunit

The distribution of the LSB-T subunit represents the major pathways of turbidity currents delivered in the early Miocene (Fig. 3.11). The LSB-T subunit clearly appears along the

northern slopes of KK including the ENE-trending ridge located on the northwest (Fig. 3.5). There is generally a section (~100 m) of low amplitude reflections, underneath the LSB-T subunit, that drapes over the basement (e.g. Fig. 3.4a, 3.5), but this subunit is locally absent over steep basement slopes. The thickness of the LSB-T subunit ranges from ~100-250 m; however, its seismic character is disturbed where the basement's slope is steep across a horst and graben. To the southwest, at the pair of NW-trending ridges, the upper boundary of the LSB-T subunit is sub-parallel to the underlying basement relief (Fig. 3.4a). This subunit is characterized by thinning towards the summit of KK. The LSB-T subunit onlaps the basement around the IBHs on KK's flanks, but generally is parallel to basement slopes that are less than ~5-10°, such as on the northwestern area of KK (Fig. 3.4a, 3.6).

Reflection amplitude is relatively low and the internal structure is relatively horizontal on the eastern flank of KK where the slope is steep. On these steep slopes, the high amplitude reflections that characterize the LSB-T subunit are poorly defined or absent (Fig. 3.4a, S.P. 2000-2050). Similar relationships between the basement structure and the seismic character of the LSB-T subunit occur on the southern slope of KK where the steepest (~20°) basement slope correlates with the steep bathymetric slope (Fig. 3.2b,

3.5). The LSB-T subunit is also absent near the southern flank of KK.

Away from KK, the LSB-T subunit laps onto basement highs and fills basement lows (Fig. 3.7, S.P. 2600-3600). To the west, it has low amplitude discontinuous reflections (Fig. 3.7, S.P. 2300-2600). Within the LSB sequence in this area, but above the LSB-T subunit, there are high amplitude reflections suggestive of a channel and levee structure. This channel and levee structure also occurs near the relative basement high to the west in a similar depth (Fig. 3.7, S.P. 1600-1800). On the northwestern side of KK, the LSB-T subunit's reflections are parallel with the local basement high and become unclear towards the west underneath the trench sediments (Fig. 3.7, S.P. 1000-2200). There is a section (~100 m) of low amplitude reflections in between the LSB-T subunit and the basement (Fig. 3.7).

On the southwestern side of KK, the LSB-T subunit has high amplitude reflections in the upper half of the unit, although the reflection amplitudes decrease in the lower half. The LSB-T subunit is parallel with the basement relief and also laps onto local basement highs (Fig. 3.8, S.P. 2520-3300). To the south, the LSB-T subunit shows discontinuous low amplitude reflections over the basement relief (Fig. 3.8: S.P. 1000-2500). The low amplitude reflections within the LSB-T subunit clearly appear on the trench-parallel

seismic cross-line ODKM-104 (Fig. 3.9).

The LSB-T subunit clearly appears in basement lows on the southwest side of KK, and it is poorly defined over the basement highs towards the east. The thickness of the LSB-T subunit on the southwest side of KK is ~200 m and is roughly constant over the basement relief, similar to the northwestern slopes of the knoll. In detail, the thickness of the LSB-T subunit locally increases up to 400 m between S.P. 2300-2600 associated with eastward thinning (Fig. 3.9). The thinning is similar to the western (Fig. 3.4a, S.P. 1500-1650) and northeastern (Fig. 3.7, S.P. 3400-3600) slopes of KK in terms of its deposition against basement highs. To the east, over the relative basement high between S.P. 2800-3900, the LSB-T subunit is characterized by low amplitude discontinuous reflections, and its thickness is less than 100 m, similar to its character at the summit of KK (Fig. 3.9). The subunit is poorly defined or absent from S.P. 3900-4600, similar to areas along the eastern slope of KK.

USB Sequence

The USB sequence clearly appears over and around KK (Fig. 3.5 to 3.10). The internal reflections in the USB sequence have parallel relationship with the upper boundary of the

LSB sequence; however, they show low -amplitude reflections characterized by sub-parallel relationship over IBH. Around KK, the seismic character of the USB sequence shows relatively subdued and lower amplitude reflections compared with the upper boundary of the LSB sequence. The upper portion of the USB sequence has low amplitude reflections where they are not overlain by the Quaternary turbidites. The thickness variation in the USB sequence is roughly up to 40 % of the total sediment thickness over KK (~100-350 m). This trend holds on the northern and western slopes of KK; however, it is disrupted where the USB sequence is overlain by the Quaternary trench turbidites or where the total sediment thickness is less than ~400 m, such as over the IBH and near the basement summit similar to the LSB sequence (Fig. 3.4a, 3.6, 3.7).

Quaternary Turbidites

Overlying the USB sequence, the majority of the Quaternary turbidites accumulate around the knoll; such as along the trench, between KK and ZR, and partly on the southern side of KK towards the southwest filling the topographic lows (Fig. 3.7, 3.9).

The Quaternary turbidites are not deposited over KK (Fig. 3.4a).

Sediments between Kashinosaki Knoll and Zenisu Ridge

The seismic character of the LSB and USB sequences is different between KK and ZR than in other parts of the study area (Fig. 3.9, 3.10). The LSB sequence is dominated by low amplitude, discontinuous reflections that generally drape over the basement relief. Some reflections within the LSB sequence may be the candidates for the LSB-T subunit; however, we find that the LSB-T subunit in this area is usually isolated to structural lows (Fig. 3.10, S.P. 1000-2600). For instance, on line ODKM-100 at ~S.P. 4000, the LSB-T subunit is absent, whereas the subunit laps onto the basement high at ~S.P. 3500 (Fig. 3.7). Overlying the LSB sequence, the USB sequence is characterized by high amplitude continuous reflections that partially lap onto the upper boundary of the LSB sequence (Fig. 3.10, S.P. 2000-2350). The USB sequence in this area is characterized by high amplitude continuous reflections that are distinct from other areas. We define the upper boundary of the USB sequence by an unconformity at the lower boundary of the trench wedge turbidites. The unconformity is difficult to distinguish from other reflections towards the south, indicating that the young trench wedge sediments are transported not only along the trench but also out of the axial trench channel towards the south, between KK and ZR, and on the southern side of KK. In addition, within this

area, high angle normal faults displace all of the sediment sequences (Fig. 3.10). The dip angles of these faults range from 75 to 85 ° and offset the entire sediment column for 10-30 m. The geometry of these faults is not correlated with the basement relief. We do not find strong evidence for similar fault displacement on the west side of KK (Fig. 3.8).

DISCUSSION

THE ORIGIN OF KASHINOSAKI KNOLL

Our new bathymetric, seismic reflection and magnetic anomaly data provide insight into the origin of KK, and processes of sedimentation over and around this isolated topographic high in the eastern Nankai Trough. Several interrelated processes are responsible for shaping the present structure of the knoll: the location of its origin, variations in local sedimentation, and late stage normal faulting associated with basement deformation.

The high amplitude dipolar magnetic anomaly pattern observed over KK indicates that the knoll's origin is volcanic (Parker 1991). The amplitude of the dipolar anomaly over KK, which is of lower amplitude than that over the seamounts along the Izu-Bonin

arc, implies that the knoll is not affected by young volcanic intrusions that would superimpose their signal over the pre-existing magnetic anomaly. The lowest sedimentary unit, (LSB-T subunit) onlaps the basement flank of KK, indicating that the knoll was already in place before LSB-T sedimentation began. Therefore, KK must have been formed soon after the crust was formed by seafloor spreading in the middle Miocene (20-21 Ma). Given the age of the knoll and the estimated subduction rate (10 cm/yr during 17-12 Ma, 1 cm/yr during 12-4 Ma, 4 cm/yr during 4-0 Ma, Kimura *et al.* (2005)), the Knoll formed more than 700 km southeast of its present location and has been transported to the northwest by subduction of the Shikoku Basin beneath Japan (Fig. 3.12). The striking differences in the magnetic and gravity anomalies over KK and ZR, and the lack of continuity of anomalies between the two areas strongly suggest that the two features have different geologic origins (Fig. 3.1b, 3.1c). ZR is clearly related to the Izu-Bonin collision to the east (Le Pichon *et al.* 1987), whereas KK appears to be an isolated feature, contrary to previous interpretations that it is an extension of ZR (Lallemant *et al.* 1989).

However, KK's bathymetry and basement relief show an elongation parallel to the trench axis than cinder cone morphology. These observations may imply that the knoll

is not affected by single conduit volcanic intrusions that would form a cinder cone but also by multiple intrusions that are aligned parallel to the trench axis. The formation mechanism of KK may be affected by Izu-Bonin volcanism or pre-existing zone of weakness due to seafloor spreading.

EXTENSIONAL DEFORMATION OVER KASHINOSAKI KNOLL

Bathymetry data show two NE-trending scarps on the southeastern slope of KK. The apparent offset of these scarps is 250-300 m. Seismic profiles crossing these scarps show normal faulting displacement of the basement with ~500 m offset (Fig. 3.4a, S.P. 1880, 2050). The sediment layers between the two bathymetric scarps are nearly horizontal. Towards the east, the sediment package between KK and ZR shows normal faults that appear to cut through most of the deep as well as shallow sediments (Fig. 3.9, 3.10). Normal faults and large scale slumping are common on the flanks of most oceanic seamounts (e.g. Mitchell 2003; Morgan *et al.* 2003; Kerr *et al.* 2005). Given the proximity of KK to the trench outer slope, it is likely that the normal faulting was enhanced by bending stresses as the knoll approached the trench.

In contrast, previous authors have suggested that KK is the western extension of ZR

and that the north-dipping thrust fault underlying ZR continues westward under KK (Aoki *et al.* 1982; Le Pichon *et al.* 1987). If the effect of tectonic shortening occurs along ZR and continues over KK, then the reverse faults should also occur within the sediment package between KK and ZR. However, we only observe high-angle normal faults that cut the sediment package between KK and ZR (Fig. 3.9, 3.10). Therefore, the tectonic shortening affecting ZR probably does not extend westward to influence the deformation of KK. Indeed the high-resolution bathymetry (Fig. 3.1a) shows the thrust front ridges curving to the NW at the WSW end of ZR.

SEDIMENTATION OVER AND AROUND KASHINOSAKI KNOLL

The onlap of the LSB-T subunit onto IBHs and other relative basement highs indicates the basement relief of KK was reached by Miocene turbidity currents coming from Japan (Fig. 3.4a, 3.6, 3.9, 3.11). Turbidites from Shikoku are not currently able to reach very far out onto the Shikoku Basin because they are trapped either in the forearc basins, in small basins on the accretionary prism, or in the trench. Thus, the occurrence of the LSB-T subunit over the knoll suggests that the margin must have been very different in the Miocene, with no morphologic trench or forearc basins. There may be two scenarios

for having no morphologic trench; high sedimentation rate or shallow trench depth (Wdowinski, 1992). Both scenarios are consistent with the inference of extremely low subduction rates during this time (Kimura *et al.* 2005). The LSB-T subunit probably represents turbidites that flowed from Shikoku and western Honshu, filling topographic lows in the Shikoku Basin floor (Fergusson, 2003). Infrequent higher-energy flows may have climbed up the northwest-facing slope of KK as well (e.g., Muck & Underwood 1990; Ricci-Lucchi & Camerlenghi 1993).

Above the LSB-T subunit, high amplitude continuous reflections characteristic of turbidite deposits are absent in both the LSB and USB sequences north, south and west of KK. This observation is consistent with the inference of rejuvenation of Philippine Sea subduction in the late Miocene (Kimura *et al.* 2005). Accelerated subduction would have led to formation of the trench and rapid outbuilding of the accretionary prism and formation of forearc basins that would have inhibited flow of turbidity currents from Japan out onto the Shikoku Basin floor. Here we assume that the regional-scale outbuilding of the accretionary prism outpaces local sediment erosion caused by submarine canyons.

In the region between KK and ZR, the USB sequence exhibits high amplitude

continuous reflections characteristic of turbidite deposition (Fig. 3.9, 3.10). The thick accumulation of these turbidites indicate that they were not affected by the two scenarios presented above. We interpret the majority of these high amplitude reflections observed between KK and ZR to be turbidites that were sourced from the Izu-Bonin arc to the east. They are restricted to the regional low southeast of KK because the volume of flows was not great enough to fill the basin and flow around KK.

Quaternary deposits that overlie the LSB and USB sequences in the Nankai Trough are dominated by thick turbidites sourced from the Izu collision zone to the NE (e.g., Taira and Niitsuma, 1986; Fergusson, 2003), and spill-over from Tenryu-Canyon that forms a canyon-mouth fan superimposed on the axial-channel system (Soh et al., 1991). North and west of KK, these deposits form a classic trench wedge (Fig. 3.7, 3.8), similar to the wedge off Shikoku (Moore *et al.*, 2001). Similar deposits of thick Quaternary turbidites onlap the southern and eastern margins of KK (Fig. 3.9, 3.10) and also overlie the USB sequence east of KK (Fig. 3.7, 3.10). These observations suggest that KK's approach to the Nankai Trough partially dammed the path of Quaternary turbidity currents flowing along the trench axis, diverting part of the flow between KK and ZR onto the Shikoku Basin floor. The introduction of these topographic highs into the

trench disrupts the normal flow of trench turbidites, in turn leads to significant along-strike variations in sediment thickness and type entering the subduction zone, and towards the seismogenic zone.

SUBDUCTION OF BASEMENT HIGHS IN THE KUMANO AREA

Several models describe the deformation that accompanies subduction of topographic features like KK (e.g. Dominguez *et al.* 2000; von Huene *et al.* 2000). Following the analysis of Lallemand & Le Pichon (1987) for deformation due to a subducting seamount, we anticipate the generation of a large slump in the accretionary prism that will result in a wide embayment in the trench landward slope. The basement slope landward of KK is $\sim 5\text{-}15^\circ$ (Fig. 3.5), while the seaward slope of the knoll is $\sim 20\text{-}30^\circ$ ($\sim 15^\circ$ steeper than the landward side). Thus, as the accretionary prism rides up the knoll's landward flank, the décollement slope will increase, leading to rapid accretion of the sediment overlying the knoll. As the toe of the prism reaches the steep seaward slope of the knoll, it will be unsupported and will collapse. This would lead to a large embayment (approximately 70 km) that could be the square root of three times larger than the KK's (30 x 40 km) basal surface (Dominguez *et al.* 2000).

To the west, along the Kinan Seamount chain, a ~50 km wide and ~2.0 km high seamount is identified beneath the accretionary prism, 60-70 km landward from the Nankai Trough (Kodaira *et al.* 2000). This seamount subduction is associated with a bathymetric depression called the Tosa-bae embayment on the trench landward slope. The size of this seamount is similar to the size of KK, supporting our suggestion that a wide embayment will occur after subduction of KK.

In addition to the morphological effect of seamount subduction on the trench landward slope, our study suggests that subduction of seamounts is associated with the different materials, such as presence or absence of turbidites (LSB-T subunit), deposited on top of the seamount compared to the surrounding basement lows. As KK is carried deeper into the subduction zone, thick sediments deposited on the basement will likely be detached from KK (Dominguez *et al.*, 2000), and contribute to a quick seaward-rebuilt of the accretionary prism as well as the reaccreted sediments from the prism itself. These detached sediments may lead to a local friction difference due to terrigenous sand and hemipelagic clay along the subduction interface compared to nearby regions with smoother basement topography. These results may imply that the depth of the décollement may vary its depth as it migrates over the basement high. Such a frictional

anomaly may serve as an asperity within the seismogenic zone.

CONCLUSIONS

Analysis of regional seismic stratigraphic, magnetic and gravity data provide insight into the origin of Kashinosaki Knoll and its control on sedimentation in the eastern Nankai Trough. KK is a relatively old volcanic feature of the Shikoku Basin that was formed soon after the crust was generated well south of its present location in the early Miocene (Fig. 3.12). Hemipelagic sedimentation began immediately after the knoll's formation and continued throughout the Tertiary. In the early to mid-Miocene, subduction at the Nankai Trough slowed and the trench became filled with sediment. Turbidites fed from the Japanese island arc spread more than 700 km out onto the Shikoku Basin and reached the position of KK. Turbidites are present over gentle basement slopes ($\sim 5-10^\circ$) on the northern and western sides of KK, but they are absent on the southeastern side of the knoll which has relatively steep slopes ($\sim 20-30^\circ$). As the knoll was carried northwestward close to the Nankai Trough, it began to influence the trench sedimentary regime that has been carrying turbidites down the trench axis from the Izu collision zone in the northeast. Its high topography partially dammed the flow of Quaternary turbidites

down the trench axis, forcing the turbidites to flow southward out onto the Shikoku Basin.

The knoll is not a westward continuation of ZR and is cut by normal faults rather than the reverse faults that affect Zenisu. As it is carried beneath the accretionary prism, it will deform the seaward edge of the prism, leading to a large slump and embayment within the prism of width comparable to the Tosa-bae embayment to the west, and followed by a quick rebuilt of the accretionary prism.

ACKNOWLEDGEMENTS

We thank the Captain and crew of the R/V *Kaiyo* for assistance in obtaining the seismic reflection data presented in this paper. We thank Patrizia Costa Pisani for conducting the PSDM processing. We are grateful to our colleagues at the Univ. of Hawai'i for helpful discussions and for critical reviews of the manuscript, particularly by Brian Taylor. We greatly appreciate JAMSTEC for providing seismic data.

FIGURES

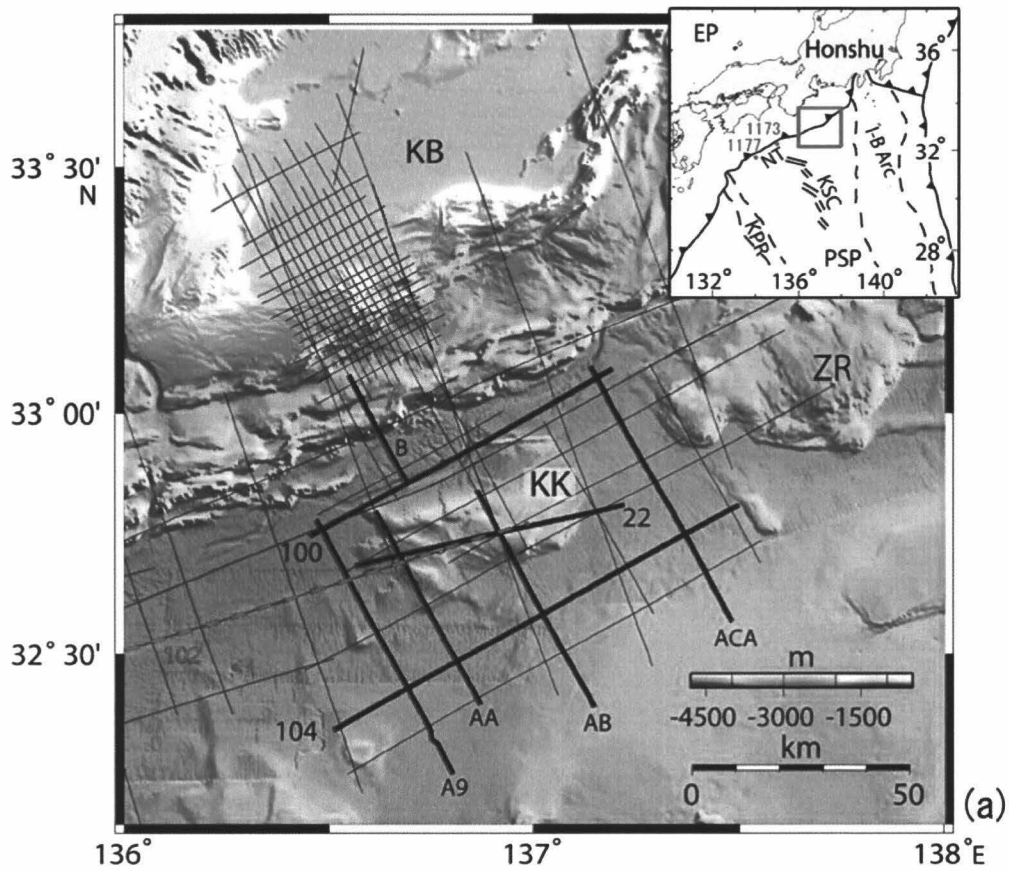


Fig. 3.1(a)

Regional bathymetric map showing the location of the seismic lines (initial-ODKM) used in this study. Solid bold lines are the track of the seismic lines presented in this paper (Fig. 4-8). Line B is used only to develop a velocity model. Insert box shows the tectonic map of the Philippine Sea Plate (PSP). EP: Eurasian Plate, I-B Arc: Izu-Bonin Arc, KB: Kumano Basin, KK: Kashinosaki Knoll, KSC: Kinan Seamount Chain, KPR: Kyushu-Palau Ridge, NT: Nankai Trough, ZR: Zenisu Ridge. Red circles show the location of ODP sites 1173 and 1177.

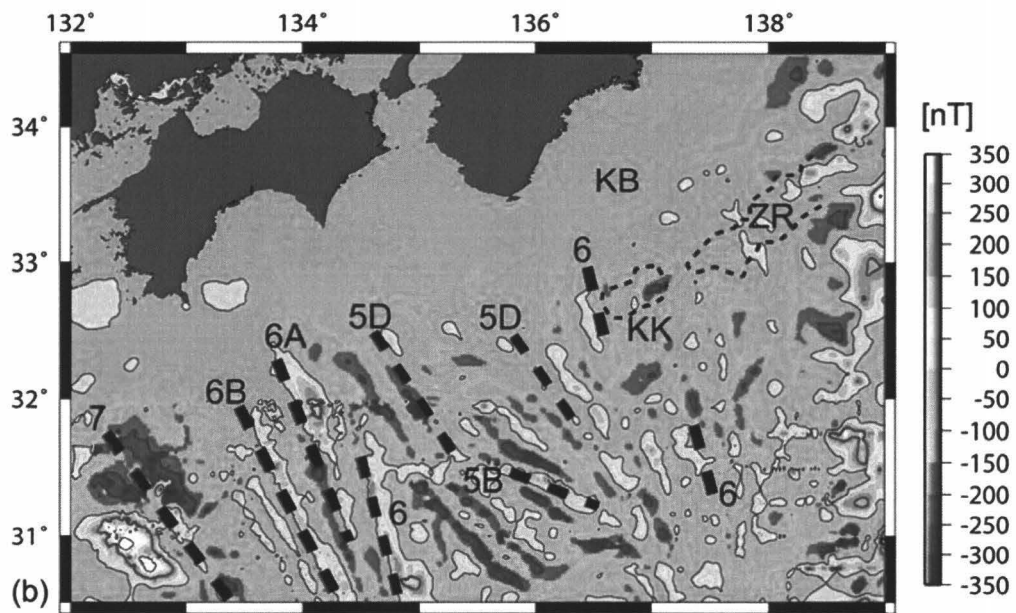


Fig. 3.1(b)

Magnetic anomaly map of the northern Shikoku Basin (Geological Survey of Japan, 1996). Thick dashed lines represent the lineation of the major anomalies. Thin dotted lines indicate the outlines of KK and Zenisu Ridge

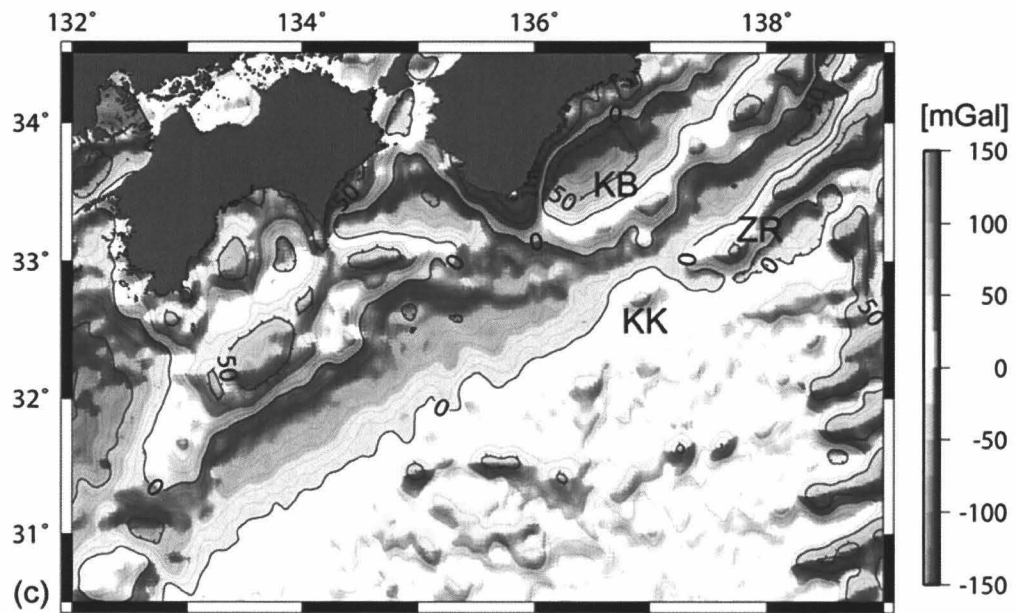


Fig. 3.1(c)

Free-air gravity anomaly map of the northern Shikoku Basin based on compiled marine gravity data (Geological Survey of Japan, 2000). Thick solid lines are contours with 50 mGal interval.

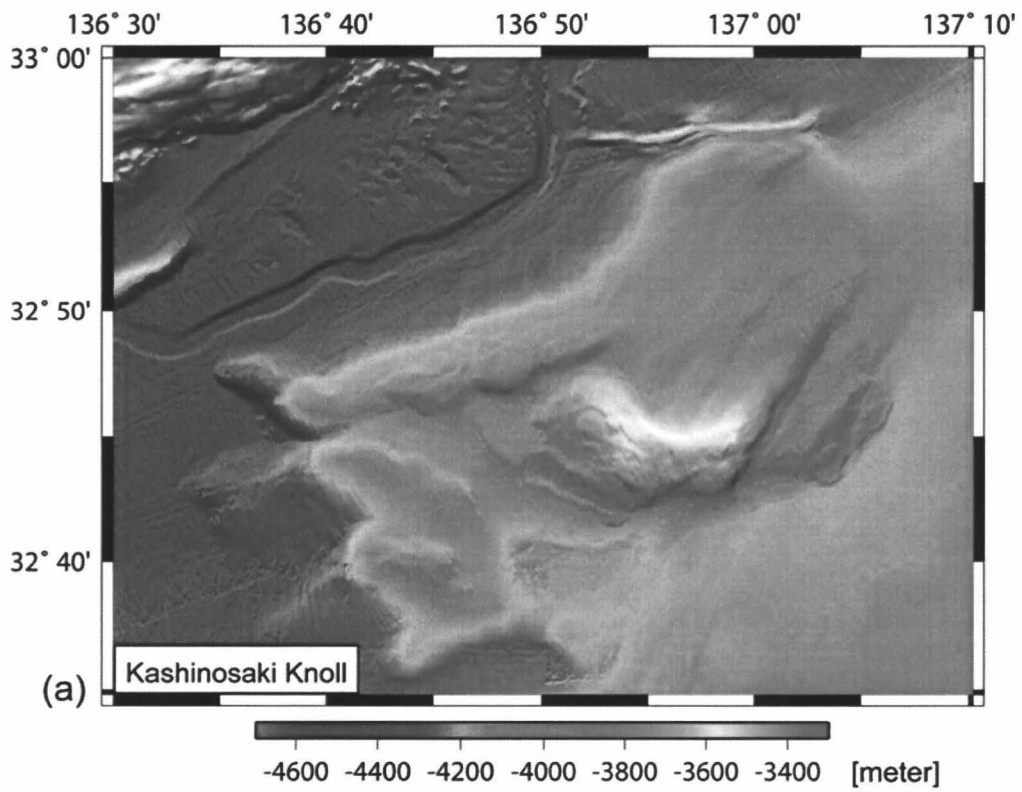


Fig. 3.2(a)

Bathymetric map of Kashinosaki Knoll. A depth color scale is shown at the bottom of the figure.

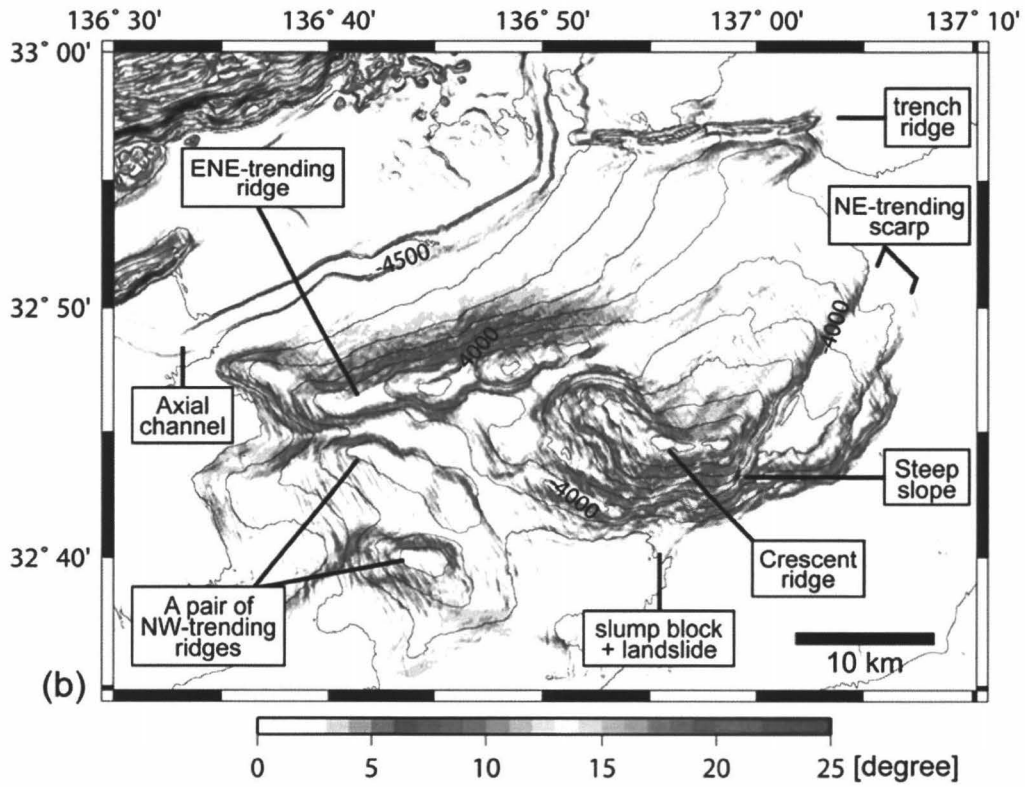


Fig. 3.2(b)

Slope angle map with interpretation of the seafloor morphology. Solid lines are the bathymetric contours with 100 m interval. A color scale for each angle is shown at the bottom of the figure.

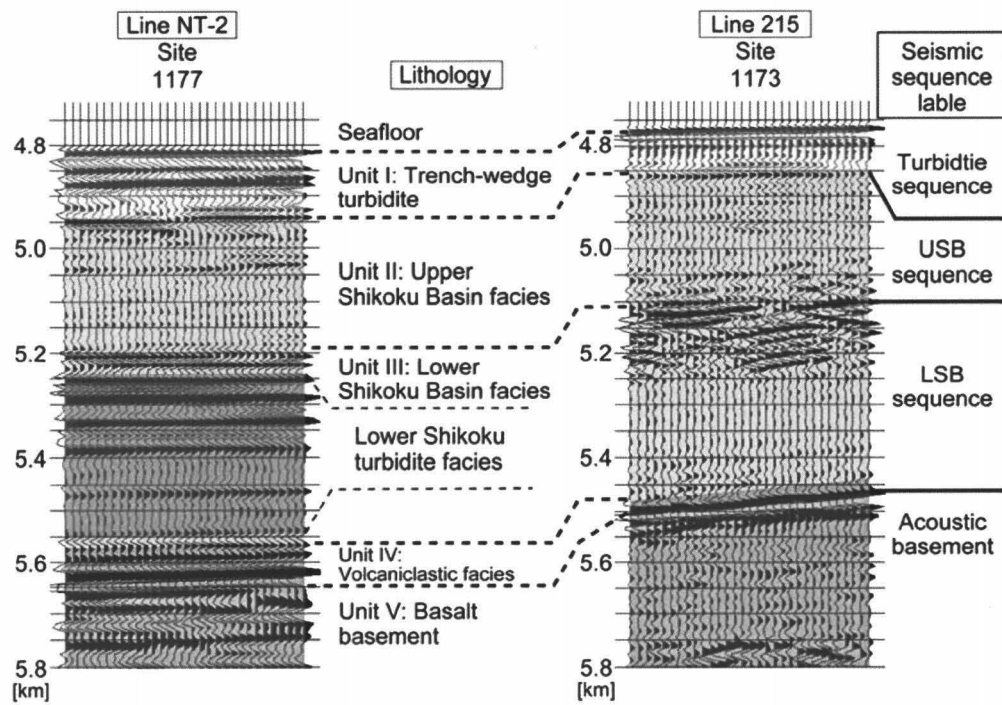


Fig. 3.3(a)

Depth converted seismic reflection data showing the seismic stratigraphy of the Shikoku Basin sediments correlated with ODP sites 1173 and 1177. Seismic line NT-2 with ODP site 1177 is on the left, and line 215 with site 1173 is on the right (Moore *et al.* 2001). Vertical axis is depth in meters.

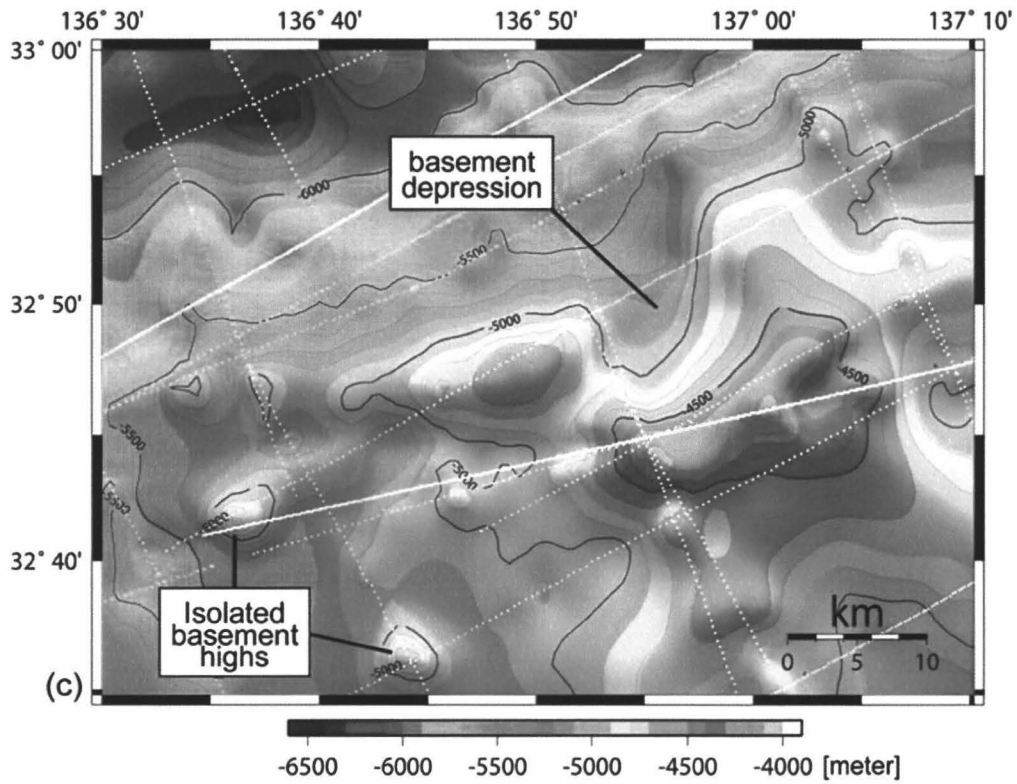


Fig. 3.3(b)

Basement topography map. Thick solid lines are the topographic contours with 500 m interval. White dots are the sampling points for the basement depths.

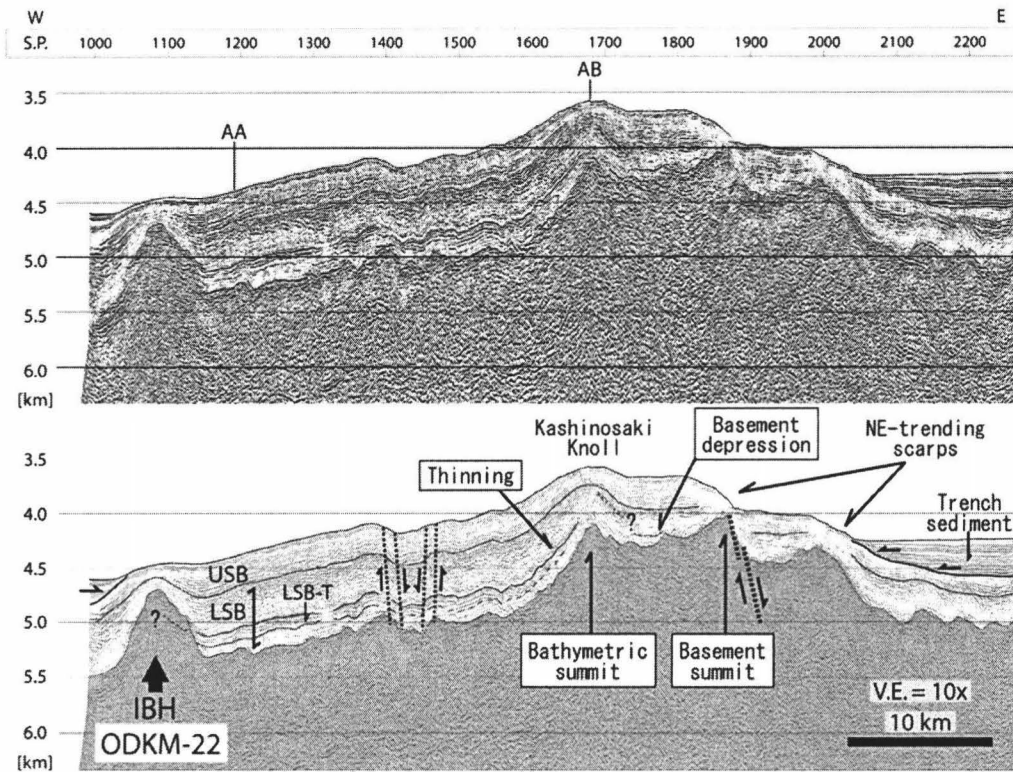


Fig. 3.4(a)

ODKM-22 is a depth section crossing over the summit of Kashinosaki Knoll, oriented approximately parallel to the trench axis. The location is shown on Fig. 1. S.P. = Shot Point, shot interval = 50 m. Upper: Uninterpreted seismic depth section. Cross lines are labeled with a vertical line and a line number. Lower: Interpreted seismic depth section. Thick dotted lines represent faults. Thick solid line represents the bottom of the Quaternary turbidite. IBH: Isolated Basement High. LSB: lower Shikoku Basin sequence, USB: upper Shikoku Basin sequence. In both sections, vertical axis distances are in kilometers. Vertical exaggeration (V.E.) is 10 x.

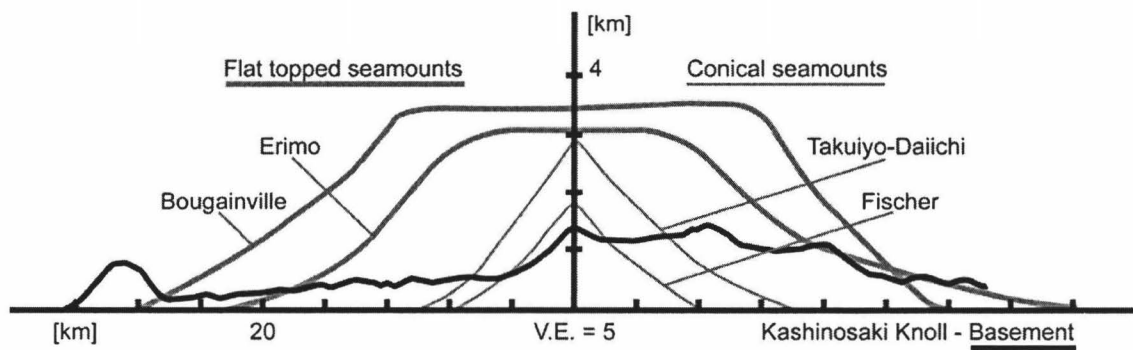


Fig. 3.4(b)

Morphological comparison of seamounts with KK after Dominguez et al 1998. Bold black line indicates basement morphology imaged along ODKM-22.

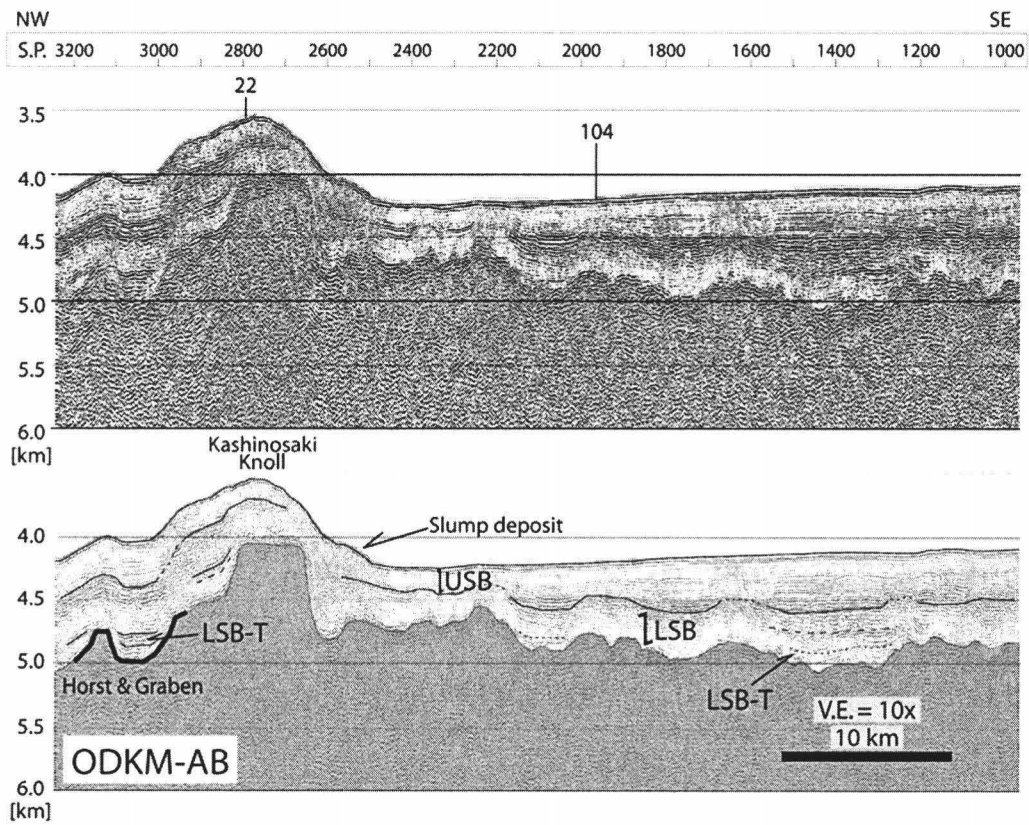


Fig. 3.5

ODKM-AB is a depth section crossing over the summit of Kashinosaki Knoll, oriented perpendicular to the trench axis. S.P. = Shot Point, Shot interval = 25 m. Vertical exaggeration (V.E.) is 10 x.

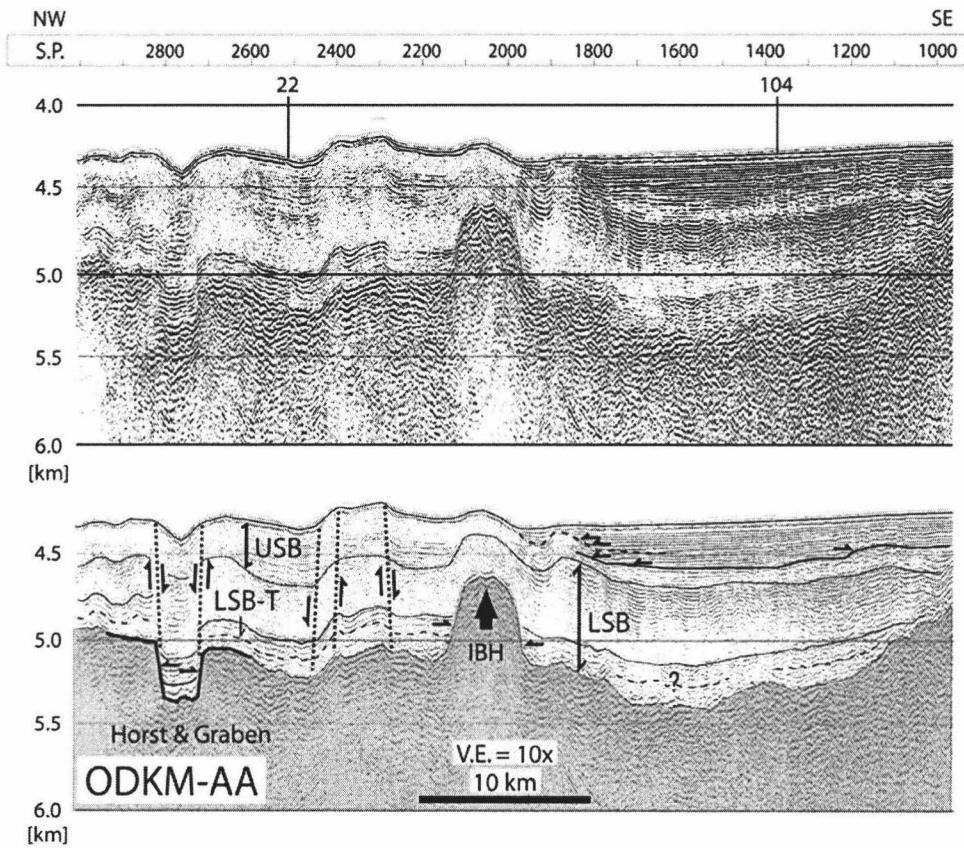


Fig. 3.6

ODKM-AA is a depth section from the western side of KK, perpendicular to the trench axis. Axes are the same as Fig. 3.5.

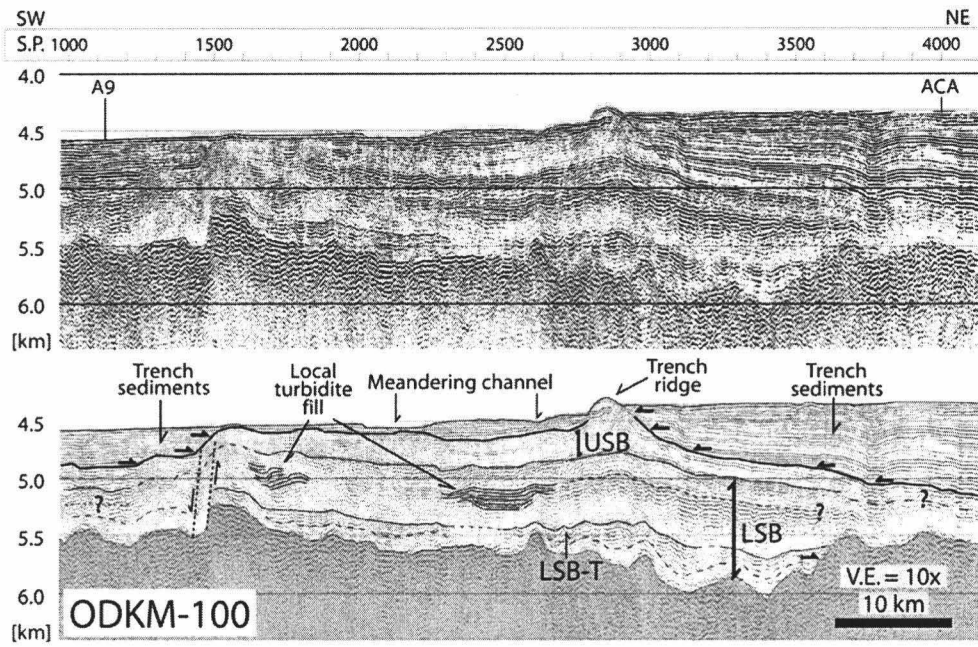


Fig. 3.7

ODKM-100 is a depth section from the northwestern end of KK, parallel to the trench. Axes are the same as Fig. 3.5.

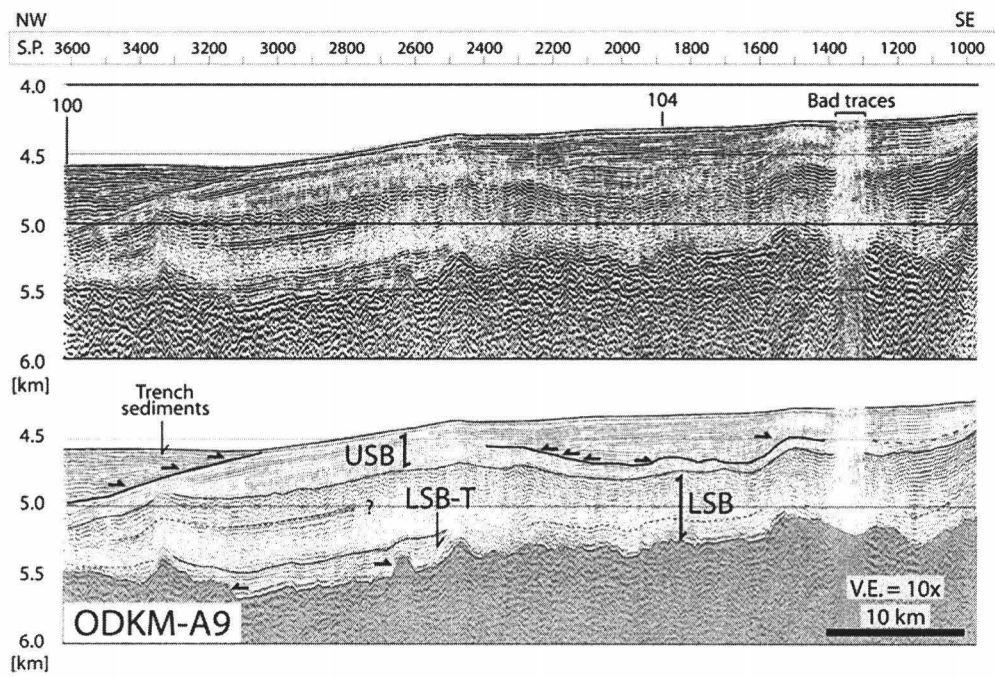


Fig. 3.8

ODKM-A9 is a depth section from the western end of KK, perpendicular to the trench axis. Axes are the same as Fig. 3.5.

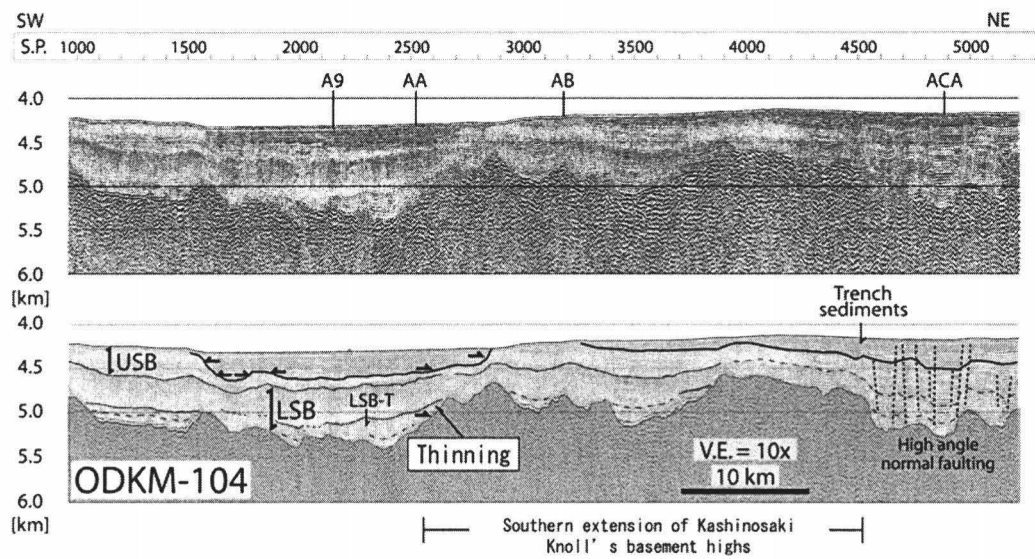


Fig. 3.9

ODKM-104 is a depth section on the south side of KK, parallel to the trench axis. Axes are the same as Fig. 3.5.

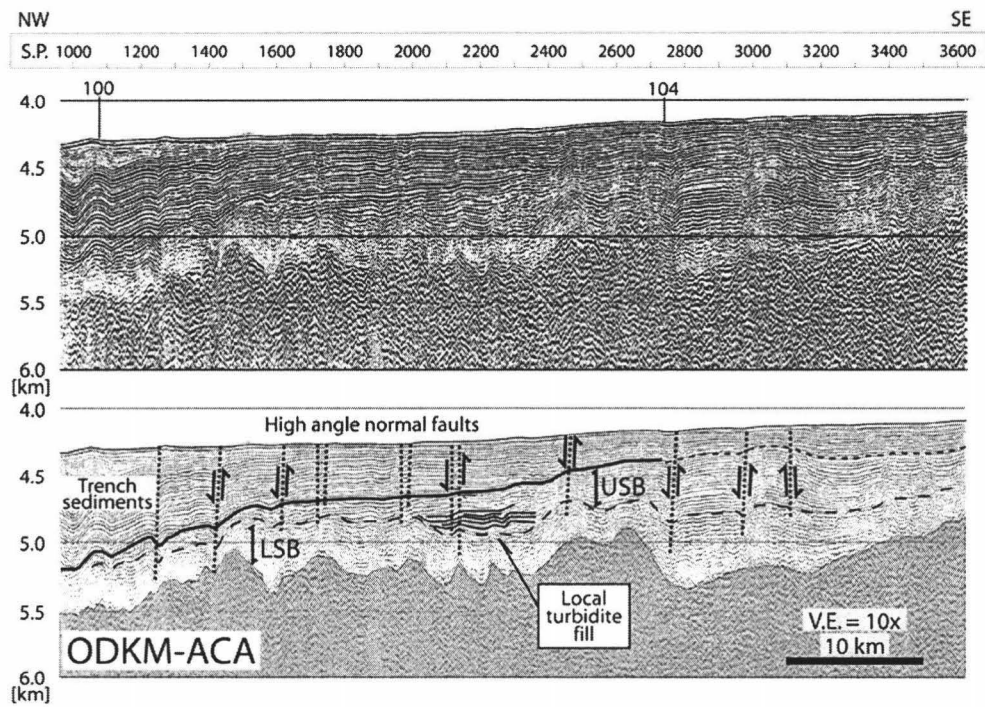


Fig. 3.10

ODKM-ACA is a depth section between KK and Zenisu Ridge, perpendicular to the trench axis. Axes are the same as Fig. 3.5.

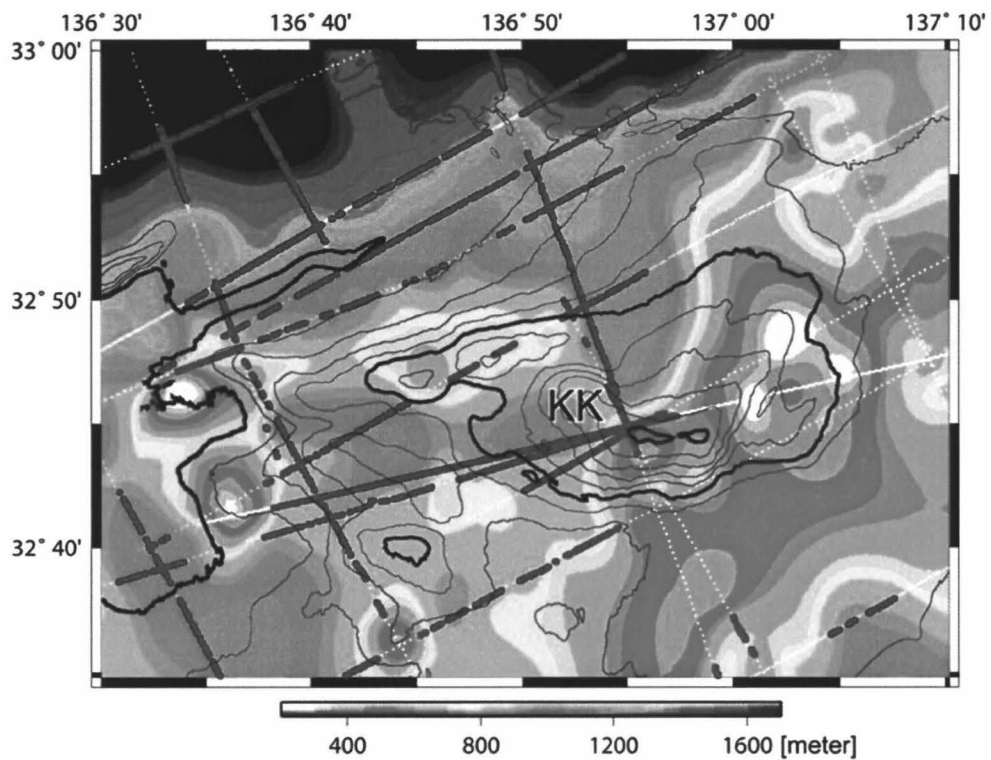


Fig. 3.11

Total sediment isopach map of KK. A color isopach scale is shown at the bottom of the figure. Solid lines are the bathymetric contours with 500 m (thick) and 100 m intervals (thin). White dots are the sampling points for the total sediment thickness. Brown dots show the location for the LSB-T subunit. KK: Kashinosaki Knoll.

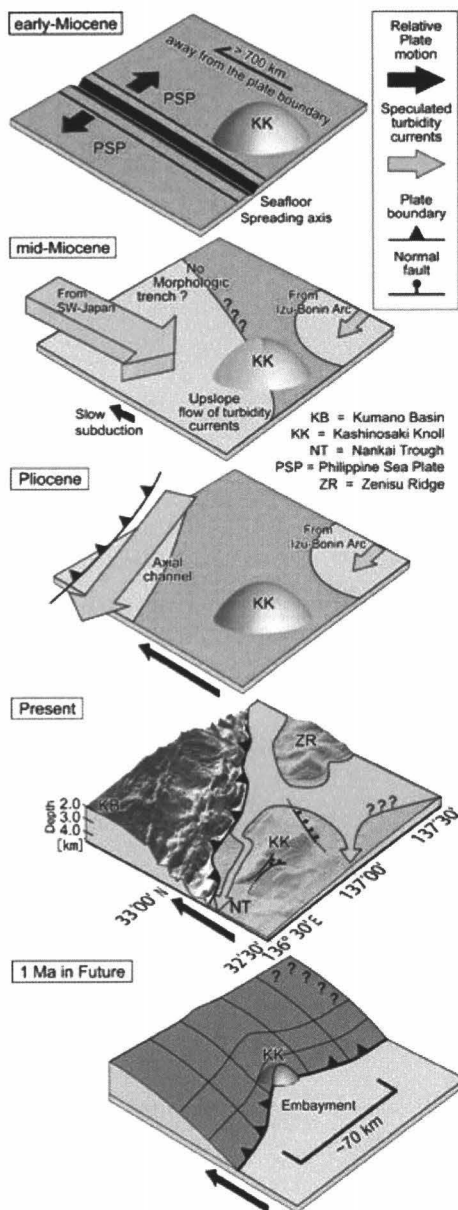


Fig. 3.12

Schematic view of turbidity currents migrated around KK since the early-Miocene. Light blue color represents pelagic and hemipelagic sedimentation, and light brown color represents turbidity currents.

Chapter IV

THE INFLUENCE OF ALONG-STRIKE VARIATIONS IN SUBDUCTING BASEMENT TOPOGRAPHY AND OVERLYING SEDIMENTS ON THE TOE STRUCTURE OF THE NANKAI TROUGH ACCRETIONARY PRISM

T. Ike¹, G.F. Moore^{1,2}, G. Kimura^{3,4}, J.O. Park^{4,5}, Y. Kaneda⁴

¹ Department of Geology and Geophysics, University of Hawaii, Honolulu, HI 96822

² CDEX/JAMSTEC, Yokohama, Japan

³ Tokyo University, Earth and Planetary Sciences

⁴ Institute for Research on Earth Evolution, JAMSTEC, Yokosuka, Kanagawa 237-0061,
Japan

⁵ Now at: Ocean Research Institute, University of Tokyo, Minamidai,

Email: tike@hawaii.edu

Phone: 808-956-3727

To be submitted to: **Tectonics**

Abstract

At subduction zones, heterogeneous incoming sediment sections and underlying basement topography affect the structural development and deformation styles of the landward trench slopes. In this paper, we present a multi-channel seismic (MCS) data set, tied to sediment stratigraphy from ODP cores, and interpret the regional structural variations along the frontal part of the Nankai Trough accretionary prism with respect to the heterogeneous incoming sediment sequences. We use Coulomb wedge theory to relate the various structural styles, such as the geometry of imbricate thrusts, to the wedge taper angle. The taper angle is significantly controlled by the thickness of accreted sediments. The underthrusting sediment type, the presence or absence of the Miocene turbidites, is strongly correlated with the effective basal friction coefficient and so also the taper angle. Lateral variations in the deformation pattern and structural styles may relate to the ratio of internal friction coefficient (μ_i) to effective basal friction coefficient (μ_b'). These variables in turn are strongly correlated with incoming sediment heterogeneity and local basement relief along the base of the accretionary prism and the subducting plate.

INTRODUCTION

Inputs to subduction zones have a direct impact on the structural diversity in convergent margins [von Huene *et al.*, 2000; Moore *et al.*, 2001; Clift and Vannucchi, 2004; Taylor *et al.*, 2005; Underwood, 2002, 2007]. In thickly sedimented margins, the incoming sediments are partially offscraped from the oceanic plate to form accretionary prisms, while the underthrust sediments continue to subduct and may affect the mechanics of the prism's base [Bekins and Dreiss, 1992; Maltman, 1993; Screaton, 2006]. The underthrust sediment section undergoes compaction, lithification, and dehydration [Spinelli and Saffer, 2004], affecting pore pressure along the base of the prism, and later becomes the input to the seismogenic zone where large earthquakes occur. Interplate earthquakes may rupture along the base and the interior of the prism and cause tsunami threats onland [Baba and Cummins, 2005]. In the deeper region along the plate boundary, the failure of micro cracks triggered by the sudden increase of fluid pressure may induce slow slip events [Rogers and Dragert, 2003; Obara *et al.*, 2004]. Topographic highs, such as fracture zones, seamounts, and ridges, could cause isolated strong coupling with the overriding plate and influence earthquake behavior [e.g., Cloos, 1992; Cloos and Shreve, 1996; Scholz and Small, 1997; Bilek, 2007].

Structural styles and the development of accretionary prisms are strongly affected by the incoming sediment section. For example, an accretionary prism of non-cohesive Coulomb material adopts a critical taper angle and this angle depends on the internal and basal coefficients of friction in the offscraped sediments [Davis *et al.*, 1983; Dahlen, 1984, 1990]. Assuming homogeneous material, various complementary models have been proposed to explain the behavior of the prism controlled by imbricate thrusts: differences in basal friction controlled by pore pressure [Moore *et al.*, 1990; Saffer and Bekins, 2006], a combination of very low basal shear stress and basal dip [Koyi and Vendeville, 2003], and strain-rate control in non-Coulomb wedges [Gutscher *et al.*, 2001]. Analogue sand-box modeling suggests that mechanical and geometrical parameters, such as incoming sediment thickness, the prism's basal friction, and the geometry of the backstop exert strong control on the style of sediment deformation [Calassou *et al.*, 1993; Gutscher, 1998; Koyi and Schott, 2001]. The accreted sediment thickness also affects the thrust spacing, which controls the thickening and shortening of the prism in its early stage of deformation [Schott and Koyi, 2001]. Moreover, recent modeling, using critical taper theory, indicates how accretionary prisms respond specifically to the basal friction and earthquake rupture behavior of the décollement in the coseismic and inter-seismic cycle

[Wang and Hu, 2006].

Despite these extensive studies, the detailed effects of subducting basement topography and associated sediment thickness and type on the structural development and deformation style along subduction zones are poorly understood. By focusing on regional variations in incoming sediment thickness and sediment heterogeneity in a single subduction zone, we eliminate the effects of some variables, such as the age and rate of the subducting plate, on an accretionary prism's geometry and growth history.

The Nankai Trough convergent margin has long been considered to be the type area for study of subduction zones accreting thick terrigenous sediment sections. Therefore this margin has been extensively studied in recent years, yielding large amounts of data, such as seafloor bathymetry [Kaiko I Research Group, 1986; Ashi *et al.*, 1989; Okino *et al.*, 1994], seismic reflection [Aoki *et al.*, 1986; Bangs *et al.*, 1999; Park *et al.*, 1999, 2000, 2002a, 2002b, 2003; Moore *et al.*, 2001]. There are nine major drill sites along the Nankai Trough. Three of the drill sites are located seaward of the prism, Deep Sea Drilling Program (DSDP) Site 582 [Shipboard Scientific Party, 1986] and Ocean Drilling Program (ODP) Sites 1173 and 1177 [Moore *et al.*, 2001] (Fig. 4.1a). These sites provide a reference for the geological characteristics of the incoming sedimentary section before

deformation. Other sites sampled a landward progression of the prism's structure, such as incipient deformation, a major out-of-sequence thrust, and landward slope sediments.

In this paper, we present a series of 2-D seismic reflection lines along the entire length of the Nankai Trough to describe the structure of the accretionary prism, with particular focus on its seaward-most part (Fig. 4.1 a). We previously defined the regional variations in basement morphology and associated sediment thickness and type across the subducting northern Shikoku Basin [*Ike et al.*, in prep.]. The present study focuses on the accretionary prism with the aim of establishing a relationship between the thickness and type of sediment and morphology of the underlying basement entering the subduction zone and the resulting structure of the frontal part of the accretionary prism [*Moore et al.*, 2001b]. In addition, we apply Coulomb wedge theory to the seismic data set to estimate the internal friction coefficient and the effective basal friction coefficient. Comparison of the inferred mechanical properties with the heterogeneous incoming sediments provides a better understanding of the mechanical effects of sediment stratigraphy on structural development and deformation styles. This study also constraints on dewatering history and inputs to the seismogenic zone.

GEOLOGICAL SETTING AND PRISM GEOMETRY

The Philippine Sea plate (PSP) is subducting at the Nankai Trough subduction zone at a rate of approximately 40-50 mm/yr at an azimuth of $\sim 305^\circ$ [*Seno et al.*, 1993; *Miyazaki and Heki*, 2001; *Zang et al.*, 2002]. The northern margin of the PSP, the Shikoku Basin, is characterized by large variations in basement relief with associated variations in the overlying sedimentary section [*Ike et al.*, in prep.]. Large-scale structural variations along the entire Nankai Trough forearc, from the Kyushu-Palau Ridge in the west to the Izu-Bonin Ridge in the east, have been documented [e.g., *Aoki et al.*, 1982; *LePichon et al.*, 1987; *Moore et al.*, 1990, 2001; *Okino and Kato*, 1995; *Park et al.*, 2002a, 2002b; *Kimura et al.*, 2007]. At a large scale, the dip of the accretionary prism's surface slope (α) varies from 2.4° to 4.4° within a few hundreds of kilometers along-strike [*Okino et al.*, 1994]; the taper angle that is the sum of the accretionary prism's surface slope angle and the basal décollement's angle also varies with distance from the trench axis. Specifically, much of the eastern and western regions of the Nankai Trough accretionary prism are characterized by moderate wedge taper angles ($4^\circ - 10^\circ$) and regularly-spaced thrust slices of accreted trench strata [*Moore et al.*, 1990]. The central region, south of Tosa-Bae (Fig. 4.1a), has a much lower taper angle and the thrust slices include significant amounts

of Shikoku Basin hemipelagic strata in addition to the overlying trench strata. The basal décollement in the eastern and western regions is generally a normal polarity (positive) reflection, while the central region exhibits a reversed (negative) polarity décollement. These differences have been attributed by Moore et al [1990] to the differences in fluid pressures and/or basal friction along the Nankai Trough. In addition, these differences are of particular importance near the toe of the accretionary prism, where rapidly deposited trench sediments deform when rapidly being overridden by the upper plate.

Kimura et al. [2007] have shown that the regional structure of the Nankai prism can be generalized into three segments approximately parallel to the trend of the trench axis (Fig. 4.1b). These segments, as defined by variations in the surface slope, prism wedge taper angle, and character of the basal plate boundary fault, are the outer wedge, the transition zone, and the inner wedge. In the outer wedge, an imbricate thrust zone (ITZ), is characterized by closely spaced imbricate thrusts [*Moore et al.*, 2001b] typically characterizes the prism, for a length of 20 - 30 km, from the frontal thrust to the transition zone. The outer wedge is characterized by a narrow wedge taper, internal deformation by in-sequence folds and thrusts and an aseismic décollement. The inner wedge has a weakly deformed internal structure and a seismogenic plate boundary fault along its base. The

transition zone between the two wedges regionally has a large wedge taper angle with steep surface slope, internal structure of out-of-sequence thrusts, and step-down of the décollement onto the sediment–oceanic basement interface. *Kimura et al.* [2007] believe that these common aspects might be related to the lithification of both accreted and underthrust sediments and the resultant switch from seismic to aseismic of the plate boundary fault. In this paper we further address the contribution of accreted and underthrust sediments, particularly their lithologies and thicknesses, as well as that of the topography of the underlying oceanic crust. We thus accept the basic regional three-fold, trench-parallel zonation of *Kimura et al.* [2007] and concentrate on regional along-strike variations within these zones that can be attributed to variations in incoming sediment thickness and basement relief.

INCOMING SEDIMENT SEQUENCE

The stratigraphy of the incoming sediment section on the PSP provides the key to understanding sediment deformation at toe of the Nankai Trough accretionary prism [e.g., *Moore*, 1989; *Le Pichon et al.*, 1993; *Moore et al.*, 2001]. Stratigraphic sequences,

defined in the western and central Nankai Trough off Shikoku Island, have been sampled by DSDP Legs 31 and 87 and ODP Legs 131 and 190 [Karig and Sharman, 1975, Bray and Karig, 1985; Taira *et al.*, 1991; Moore *et al.*, 2001]. We defined three major seismic stratigraphic sequences in the northern Shikoku Basin based on ties to ODP drilling data [Ike *et al.*, in prep.]. The oldest unit, the Lower Shikoku Basin (LSB) sequence, overlies volcanoclastic sediments above the basement. It is characterized by low amplitude reflections in the lower section, and relatively high amplitude, discontinuous to moderately-continuous hummocky reflections at its upper boundary. This sequence is correlated with the middle Miocene to lower Pliocene hemipelagic mudstones sampled at the ODP drill sites. Within the LSB sequence, we interpret high amplitude, laterally continuous reflections as a subunit (LSB-T) that correlates with turbidite sands recovered at ODP site 1177 [Moore *et al.*, 2001]. The probable source of these turbidites is the inner zone of Shikoku Island, southwestern Japan, with delivery of sediment across the trench, perpendicular to the trench axis, and out onto the Shikoku Basin floor [Fergusson, 2003]. At a local scale, the LSB sequence off Cape Ashizuri is more smectite-rich than off Cape Muroto, which may have significant implications for the behavior of the deep seismogenic zone as this is the part of the section that is subducted beyond the prism toe

[Moore *et al.*, 2001]. The presence or absence of the turbidite sand within the underthrust sediment has significant influence on fluid migration beneath the décollement [Saffer and Bekins, 2002]. The lack of boreholes in the eastern Nankai Trough limits our direct knowledge of the geology of the incoming sediment section. Based on our seismic reflection interpretations, we infer that the LSB sequences in the region east of the subducting Kinan Seamount chain generally contain the Miocene turbidite section in the relative basement lows. Moreover, the seismic character of the Miocene turbidites, high-amplitude continuous reflections, shows multiple layers interbedded with low amplitude reflection in this area.

The second sequence, the Upper Shikoku Basin (USB) sequence, is characterized by low amplitude, moderately-continuous reflections. A facies change from the lower to upper Shikoku Basin is defined at all sites by the appearance of ash layers containing volcanic glass shards [Taira *et al.*, 1991; Moore *et al.*, 2001]. This unit boundary is thought to be sensitive to diagenesis that is affected by regional changes in the thermal structure [Underwood, 2007].

The third and youngest seismic sequence exhibits laterally continuous and high amplitude reflections that lap onto the USB sequence. We correlate it with the trench

wedge facies at the ODP sites and the distribution of Quaternary turbidites in our study area is also restricted to the morphologic trench.

Basement relief on the subducting Shikoku Basin crust, classified into three distinct provinces (Fig. 4.1 a), has a significant influence on the sedimentary facies distribution along the northern Shikoku Basin [*Ike et al.*, in prep.]. The basement depth and total sediment thickness are linearly related because turbidites are channeled into basement lows, thus increasing sediment thickness in the basement lows at the expense of the basement highs. Irregularities in the basement relief (> 1500 m) of the central province are 3-5 times larger than those in the western and eastern provinces, and the basement relief controls local sedimentation at a scale of ~ 5 -20 km [*Ike et al.*, in prep.]. In the western province, sediment sequences over the smooth basement relief uniformly contain the Miocene turbidites, similar to those recovered at ODP site 1177. In the central province, the region with the largest basement relief (Kinan Seamount chain) includes large variations in sediment thickness, and variations in the amount of Miocene turbidites in the basement lows. Over the basement highs, the sediment sequence is dominantly hemipelagic mudstones comparable to those recovered at ODP site 1173. In the eastern province, the Miocene turbidites are mostly absent over the basement highs. The

basement relief in this area is significantly rougher compared with the western province.

The basement highs in the eastern province are mostly 5-15 km wide and ~600 m higher than the surrounding basement lows. Over these basement highs, the sediment sequence is inferred to be dominantly hemipelagic mudstones comparable to those recovered at ODP site 1173; whereas, the sediments in the basement lows show multiple-layers of high amplitude reflections within the LSB-T unit, inferred to be turbidite layers interbedded with thick hemipelagic sediments. At a local scale, the basement highs with relatively shallow dip on their landward margin may allow the turbidites to climb up their north-facing flanks (e.g., Kashinosaki Knoll, *Ike et al.*, in prep.).

SEISMIC REFLECTION DATA

In this study, we use 10 seismic reflection lines that are chosen to represent regional characteristics of the prism along the Nankai Trough (Fig. 4.2a to 4.2c). The seismic lines (Table 4.1) are combined from three data sets [*Ike et al.*, in prep.]. Seismic data acquisition and initial processing through stacking was completed by JAMSTEC. We applied a second phase of data processing to this data set, including bandpass filters and

post-stack time migration. We converted the seismic lines from time to depth using a velocity model based on pre-stack depth migration (PSDM). The PSDM of the Muroto data set was constrained by depths from ODP Sites 808, 1173 and 1174 [*Costa Pisani et al.*, 2005]. Velocities along line ODKM-b were also determined by detailed PSDM [*P. Costa Pisani*, unpublished data, 2006]. We then extrapolated those velocities across the entire prism based on detailed seismic interpretation. This velocity model uses 1500 m/sec for the water column and increases to 1600 m/sec at the seafloor with a gradient of 650 m/sec² with increasing two-way travel time. The interval velocity between the décollement and the oceanic crust is approximately 2300 - 3000 m/sec at the prism toe, and gradually increases in the landward direction. Although this regional velocity estimate is probably not accurate in detail, we believe that it is sufficient for depth conversion to determine the regional structural variations, such as the angle of the forward thrusts, back thrusts, and the base of the prism.

COULOMB WEDGE MODEL

Geometric changes in wedge taper and inferred internal deformation of the prism have

been well explained by Coulomb wedge theory [*Davis et al.*, 1983; *Dahlen*, 1984, 1990]. However, these original studies considered a homogeneous material and ignored local changes in sediment deformation. These assumptions are suitable for inter-prism comparisons, but within a single prism, sediment properties may change along strike and landward into the prism. Thus, the recognition of lateral changes in sediment properties is important for quantifying local variations in structural characteristics along a single subduction zone.

We assume that the toe of the prism is at critical condition following *Davis et al.* [1983] and *Dahlen* [1984, 1990]. We take into account differences in sediment type assuming that these materials have similar frictional properties. Sandstones and siltstones from onland accretionary prisms show relatively similar orders of internal friction coefficient, suggest that this assumption is reasonable [*Hoshino and Kato*, 2001].

In applying Coulomb wedge theory to the Nankai prism, we first measure the dip of the accretionary prism's surface (α) and the décollement (β) on regularly spaced profiles perpendicular to the topographic trends of the prism (Fig. 4.3). For the angle of the accretionary prism's surface (α), we first determine the bathymetric peaks of the slope and fit a best approximation line, with measurements every 5 km along a single seismic

line. Approximation lines are designed to be asymptotic to the bathymetric relief; however, in many cases the line cuts through anomalous highs and balances the open space underneath the line in order to characterize the regional trend. To determine the angle β , we fit linear approximation lines based on the location of the décollement at the toe of the accretionary prism and then on the basement under the landward part of the prism where the décollement has stepped down to the top of oceanic crust [e.g., *Moore et al. 2001; Park et al. 2002a*]. We believe that these approximation lines are sufficient to determine the regional trend of the taper angle and thus use these approximations with the bathymetric profiles to determine the wedge taper at uniform spacing along the prism.

We then use the Coulomb wedge theory to constrain variations in the internal (μ_i) and basal (μ_b) friction coefficients (Fig. 4.3). We first determine the angles of the forward (δf) and back thrusts (δb), and then measure the geometrical determination of the internal friction

$$\theta = \{90 - (\delta b - \beta) - (\delta f - \beta)\}$$

and the direction of maximum compressive stress relative to the décollement

$$\psi = \{(\delta b + \beta) - (\delta f - \beta)\} * 0.5$$

The internal friction coefficient is calculated as

$$\mu_i = \tan \theta$$

; whereas, the effective basal friction coefficient is

$$\mu_b' = \sin(2\psi)/(1/\sin(\theta) - \cos(2\psi))$$

based on *Davis and Huene* [1987] and *Kukowski et al.*, [2001].

Calculation of both friction coefficients depends on the angle measurement of the back thrust. We obtained coefficient of friction values at 5 sites. We then constrain variations in the pore pressures at the base and the inside of the accretionary prism, and hence the basal shear stress [*Saffer and Bekins*, 2006]. The effective basal friction coefficient (μ_b') accounts for pore-fluid pressure ratio along the décollement (λ_b) and the basal friction coefficient

$$\mu_b = \mu_b'((1-\lambda^*)/(1-\lambda_b))$$

: ($\lambda^* = (P_f - P_h)/(P_l - P_h)$): normalized pore pressure ration, P_f : pore pressure, P_h : hydrostatic pressure, and P_l : lithostatic pressure). Following *Kimura et al.* [2007], we assume various fluid pressure ratios, from hydrostatic condition to over-pressured condition of $\lambda^*=0.17$

and 0.33, neglecting the water column above the prism. The internal friction coefficient $\mu_i=0.5-0.6$ is common for rock fracture in low confining pressure and sand, and $\mu_i=0.85$ is the same as Byerlee's coefficient for the upper crust [Byerlee, 1978]. Sedimentary rocks from the Nankai accretionary prism on land show a range of internal friction coefficient from 0.6 to 0.9 [Hoshino and Kato, 2001]. Coefficients for quartz gouge range from 0.49 to 0.62; typical friction coefficients for illite range from 0.22 to 0.48; and those for chlorite are 0.30– 0.45. Estimated values of effective basal friction coefficient, generally reported, range from 0.15 to 0.35 [Davis and von Huene, 1987; Lallemand et al., 1994; Kukowski et al., 2001]. Given the low estimated cohesion (η) in the sediments of the outer wedge, we apply a noncohesive model ($\eta=0$) to the study area [Kopp and Kukowski, 2003; Wang and Hu, 2006].

VARIATIONS IN STRUCTURE OF THE FRONTAL ACCRETIONARY PRISM

The internal structure of the accretionary prism along the Nankai Trough is not uniform. The toe structure of the Nankai prism can be divided into three regions, along-strike, on the basis of basement morphology, sediment thickness, and sediment type (Fig. 4.1). The surface and underlying basement morphology in the Western Shikoku Basin (Western

Region of Ike et al. [in prep.]) is relatively smooth, whereas large ridges and seamounts are present along the Kinan Seamount chain in the Central Region, and numerous smaller seamounts characterize the Eastern Region. Bathymetric profiles spaced 50 km along with seismic reflection profiles spaced 10-100 km apart along the Nankai Trough exhibit along-strike variations in wedge taper angles and internal structures, which we infer to indicate variations in internal and basal friction values. Measurements of the incoming sediment thickness south of the toe of the prism (black arrow, Fig. 4.4a to 4.4c) further distinguish the regions defined above. We define measurement error ($\pm 0.5^\circ$) of the fore thrust and back thrust. The uncertainties in the velocity model also contain errors in the angle of the thrusts. For example, if we use a constant velocity model of 1.800 km/sec for the sediment column and measure a fore thrust (25°) fitting in a 2.00 km wide and 0.93 km tall block that is approximate to the fault block in our study, then the 0.93 km is equivalent to 0.518 sec (or 1.036 sec in Two-way travel time). When the same forward thrust, within the 2.00 km wide and 0.518 sec tall block, happens to be imaged as 24.5° , then the velocity should be 1.759 km/sec. Therefore, uncertainties in constant velocity of ± 0.041 km/sec also cause errors of measuring the angles of thrusts ($\pm 0.5^\circ$). In the following section we describe the distinctive morphologic and structural styles that

characterize each tectonic province from the western Nankai Trough toward the east.

THE WESTERN PROVINCE: NORMAL PRISM

We present two seismic reflection profiles, kr9810-1 and kr0114-5, from the western province (Fig. 4.2a). These profiles show a classic leading imbricate fan with a gradual thickening of the prism associated with fault-bend fold structures [Moore *et al.*, 2001], and the accretionary prism's surface slope has a smooth and coherent ridge-and-trough morphology that has not been significantly modified by seamount or ridge subduction. Therefore, we call this region the "normal" prism. The normal prism has four characteristics (Fig. 4.4a); 1) the thickness of the incoming sediment is 1270-1350 m, 2) its sediment sequence is comparable with defined at ODP site 1177, 3) the underthrust sediment contains a significant thickness (~300 m) of the LSB-T unit (Miocene turbidite), 4) the boundary between the outer wedge and transition zone occurs at the depth of 3500-4000 m (Fig. 4.1a).

Seismic line kr9810-1 is located 80 kilometers east of Kyushu-Palau ridge (Fig. 4.1a). The taper angle at the prism toe is approximately 5.5° and it increases to 8° to the north (Table 4.2). Seaward of the prism, the incoming sediment section is ~1350m thick, of

which ~890 m are accreted and 460 m are underthrust beyond the toe of the prism (the accreted/underthrust ratio = 1.93). The angle of the frontal thrust is 20°, and the dip of the thrusts in the ITZ increase landward to ~20°. In the outer wedge, the angle of the seaward-most back thrust is 33°. Based on the geometry of these faults, we estimated values for the internal friction coefficient $\mu_i = 0.75$, and the effective basal friction coefficient $\mu_b' = 0.39$.

Approximately forty kilometers east of seismic line kr9810-1, line kr0114-5 has a taper angle of ~6°, similar to that of line kr9810-1. Seaward of the prism, the incoming sediment is separated by the décollement into 940 m of accreted sediments and 330 m of underthrust sediments (the accreted/underthrust ratio = 2.82). The sediments between each thrust show thickening without major fold or vertical displacement along the thrusts. Over the ITZ packages the angle of the accretionary prism's surface slope is 4°. The slope angle decreases to 3.5° toward the north. On seismic line kr0114-5, the angle of the frontal thrust and the thrust sheets in the ITZ package are ~22°. These thrusts are characterized by high amplitude reflections. The angle of the back thrust is difficult to define, thus unable to estimate μ_i and μ_b .

THE CENTRAL PROVINCE: MAJOR RIDGE SUBDUCTION

We present five seismic reflection profiles, kr9704, lline210, kr9806-8, kr0114-4, and kr0114-3 from the central province, south and southeast of Tosa-Bae, to characterize the internal structure of the accretionary prism's toe (Fig. 4.2a, 4.2b). The basement topography in this province is the roughest within our data set. The accretionary prism in this province has been affected by the subduction of large topographic features, therefore we define this region as having suffered "major ridge subduction".

Seismic line kr9704 is located on the western rim of the Tosa-bae embayment. The accretionary prism's surface slope has a local bathymetric step (surface slope 10°), ~20 km north of the frontal thrust (Figs. 4.2a). *Park et al* [1999] suggests that a seamount subduction is the cause of this bathymetric step. The accretionary prism's surface slope becomes flat on the landward of the step. Seaward of the prism, the incoming sediment is the thinnest in the Nankai prism (~970 m), with ~620 m accreted and ~350 m underthrust (accreted/underthrust ratio = 1.77). The incoming sediment sequence may not contain the LSB-T unit beneath the prism [*Ike et al.*, in prep.]. The outer wedge segment has a gentle slope (2.5° ; Fig. 4.2a). The internal structure of the prism is incoherent compared with the western province. The taper angle at the toe is approximately 4.5° , and the angle of the

frontal thrust is 24° . The dip of the thrusts in the outer wedge is approximately 24° (Fig. 4.4a). We were not able to measure a clear back thrust on this line, thus unable to estimate μ_i and μ_b .

South of Cape Muroto, the basement topography is generally shallower than the western province because of the shallow topography of the subducting Kinan Seamount chain [Moore et al., 2001a]. This region, exemplified by seismic line Iline210, has three distinct characteristics compared with the other regions: 1) a thin incoming sediment package (~ 1160 m), 2) the sediment sequence is comparable with ODP site 1173, and the LSB-T unit is absent in the underthrust sediments, 3) the prism has been rejuvenated after suffering a giant landslide due to the subduction of a seamount, creating the Tosa-Bae embayment (Fig. 4.1a). Seismic line Iline210 is located on the western side of the Tosa-bae embayment (Fig. 4.1b). The taper angle at the toe is approximately 3.5° increasing to 6.0° toward the north (Table 4.2). Locally the taper angle increases to $>10^\circ$ where the out-of-sequence thrusts develop in the transition zone (Fig. 4.2a). Seaward of the prism, the incoming sediment is separated by the décollement into 680 m of accreted sediments and 480 m of underthrust sediments (the accreted/underthrust ratio = 1.38). In the Outer wedge (Fig. 4.4a), the angle of the frontal thrust and the thrust sheets in the ITZ

are nearly constant (28°). In one of the thrust sheets, the angle of the back thrust is 41° .

The estimated value for the internal friction coefficient is $\mu_i = 0.38$, and the effective basal friction coefficient is $\mu_b' = 0.16$.

Seismic line kr9806-8 is located on the eastern rim of the Tosa-bae embayment. The seismic profile shows a steep bathymetric slope ($\sim 5^\circ$) in the outer wedge, although the accretionary prism's surface slope has a low angle (2.5°) in general (Fig. 4.2b). The taper angle at the toe is approximately 7° , increasing to 7.5° toward the north. The incoming sediment seaward of the prism is ~ 2170 m thick, with ~ 1340 m accreted and ~ 830 m underthrust (accreted/underthrust ratio = 1.61). The incoming sediment sequence partially contains the LSB-T unit in the lower portion, and is the thickest in this study. The prism's surface slope has a local bathymetric step 7 km north of the frontal thrust. The internal structure of the prism is similar to Iline210 seaward of the step, showing typical in-sequence imbricated thrust sheets (Fig. 4.4b). The angle of the frontal thrust is 28° , and the dip of the thrusts in the ITZ increases landward to $\sim 33^\circ$. We were not able to measure a clear back thrust on this line, thus unable to estimate μ_i and μ_b . In addition, the structure becomes hard to interpret more than 10 km north of the frontal thrust.

Seismic line kr0114-4 is located approximately 10 km east of line kr9806-8. The

geometry of the local bathymetric step is similar to line kr9806-8 (Fig. 4.2b). Seaward of the prism, the incoming sediment is ~1260m, with 790 m accreted and 470 m underthrust (accreted/underthrust ratio = 1.68). The underthrust sediment partially contains the LSB-T unit. The seismic profile shows a gentle (2.8°-3°) angle along the accretionary prism's surface slope. The taper angle at the toe is approximately 5°, increasing to 8.8° toward the north (Table 4.2). The internal structure of the prism is also similar to seismic line kr9806-8 (Fig. 4.4b). The angle of the frontal thrust is 23°, and the angles of the thrusts in the ITZ increase landward to ~28°. At the seaward-most thrust sheet, the angle of the back thrust is 30°. The estimated value for the internal friction coefficient is $\mu_i = 0.75$, and the effective basal friction coefficient is $\mu_b' = 0.28$. The bathymetric relief shows a dip increase landward of the fourth thrust, 10 km north of the frontal thrust.

Seismic line kr0114-3 is located fifteen km east of line kr0114-4, SSW of Kii Peninsula. Along this line the dip of the subducting basement, and the internal structure of the prism are similar to line kr0114-4. The accretionary prism's surface slope has a local bathymetric step 13 km north of the frontal thrust (Figs. 4.2b, 4.4b). The incoming sediment package seaward of the prism is separated by the décollement into 1020 m of accreted sediments and 610 m of underthrust sediments, both thicker than that of seismic

line kr0114-4, but the accreted/underthrust ratio (1.65) and underthrust sediment type are approximately the same. The major differences between seismic lines kr0114-3 and kr0114-4 are 1) the angle of the accretionary prism's surface slope is approximately constant (2°) on line kr0114-3; whereas, it increases to 2.8° toward the north on line kr0114-4, and 2) the local step occurs ~ 10 km from the frontal thrust on line kr0114-3; whereas it occurs ~ 7 km on line kr0114-4. In the ITZ package, the angles of the frontal thrust and the thrust sheets are constant (24°), and the angle of the back thrust is 32° (Fig. 4.4b). The estimated value for the internal friction coefficient is $\mu_i = 0.67$, and the effective basal friction coefficient is $\mu_b' = 0.26$.

THE EASTERN PROVINCE" SEAMOUNT AND RIDGE SUBDUCTION

We present three seismic reflection profiles, kr0114-1, kr0108-5, and ODKM-b from the eastern province to characterize the internal structure of the accretionary prism's toe from the Shiono-misaki Canyon toward the east (Fig. 4.2). The prism in this area is modified by seamount and ridge subduction. The seismic lines have six characteristics in common (Fig. 4.4c); 1) the thickness of the incoming sediment is >1600 m, 2) the incoming sediment sequence is comparable with ODP site 1177; however, the seismic character of

the LSB-T unit differs from the western province (See section 3), 3) the underthrust sediment is associated with the LSB-T unit (Miocene turbidite, ~500 m thick), 4) the basement topography is rough compared with the western province, 5) the prism's taper angle ranges from 6°-8° on a large scale, 6) the prism toe is characterized by two convex upward mounds is approximately 5 km wide.

Seismic line kr0114-1 is located near the Shiono-misaki Canyon, south of the Kii Peninsula. The seismic profile shows two ridges on the outer wedge. Despite the rough bathymetric relief, the regional trend of the accretionary prism's surface slope is approximately 3°. The incoming sediment package (~1620 m), is separated by the décollement into approximately 1110 m of accreted sediments and 510 m of underthrust sediments (the accreted/underthrust ratio = 2.19). The angle of the frontal thrust is 23°, and the angles of the thrusts in the ITZ increase landward to ~24°. We were not able to measure a clear back thrust on this line, thus unable to estimate μ_i and μ_b .

Seismic lines kr0108-5 and ODKM-b are located approximately fifty kilometers east of Shiono-misaki canyon. Compared with seismic line kr0114-1, there is an increase in the amplitude of the relief of the two ridges on these profiles. Moreover, the width of the ridges is 1-2 km greater than that shown in seismic line kr0114-1. The overall angle of

the accretionary prism's surface slope is 4.0° - 4.2° along these seismic lines. Landward of the two ridges, both seismic lines show a local increase in the angle of the accretionary prism's surface slope at the transition zone, similar to line Iline210, followed by a relatively flat forearc basin fill toward the north (Fig. 4.2c). The angle of the frontal thrust is 20° , and increases the angles of the thrusts in the ITZ to $\sim 25^{\circ}$. In line kr0108-5, the angle of the back thrust is 34° (Fig. 4.4c). The estimated value for the internal friction coefficient is $\mu_i = 0.73$, and the effective basal friction coefficient is $\mu_b' = 0.45$. Seaward of the prism, the incoming sediment section is ~ 1640 - 2000 m, with ~ 980 - 1200 m accreted and ~ 660 - 800 m underthrust (accreted/underthrust ratio = 1.48-1.5). Although these two seismic lines are ~ 10 km apart, the total incoming sediment on line ODKM-b is ~ 500 m thicker than on line kr0108-5. The thicker sediment is attributed to a basement low. Comparison of these two lines demonstrates that local basement relief controls incoming sediment thickness.

DISCUSSION

The Coulomb wedge analyses and seismic reflection data presented above illustrate the characteristics of three regions of the outer wedge of the accretionary prism along-strike

of the Nankai Trough. We subdivide the Nankai prism into three regions; “normal” (Western Province), “major ridge subduction” (Central Province), and “ridge and seamount subduction” (Eastern Province). These regions are correlated with the regional provinces of the Shikoku Basin defined by *Ike et al.* [in prep.], based on variations in basement morphology, and the thickness and type of incoming sediments. We compared measurements of incoming, accreted, and underthrust sediment thicknesses to along-strike variations in the prism’s taper angle and friction properties based on internal structure. We also examined sediment type and its affect on the prism. These comparisons allow us to determine which of these factors has the greatest control on the structure of the outer wedge along the entire accretionary prism and within each province, and to understand the relationship between the taper angle and incoming sediment properties controlled by basement relief.

SEDIMENT THICKENSS AND THE OUTER WEDGE

Each province along the Nankai Trough shows unique values for the thickness of incoming sediment, accreted sediment, and underthrust sediment. In this section, we examine the relationships between prism taper angle and these thicknesses. In our study,

the thickness of total incoming sediment is positively correlated with the taper angle (Fig. 4.5, colored in pink). In detail, along the Nankai Trough, ten samples ($n = 10$, degrees of freedom = $n-2 = 8$) show different values of correlation coefficient (r) from the taper angle and the thickness of the accreted sediment ($r = 0.79$, colored in yellow), and the thickness of the underthrust sediment ($r = 0.54$, colored in blue) (Fig. 4.5). Testing for the significance of the correlation coefficient

$$t = r * \text{sqrt}[(n-2)/(1-r^2)]$$

for $r = 0.79$ shows that calculated value ($t = 3.644$) exceeds critical value ($t = 3.355$, level of significance = 0.5%) so the null hypothesis is rejected. Therefore, there is a significant correlation between the taper angle and the thickness of the accreted sediment. On the other hand, the null hypothesis of no relationship can not be rejected for $r = 0.54$, that calculated value ($t = 1.814$) does not exceed critical value ($t = 3.355$, level of significance = 0.5%). Therefore, there is no significant correlation between the taper angle and the thickness of the underthrust sediment. These results suggest that the thickness of the accreted sediment has significant correlation with the taper angle of the outer wedge.

In addition, the majority of accreted sediment is composed of interbedded Quaternary turbidites and hemipelagic clay. Accreted sediment heterogeneity have strong affect on

sediment properties, such as an increase in accreted sediment thickness leads to higher sand-to-clay ratio. Higher sand content may increase permeability; therefore, it will cause friction properties to increase [Kopf and Brown, 2003]. On seismic profile Iline210, we see thin incoming sediment thickness with the lowest internal friction coefficient ($\mu_i = 0.38$); whereas on lines such as kr0114-3/4 and kr0108-5 a thicker incoming sediment package corresponds to a higher internal friction coefficient (0.71-0.73). Assuming relatively constant basal friction along the décollement, these results suggest that thin incoming sediment results in low internal friction within the accretionary prism. The thickness of accreted sediments correlates with the prism's taper angle and internal structure; however, we need to take into account the variations in basal friction properties in order to fully explain the changes in the prism structure.

Here, we examine the effect of friction properties on the prism taper angle (Table. 4.2). Along the Nankai Trough, four samples ($n = 4$, degrees of freedom = $n-2 = 2$) show different values of correlation coefficient (r) from the taper angle of the outer wedge and the internal friction coefficient ($r = 0.72$, colored in pink), and from the taper angle and the effective basal friction coefficient ($r = 0.96$, colored in blue) (Fig. 4.6). Testing for the significance of the correlation coefficient for $r = 0.96$ shows that calculated value ($t =$

4.848) exceeds critical value ($t = 4.303$, level of significance = 2.5%) so the null hypothesis is rejected. Therefore, there is a strong correlation between the taper angle of the outer wedge and the effective basal friction coefficient. On the other hand, the null hypothesis of no relationship can not be rejected for $r = 0.72$, that calculated value ($t = 1.467$) does not exceed critical value ($t = 1.886$, level of significance = 10 %). Therefore, there is very low correlation between the taper angle and the internal friction coefficient. These results suggest that the correlation between the outer wedge taper angle and the effective basal friction coefficient is more reliable than the correlation between the taper angle and the internal friction coefficient. Note that the sample size for correlating frictional properties with other parameters is small ($n = 4$).

UNDERTHRUST SEDIMENT TYPE AND THE OUTER WEDGE

We have shown that the taper angle of the accretionary prism is not correlated with the thickness of the underthrust sediment, although there is a good correlation between taper angle and presence or absence of turbidites in the accreted section. Here, we examine the effect of heterogeneous sediment type on the effective basal friction coefficient (Table. 4.2). We focus more on the presence or absence of LSB-T unit (Miocene turbidites)

because this could affect friction properties at the base of the prism. The effective basal friction coefficient in the central province (0.16), where the LSB-T unit is absent in seismic line Iline210, is significantly lower (approximately half) than the western province (0.39) and eastern half of Shikoku Basin (0.27-0.45) where the LSB-T (Miocene turbidite) is present (Table. 4.2). In the Muroto region, along line Iline210, the narrow taper angle may represent low basal friction controlled by unconsolidated and mud-dominated sediments without Miocene turbidites, in contrast with profiles from Ashizuri and Kumano Basin where turbiditic sands are abundant [Taira *et al.*, 1991; Moore *et al.*, 2001]. The systematic increase in effective basal frictions within the eastern half of Shikoku Basin may represent a decrease of pore pressure along the décollement towards east. These observations indicate that sediment type differences in the underthrust sediments, such as the regional variations in the presence or absence of LSB-T unit, may have strong effect on accretionary prism structure than variations in underthrusting sediment thickness.

Sediment type potentially controls the physical properties of the décollement. Sandy turbidites, overlain by impermeable hemipelagic sediments, allow rapid dewatering and decrease fluid pressure along the décollement [Moore *et al.*, 1990]. We propose that the

presence of high permeability Miocene turbidites in the underthrust sediment package enables drainage, leading to a decrease in pore pressure and an increase in basal friction along the décollement. This results in a higher taper angle at the toe of the accretionary prism.

INFLUENCE OF INCOMING SEDIMENT TYPE ON FRICTIONAL PROPERTIES ALONG THE PLATE BOUNDARY

We have shown that the wedge taper angle is correlated with regional variations in frictional properties within and at the base of the prism. Coulomb wedge theory assumes that the taper angle is a function of both internal (μ_i) and basal friction (μ_b'). Here we focus on the ratio μ_i / μ_b' because it expresses the strength ratio between the décollement zone and the accreted sediment above [Davis and von Huene, 1987; Kukowski et al., 2001]. Our observations show that the ratio is highest in the central province (2.41-2.66), followed by the western province (1.91), and the eastern province (1.62) in the outer wedge (Table 4.2). Correlation coefficient (r) between the μ_i / μ_b' and the taper angle is -0.87 (Fig. 4.7). Testing for the significance of the correlation coefficient in four samples ($n = 4$, degrees of freedom = $n-2 = 2$) shows that calculated value ($t = 2.495$) exceeds

critical value ($t = 1.886$, level of significance = 10%) so the null hypothesis is rejected.

Therefore, there is a correlation between μ_i / μ_b' and the taper angle in the outer wedge

Here we discuss regional variations in the sediment type that affect friction properties, such as the μ_i / μ_b' ratio. The majority of accreted sediment along the Nankai Trough is composed of Quaternary turbidites that come from the Izu-Bonin collision zone [Taira *et al.*, 1991]. Therefore, assuming homogeneous sediments, differences in the internal friction coefficient may indicate local variations in pore pressure or drainage pathways along the faults in the ITZ package. High pore pressure, resulting in low friction coefficients, may be caused by the combination of rapid burial and low sediment permeability related to sediment accretion processes [Saffer and Bekins, 2002]. The high μ_i / μ_b' ratio along seismic line Iline210 suggests that the accreted sediments in this region are not overpressured and are able to drain effectively more than the underthrust sediment. Sediments at the base of the prism are overpressured due to the absence of the Miocene turbidite in the underthrust sediment. On the other hand, the high μ_i / μ_b' ratio along seismic line kr0114-3/4 suggests that accreted sediments in this region are able to drain more than the sediments shown in the line210. These results may indicate that the eastern rim of the Tosa-bae embayment have high drainage system caused by reaccrction

processes compared to the western rim. We argue that the regional differences in both accreted and underthrust sediments friction properties, the μ_i / μ_b ' ratio, may represent the degree of drainage caused by seamount or ridge subduction more than the sediment type within the Central province.

Here we focus on the cause of the decrease in the ratio μ_i / μ_b ' that increases the effective basal friction coefficient by decreasing pore pressure in the western and eastern provinces. Within the underthrust sediment section, the probable source of the Miocene turbidites is southwestern Japan. The sediments were delivered across the trench and deposited on the Shikoku Basin floor [Fergusson, 2003]. Although both the western and eastern provinces have Miocene turbidites in the underthrust sediment, the western province has relatively smooth basement relief compared with the eastern province of the Shikoku Basin [Ike *et al.*, in prep]. The distribution of the Miocene turbidites, preferentially deposited in basement lows, may be uniform throughout the western province; whereas, it may have a patchy distribution in the eastern province due to the rough basement relief. Accretion of homogeneous incoming sediment with constant thickness overlying a flat basement should not create significant variations along-strike of the accretionary prism's surface slope [Calassou *et al.*, 1993]. The uniformly distributed

Miocene turbidites in the western province may have a well connected network allowing for the dewatering of underthrust sediments. The μ_i / μ_b ' ratio is lower in the eastern province than in the western province, suggesting that the variable basement topography and heterogeneous sediment distribution may result in less drainage from accreted sediment or higher drainage from underthrust sediment and decreased overpressuring along the décollement. Therefore, the heterogeneous incoming sediment properties controlled by the basement relief in turn control variations in the friction properties along the prism's base. Therefore, basement topography, which controls sediment distribution within each region of the Nankai Trough, is a primary control on the structure of the accretionary prism.

MODIFICATION OF THE PRISM BY SUBDUCTION OF SEAMOUNTS AND RIDGES

We have shown that the regional variations in basement topography control the thickness and type of subducting sediments, which, in turn, affect the frictional properties at the base of the prism as well as the prism's taper angle. Subducting basement relief also directly affects the structure of the accretionary prism. The relative ramps and flats of the

outer wedge indicate that either the deformation history of recent subduction materials has changed material properties of the internal prism. These changes in material properties may no longer hold the non-cohesive assumption. Here, we compare the local bathymetric relief along the outer wedge and transition zone within the three provinces and discuss the regional differences in the structure of the accretionary prism in relation to basement topography without assuming non-cohesive Coulomb wedge theory.

In the western province, the Nankai prism is characterized by a relatively high, uniform taper angle and landward increase in the displacement of faults in the outer wedge. No large seamounts or ridges are subducted in this region and incoming sediments of uniform thickness and type overlie smooth basement (Fig. 4.1a). We therefore refer to this province as a “normal prism” that approximates the ideal accretionary prism created in sandbox models in the absence of large bathymetry relief. The accretion of uniform sediments over time maintains the morphology of the normal prism.

In comparison, the accretionary prism in the central province is affected by the subduction of young and large topographic features, such as seamounts, ridges, and large basement lows along the Kinan Seamount Chain. Periodically, young seamounts and

ridges covered by relatively thin pelagic sediments collide into the accretionary prism. As these topographic features approach the trench, the Quaternary trench turbidites are channeled around them, so there will be no accretion of Quaternary turbidites to the prism. The subduction of seamounts may locally uplift the toe of the overriding plate, which then collapses as the seamount passes under the slope, forming an embayment [e.g., *Dominguez et al.*, 2000]. The material that is eroded from the accretionary prism's surface slope may reaccumulate into the prism seaward of the subducting seamount. The process of sediment erosion and reaccumulation may create different frictional properties within the accreted sediment section of the prism. For instance, the eroded sediments from the prism toe may not be well sorted with respect to the trench wedge turbidites that normally transport a long distance along the Nankai Trough. Assuming constant effective basal friction relative to the internal friction in the prism, difference in the initial condition of the internal friction or accreted sediment thickness, based on the discussion above, may cause to form a local bathymetric high in the accretionary prism's surface slope. In this area, there is a local change in the prism's thickness at the step without a large corresponding change in the prism's taper angle (Fig. 4.2b). Along-strike and along-dip variations in incoming sediment type, related to large topographic features,

especially the periodic presence or absence of Quaternary turbidites, may cause the development of the step feature visible in the prism of the central province.

The eastern province is an intermediate case between the central province's rough topography and variable sediment thickness and type, and the western province's smooth and uniform sediments. The accretionary prism in the eastern province is affected by the subduction of relatively old, small seamounts and ridges that are covered by thick hemipelagic sediments [Park et al, 2003; Ike et al, in prep]. Because of the smaller size of these features, it is less likely that the Quaternary turbidites will completely bypass the seamounts and ridges in the trench as they do in the central province. The same seamount collision processes may affect both the central and eastern province; however, the scale of disturbance and erosion of the accretionary prism's surface slope should be smaller in the eastern province not only because the size of the topographic highs but also because of the large amount of sediments deposited over them. The characteristics of the prism in the eastern province may be caused by the subduction of seamounts and ridges associated with thick and relatively uniform sediments, causing periodic erosion and reaccretion of material to the accretionary prism's surface slope on a smaller scale than the central province. This accretion process may be one of the causes for developing the

large bathymetric relief, visible in the eastern province. Distinct from the western and central provinces, the approximation line over the accretionary prism's surface slope cuts through two bathymetric ridges in the eastern province (Fig. 4.2c). Each ridge has a large thrust package formed by multiple thrusts associated with difference in displacement (Fig. 4.4c). The process of sediment erosion and reaccrion in the eastern province may create different frictional properties within the accreted sediment section, in a smaller scale than the central province. These local differences in friction properties may cause non-linear increase in displacement along the thrusts within the outer wedge. We propose that local variations in incoming basement relief, primarily the subduction of seamounts and ridges, have significant effect on the development of the accretionary prism; and therefore, the morphology of the accretionary prism's surface slope along the Nankai Trough.

CONCLUSIONS

Our data indicate that accreted and underthrust sediments have significant control on the geometry of the Nankai Trough accretionary prism. The conceptual model of a critically tapered wedge has been modified to take into account the heterogeneity of the incoming sediment sequence and explain significant variations in the along-strike structure of the prism. Perhaps the most important result of this study is the along-strike comparison of the incoming sediment thickness, accreted thickness, and underthrust thickness associated with the internal structure, critical taper angle, internal friction coefficient, and effective basal friction coefficient of the prisms in a single subduction zone. We define three prism styles: "normal", "major ridge subduction", and "ridge and seamount subduction" along the outer wedge. These varieties of prism style, deformation pattern, and taper angle are best explained by the initial condition of the accreted sediment thickness, underthrust sediment type, and local basement relief on the subducting plate.

ACKNOWLEDGMENTS

We thank the Captain and crew of the R/V Kaiyo for assistance in obtaining the seismic reflection data presented in this paper. We thank Gaku Kimura for discussions and a critical review of an earlier review of this manuscript. We greatly appreciate JAMSTEC for providing seismic data.

TABLES

Table 4.1 Seismic Reflection Data Acquisition and Processing Parameters

Acquisition Parameters

Survey initial	Iline210	ODKM	KR
Survey vessel	R/V <i>Ewing</i>	M/V <i>Polar Princess</i>	R/V <i>Kairei</i>
Recording year	1999	2003	~2001
Seismic source	Tuned air-gun array	Tuned air-gun array	Non-tuned air-gun array
Gun volume, l, in3	70, 4276	70, 4240	~196, ~12,000
Shot interval, m	50	50	50
Number of channels	240	480	~156
Channel interval, m	25	12.5	25

Processing sequence

Spiking Deconvolution	Bandpass Filter
Bandpass Filter	(3-5-100-120Hz)
(12-24-100-150Hz)	deconvolution
deconvolution	Spike & Noise Edit
Velocity analysis	Velocity analysis
Dip moveout	Normal moveout
correction (DMO)	correction (NMO)
NMO	Mute
Mute	Stack(by JAMSTEC)
Stack	F-K time migration
F-K time migration	Depth conversion
Depth conversion	

Table. 4.2

Line #	kr9810-1	lline210	kr0114-3/4	kr0108-5
Province	Western	CentralWest	CentralEast	Eastern
Alpha [°]	4	1.5	2.5	4.2
Beta [°]	1.5	2	2	3
Taper [°]	5.5	3.5	4.5	7.2
fore thrust [°]	20	28	23.5	20
error	±0.5	±0.5	±0.5	±0.5
back thrust [°]	33	41	31	34
error	±0.5	±0.5	±0.5	±0.5
θ [°]	37	21	35.5	36
error	±1.0	±1.0	±1.0	±1.0
ψ [°]	8	8.5	5.75	10
μ_i	0.75	0.38	0.71	0.73
error	±0.027, 3.6%	±0.020, 5.2%	±0.026, 3.6%	±0.026, 3.5%
μ_b'	0.39	0.16	0.27	0.45
error	±0.021, 5.3%	±0.011, 6.8%	±0.015, 5.5%	±0.024, 5.3%
μ_i/μ_b	1.91	2.41	2.66	1.62
sediment thickness [m]				
total	1350	1160	1445	1650
accreted	890	680	905	990
underthrust	460	480	540	660
underthrust turbidite	present	absent	present	present

FIGURES

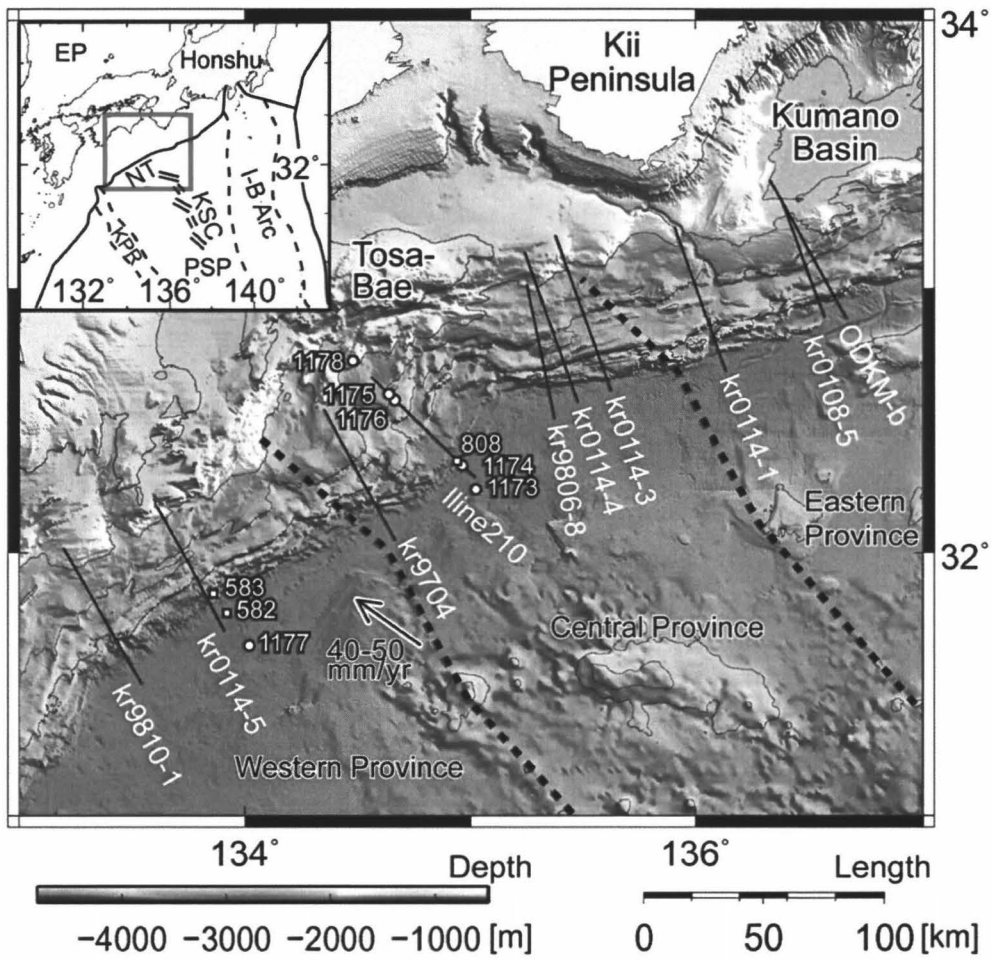


Fig. 4.1(a) Regional bathymetric map showing the location of the seismic lines (solid lines) used in this study. Contour intervals are 1000 m. ODP Leg 190 (solid circles) and previous ODP/DSDP drill sites (solid squares) are shown in numbers. The heavy dashed lines are the boundaries of the basement provinces within the Philippine Sea plate. Insert box is showing the tectonic map of the Philippine Sea Plate (PSP), and Japan Arcs. EP: Eurasian Plate, I-B Arc: Izu-Bonin Arc, KSC: Kinan Seamount Chain, KPR: Kyushu-Palau Ridge.

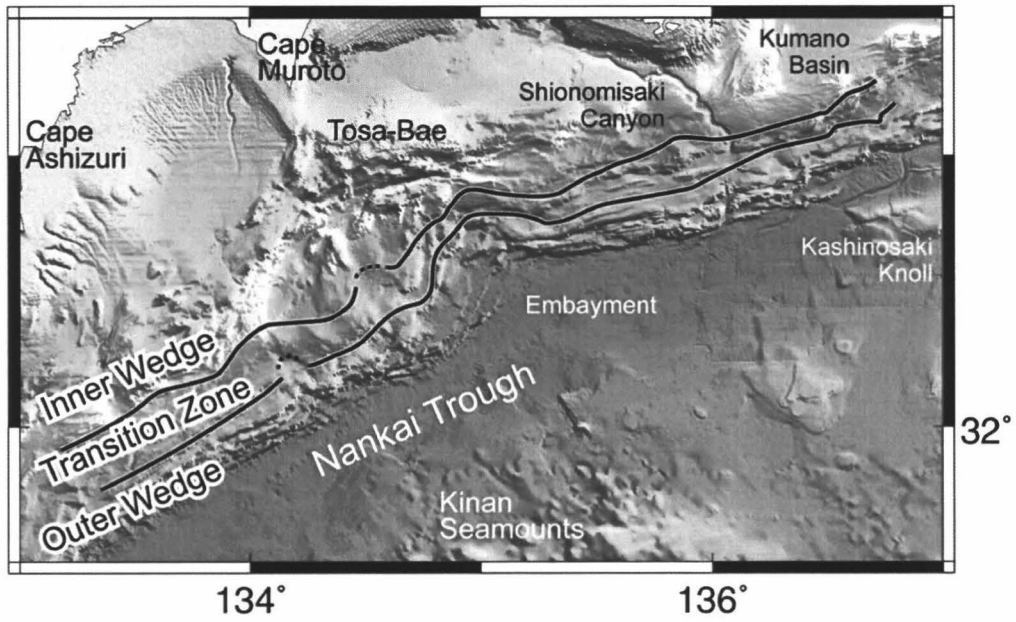


Fig. 4.1(b)

Regional bathymetric map showing the distribution of Inner wedge, Transition zone, and Outer wedge defined by *Kimura et al.*, [2007].

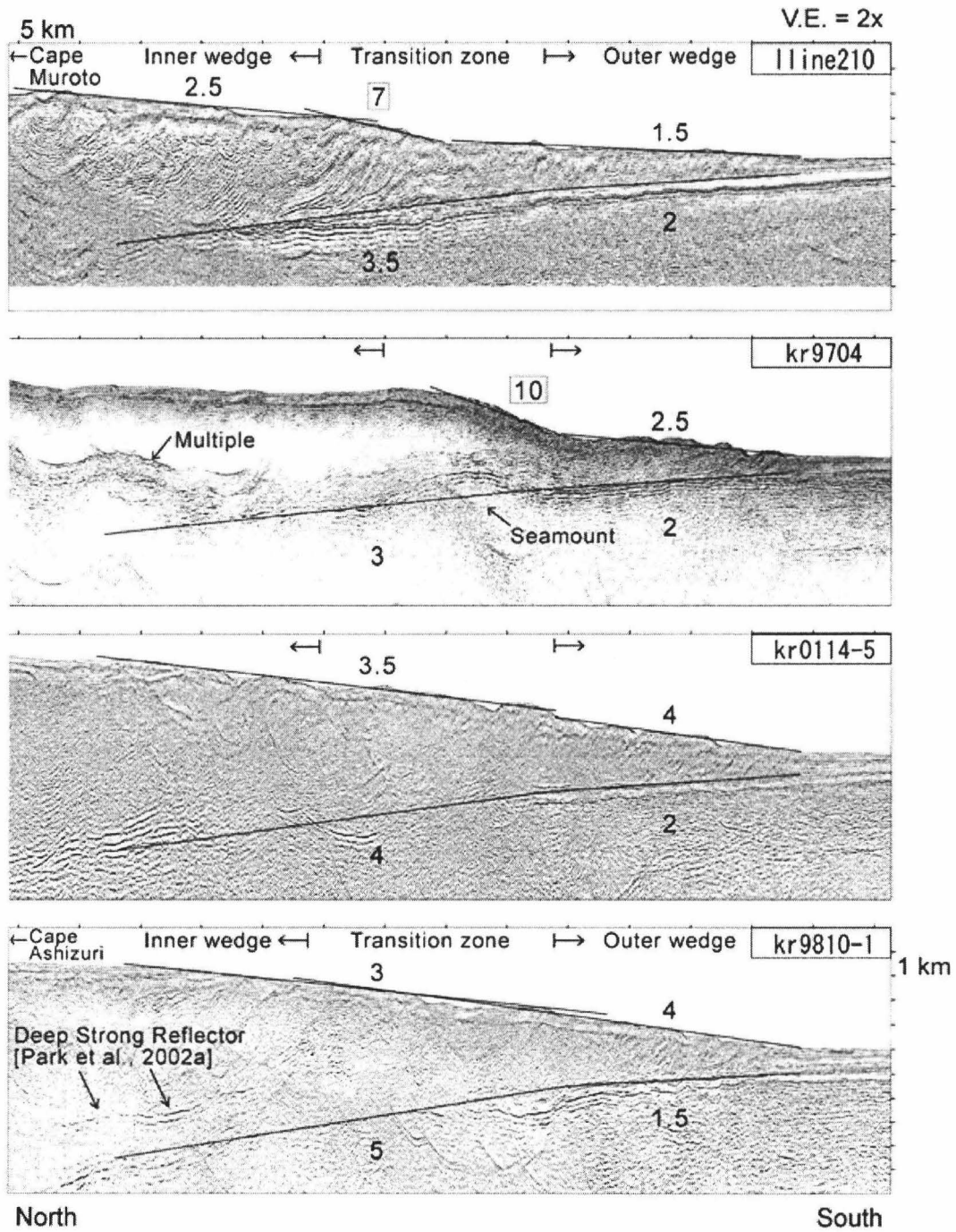


Fig. 4.2(a) Depth converted seismic reflection profiles showing approximation lines for the accretionary prism's surface slope and the base of the accretionary prism. Vertical scale is in depth. Vertical exaggeration is 2.0 in these profiles. Over the accretionary prisms, numbers show the angle of the approximation lines. The numbers with squares indicate the angle of local approximation lines. (a) The western province and kr9704 and Iline 210 from the central province.

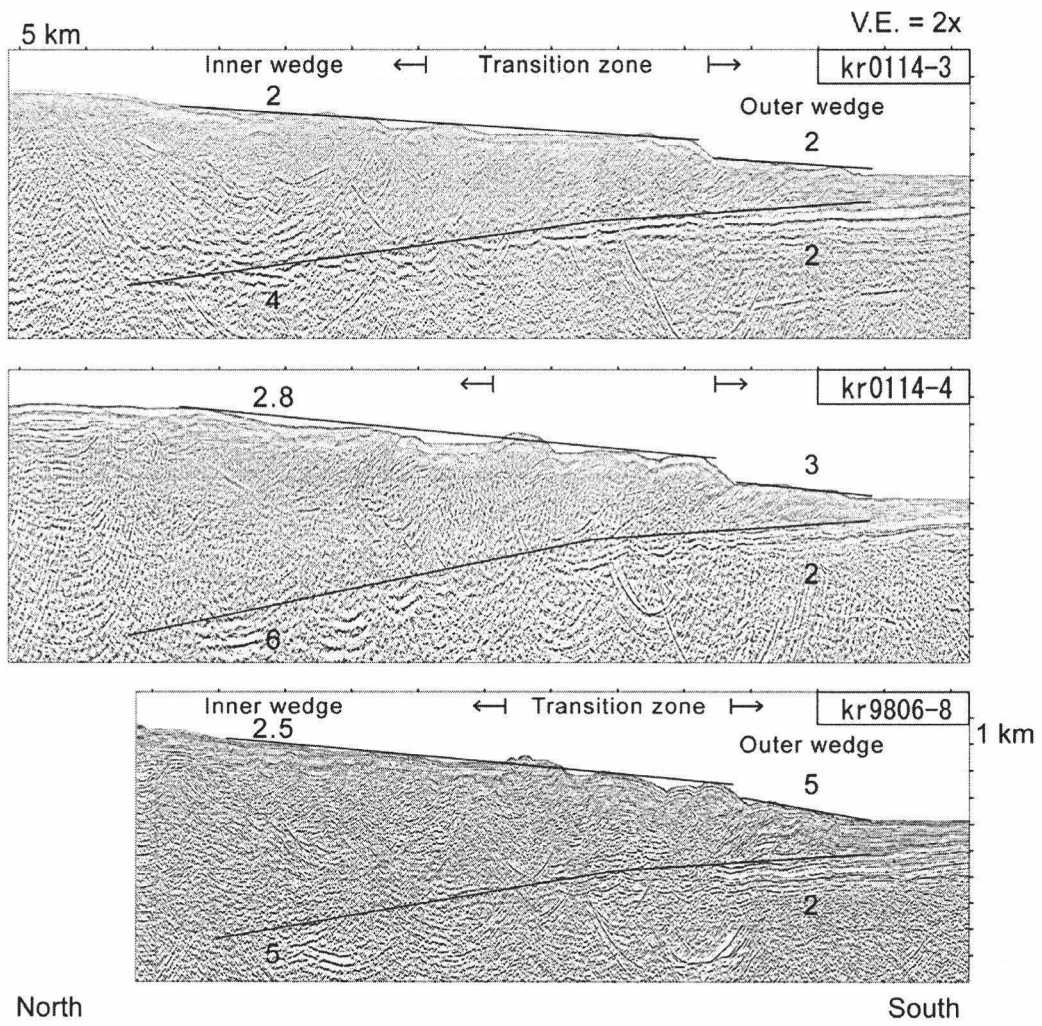


Fig. 4.2(b) Depth converted seismic reflection profiles showing approximation lines for the accretionary prism's surface slope and the base of the accretionary prism. Vertical scale is in depth. Vertical exaggeration is 2.0 in these profiles. Over the accretionary prisms, numbers show the angle of the approximation lines. The numbers with squares indicate the angle of local approximation lines. (b) the central province.

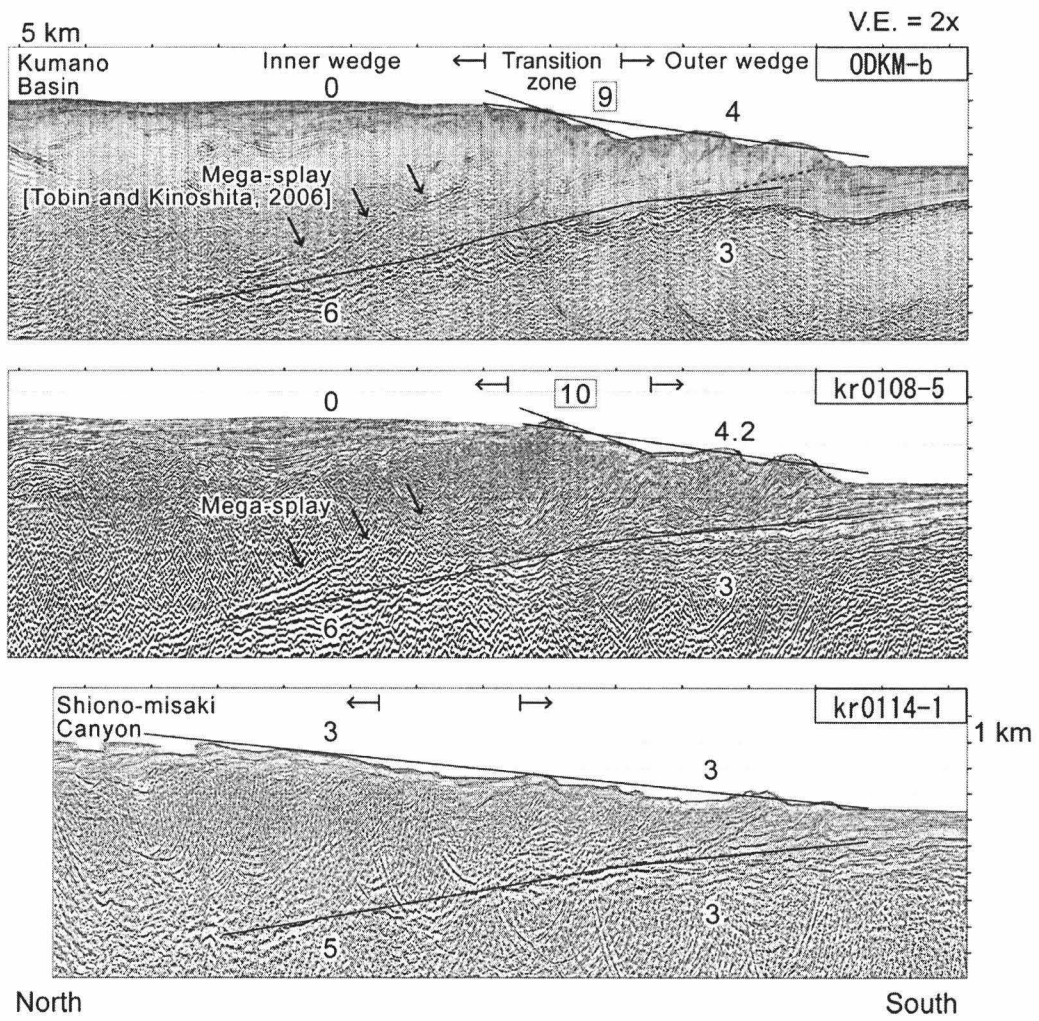


Fig. 4.2(c) Depth converted seismic reflection profiles showing approximation lines for the accretionary prism's surface slope and the base of the accretionary prism. Vertical scale is in depth. Vertical exaggeration is 2.0 in these profiles. Over the accretionary prisms, numbers show the angle of the approximation lines. The numbers with squares indicate the angle of local approximation lines. (c) the eastern province.

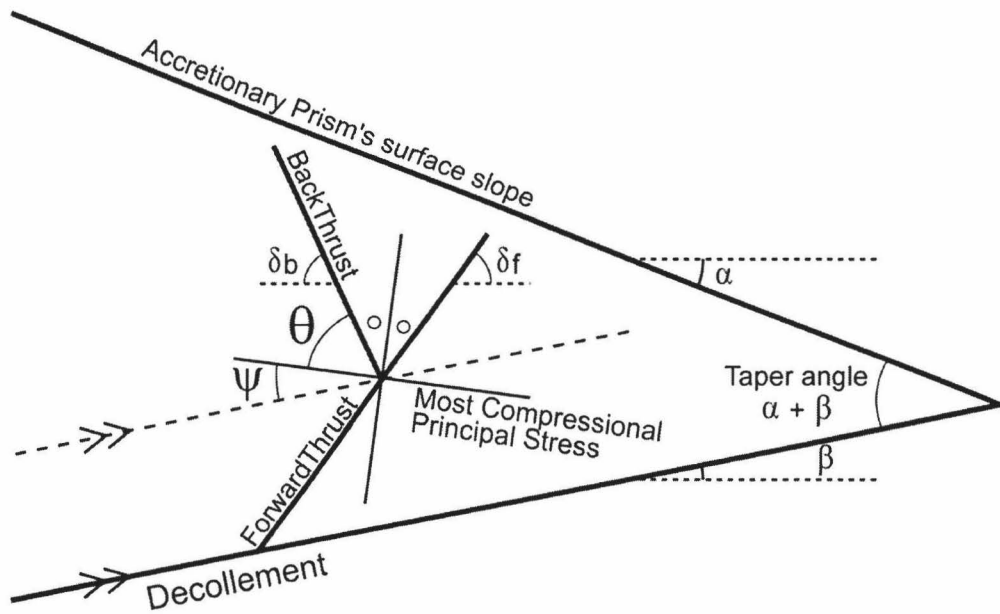


Fig. 4.3

Cartoon illustration of a critical or stable wedge coordinate system based on a similar figure by *Davis and Huene*, [1987]. Parameters include surface slope α , basal dip β , the geometrical determination of the internal friction θ , and the direction of maximum compressive stress relative to the décollement ψ .

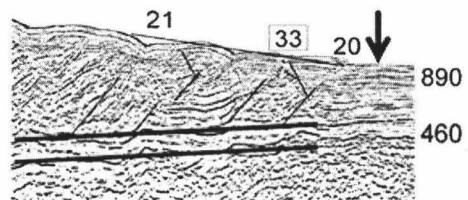
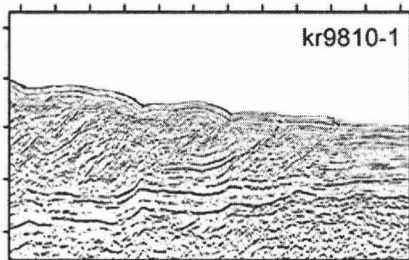
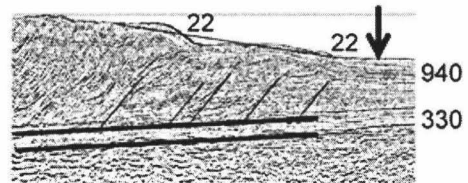
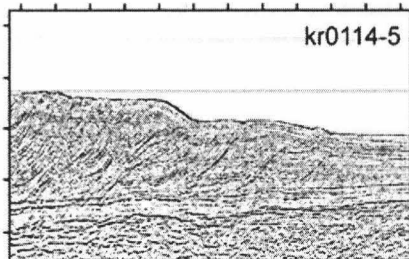
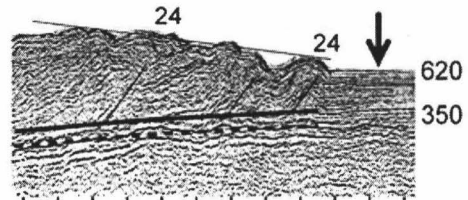
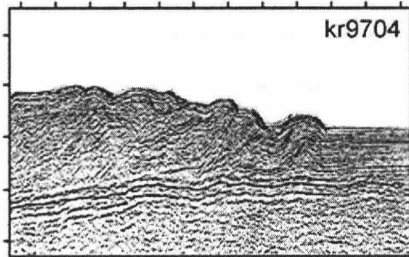
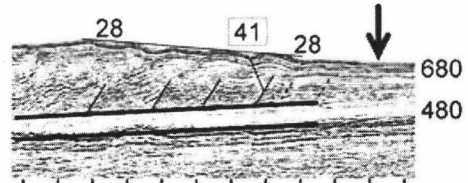
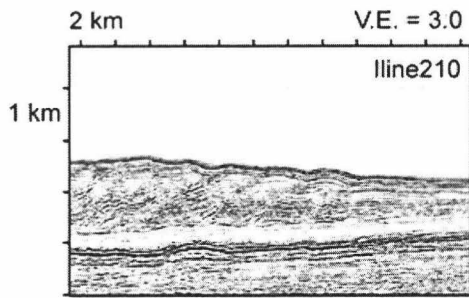


Fig. 4.4(a) Parts of the seismic profiles focusing the toe structure of the accretionary prism. Vertical scale is in depth and the vertical exaggeration is 3.0. Along the surface of the prism, seaward-dipping linear lines indicate the approximation lines for the accretionary prism's surface slope. Thin linear lines within the prism indicate the angle of the forward and back thrusts. Numbers over the prism indicate the angle of the forward thrusts; whereas, the numbers in a square box indicate the angle of the back thrusts. Thick linear lines (partially dotted) at the base of the prism indicate the angle of the décollement and the basement trend. On the seaward of the prism, the down pointing black-arrow indicates the location of the measured incoming sediment thickness for each seismic profile. (a) The western province and kr9704 and Iline 210 from the central province

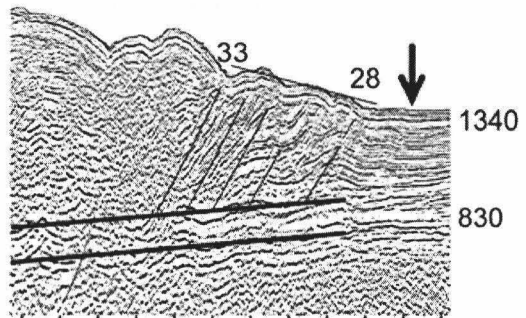
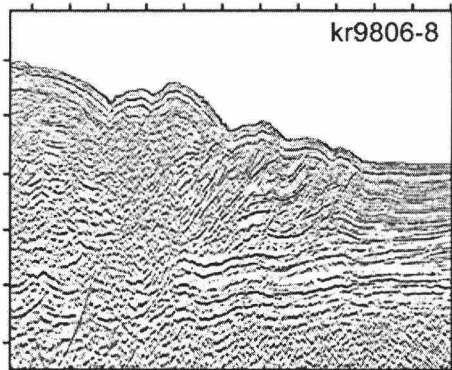
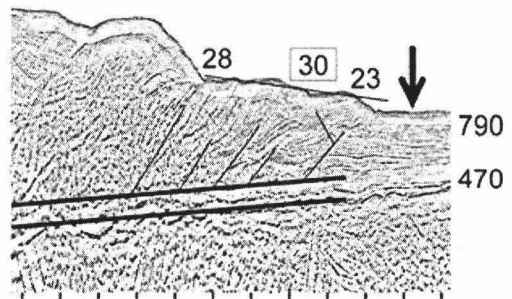
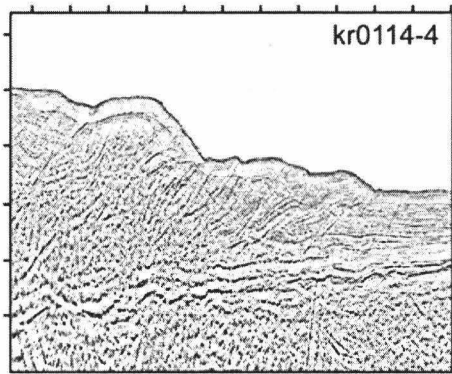
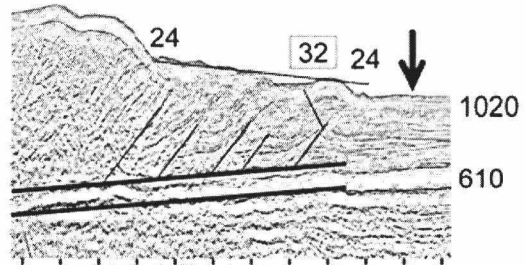
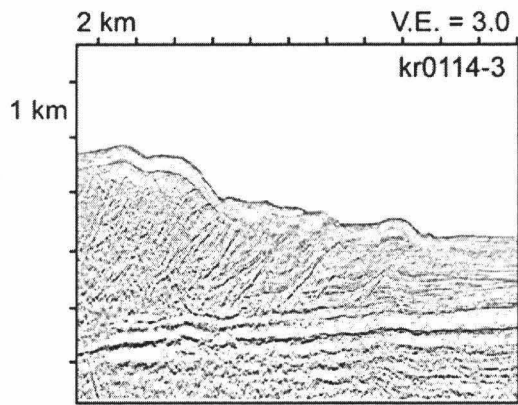


Fig. 4.4(b) Parts of the seismic profiles focusing the toe structure of the accretionary prism. Vertical scale is in depth and the vertical exaggeration is 3.0. Along the surface of the prism, seaward-dipping linear lines indicate the approximation lines for the accretionary prism's surface slope. Thin linear lines within the prism indicate the angle of the forward and back thrusts. Numbers over the prism indicate the angle of the forward thrusts; whereas, the numbers in a square box indicate the angle of the back thrusts. Thick linear lines (partially dotted) at the base of the prism indicate the angle of the décollement and the basement trend. On the seaward of the prism, the down pointing black-arrow indicates the location of the measured incoming sediment thickness for each seismic profile. (b) The central province.

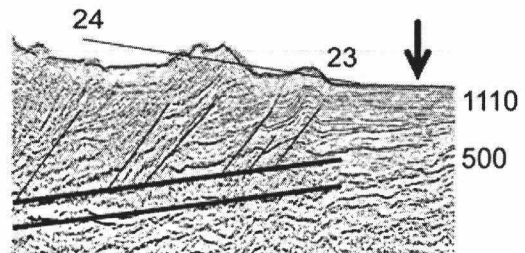
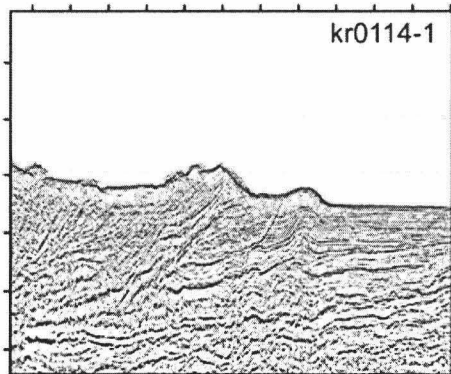
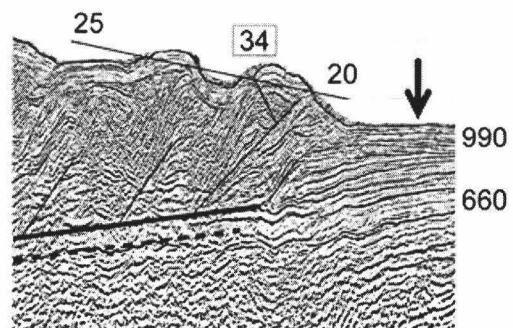
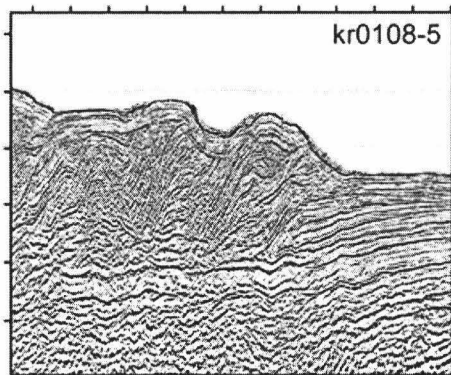
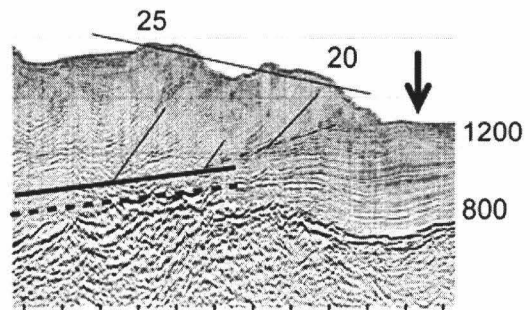
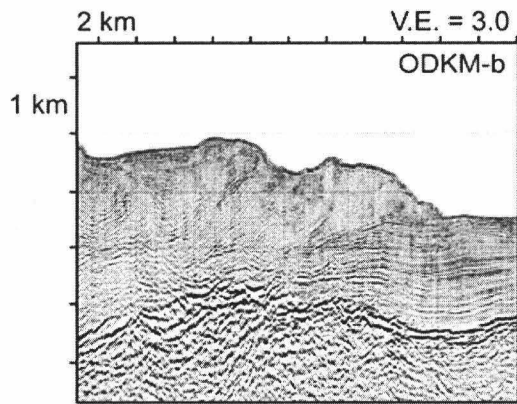


Fig. 4.4(c) Parts of the seismic profiles focusing the toe structure of the accretionary prism. Vertical scale is in depth and the vertical exaggeration is 3.0. Along the surface of the prism, seaward-dipping linear lines indicate the approximation lines for the accretionary prism's surface slope. Thin linear lines within the prism indicate the angle of the forward and back thrusts. Numbers over the prism indicate the angle of the forward thrusts; whereas, the numbers in a square box indicate the angle of the back thrusts. Thick linear lines (partially dotted) at the base of the prism indicate the angle of the décollement and the basement trend. On the seaward of the prism, the down pointing black-arrow indicates the location of the measured incoming sediment thickness for each seismic profile. (c) The eastern province.

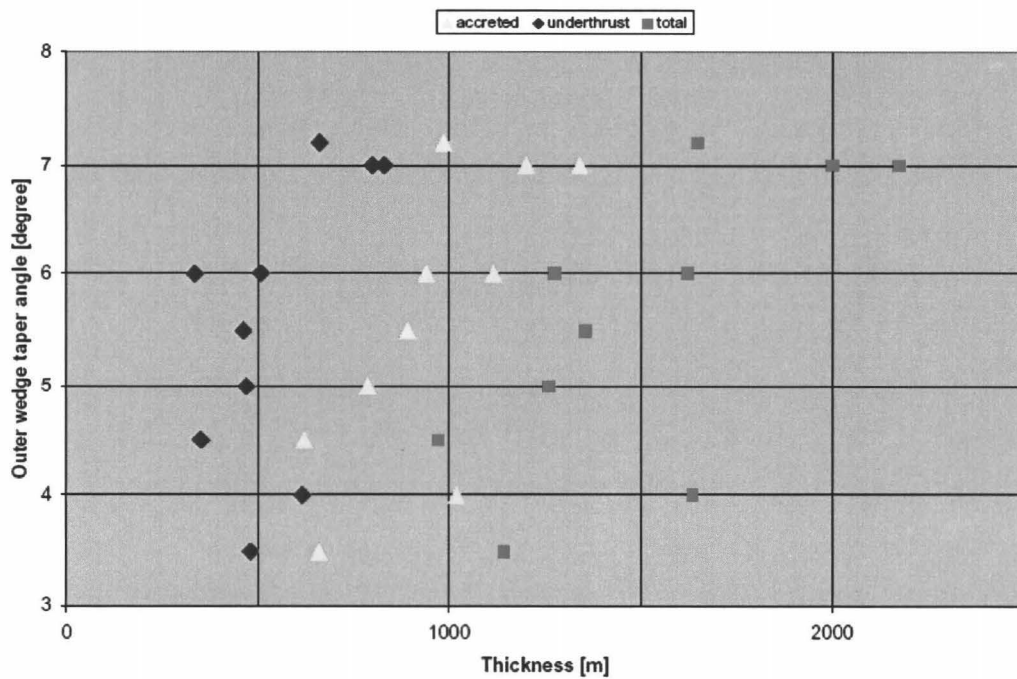


Fig. 4.5

Plotted the relationship between the sediment thickness and taper angle. Yellow triangles represent the relationship between the thickness of the accretion section and the angle of the outer wedge taper which correlation coefficient is 0.79. Blue diamonds represent the relationship between the thickness of the underthrust section and the angle of the outer wedge taper which correlation coefficient is 0.51. Pink squares represent the relationship between the thickness of the total sediment thickness and the angle of the outer wedge taper which correlation coefficient is 0.73.

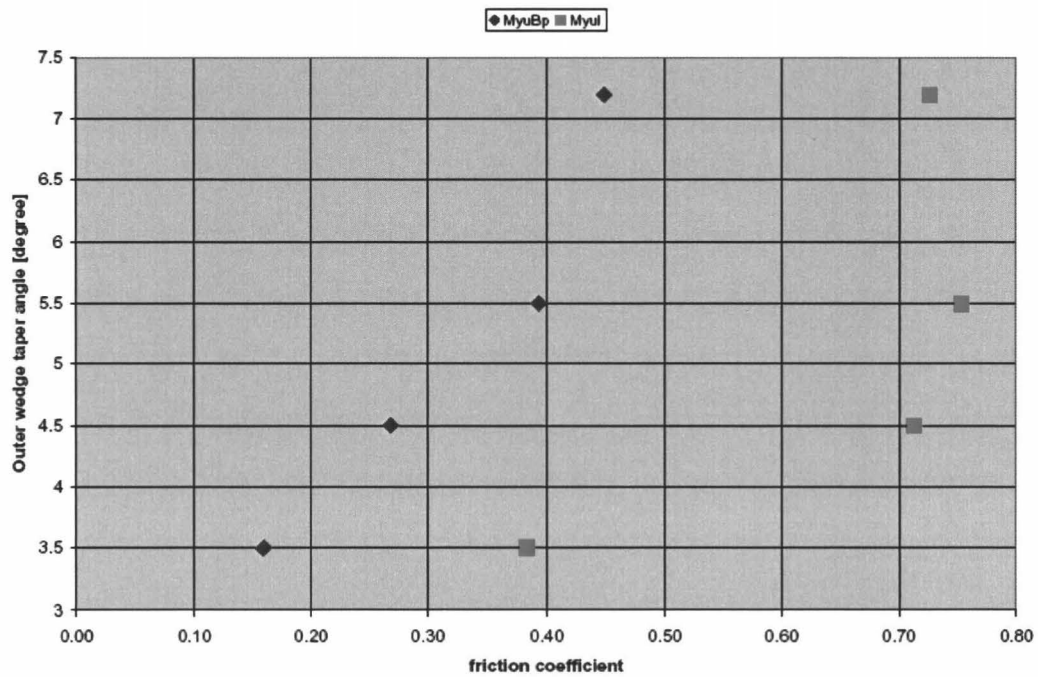


Fig. 4.6

Plotted the relationship between the taper angle of the outer wedge and effective basal friction coefficient (μ_b' , MyuBp) and internal friction coefficient (μ_i , MyuI). The correlation coefficient between the taper angle of the outer wedge and the internal friction coefficient is 0.72 (colored in pink), and the coefficient between the taper angle and the effective basal friction coefficient is 0.96 (colored in blue).

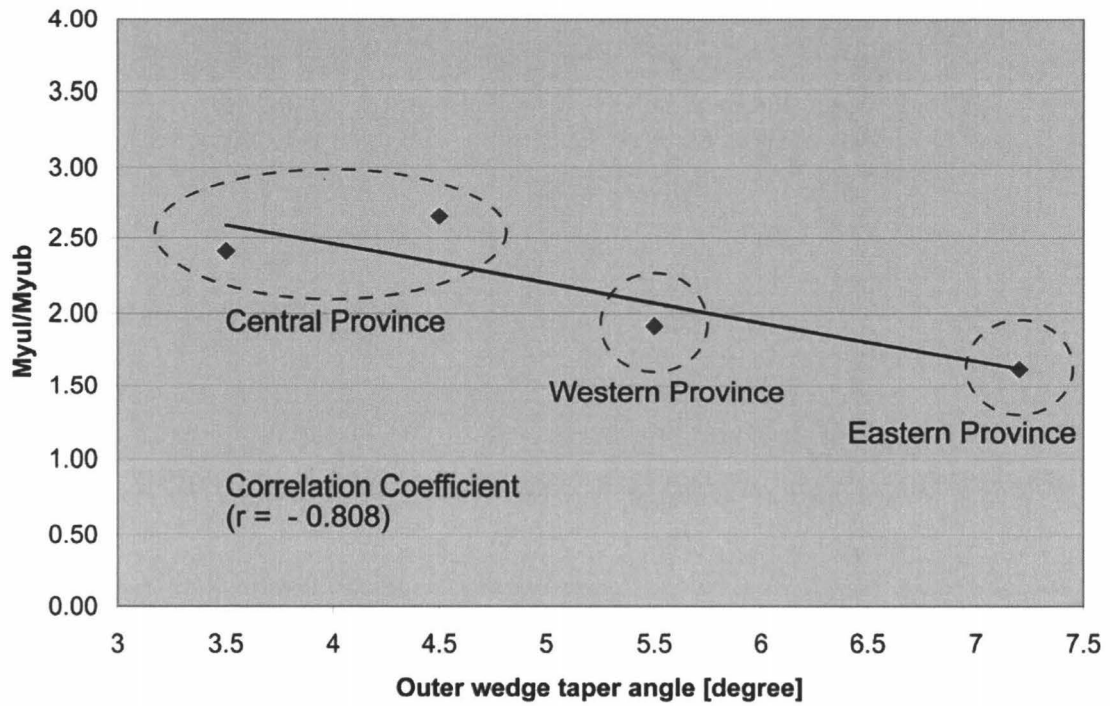


Fig. 4.7

Plotted the relationship between the internal friction to effective basal friction ratio (μ_i / μ_b' ratio) and the outer wedge taper angle that correlation coefficient is -0.87.

REFERENCES

- ALEXANDER J. & MORRIS S. 1994. Observations on experimental, nonchannelized, highconcentration turbidity currents and variations in deposits around obstacles, *Journal of Sedimentary Research*, **A64**, 899-909.
- ANDO M. 1975. Source mechanisms and tectonic significance of historical earthquakes along the Nankai trough, *Tectonophysics*, **27**, 119-40.
- AOIKE K. 1999. Tectonic evolution of the Izu Collision Zone. *Research Report of the Kanagawa Prefectural Museum of Natural History*, **9**, 113-151.
- AOKI Y. TAMANO T. & KATO S. 1982. Detailed structure of the Nankai Trough from migrated seismic sections. Studies in Continental Margin Geology. *American Association of Petroleum Geologists Memoir*, **34**, 309-22.
- AOKI Y. KINOSHITA H. & KAGAMI H. 1986. Evidence of a low-velocity layer beneath the accretionary prism of the Nankai Trough: Inference from a synthetic sonic log, *Initial Rep. Deep Sea Drill. Proj.*, **87**, 727-35.
- Ashi, J., Tokuyama H., Yamamoto F., Uyeki T., Tukioka H. & Taira a. 1989. Detailed surface features of the Nankai accretionary prism obtained by IZANAGI ocean floor imaging sonar system, *Program Abstr. Seismol. Soc. Jpn.*, **2**, 305.
- BABA T. & CUMMINS P. R. 2005. Contiguous rupture areas of two Nankai Trough earthquakes revealed by high-resolution tsunami waveform inversion, *Geophysical Research Letters*, **32**, L08305, doi:10.1029/2004GL022320.
- BANGS, N.L., TAIRA A., KURAMOTO S., SHIPLEY T. H., MOORE G. F., MOCHIZUKI K., GULICK S. S., ZHAO Z., NAKAMURA Y., PARK J.-O., TAYLOR B. L., MORITA S., ITO S., HILLS D. J., LESLIE S. C., ALEX C. M., MCCUTCHEON A. J., IKE T., YAGI H., & TOYAMA G. 1999. U.S.-Japan Collaborative 3-D seismic investigation of the Nankai Trough plate boundary interface and shallowmost seismogenic zone. *EOS*, **80**, F569.
- BEKINS B.A., & DREISS S. J. 1992. A simplified analysis of parameters controlling dewatering in accretionary prisms, *Earth Planet.Sci.Lett.* **109**, 275-87.
- BILEK S.L. & LAY T. 2002. Tsunami earthquakes possibly widespread manifestations of frictional conditional stability. *Geophysical Research Letters*, **29**, p. art. no.-1673.
- BILEK S.L., SCHWARTZ S.Y. and DESHON, H.R. 2003. Control of seafloor roughness on earthquake rupture behavior. *Geology* **31**, 455-8.
- BILEK S. 2007. Influence of subducting topography on earthquake rupture: MARGINS

- volume, chap 5, in press.
- BRAY C. J., & KARIG D. E. 1985. Physical properties of sediments from the Nankai Trough, Deep Sea Drilling Project Leg 87A, Sites 582 and 583. *Initial Reports, DSDP* (edited by Kagami, H., Karig, D.E., Coulobourn, W.T., et al.). (U.S. Govt. Printing Office) Washington, **87**, 827-42.
- BYERLEE J. 1978. Friction of rocks, *Pure Appl. Geophys.* **116**, 615–26.
- CADET J.P., KOBAYASHI K., AUBOUIN J., BOULEGUE J., ET AL. 1987. The Japan Trench and Its Juncture with the Kuril Trench: Cruise Results of the Kaiko Project, *Earth and Planetary Science Letters*, **83**, 267-84.
- CALASSOU S., LARROQUE C. & MALAVIEILLE J. 1993. Transfer zones of deformation in thrust wedges: An experimental study, *Tectonophysics*, **221**, 325-44.
- CARESS D.W. & CHAYES D. N. 1996. Improved processing of Hydrosweep DS multibeam data on the R/V Maurice Ewing, *Marine Geophysical Researches*, **18**, 631-50
- CHAMOT-ROOKE, N., RENARD V. & LE PICHON X. 1987. Magnetic anomalies in the Shikoku basin: a new interpretation. *Earth and Planetary Science Letters*, **3**, 214-28.
- CLIFT, P., VANNUCCHI P. 2004. Controls on tectonic accretion versus erosion in subduction zones: Implications for the origin and recycling of the continental crust, *Rev. Geophys.*, **42**, RG2001, doi:10.1029/2003RG000127.
- CLOOS M. 1992. Thrust-type subduction zone earthquakes and seamount asperities: A physical model for seismic rupture, *Geology*, **20**, 601-4.
- CLOOS M. & SHREVE R. L. 1996. Shear-zone thickness and the seismicity of Chilean- and Marianas-type subduction zones, *Geology*, **24**, 107-10.
- COSTA PISANI, P., RESHEF M. & MOORE G. 2005. Targeted 3-D prestack depth imaging at Legs 190-196 ODP drill sites (Nankai Trough, Japan), *Geophys. Res. Lett.*, **32**, L20309, doi:10.1029/2005GL024191.
- DAHLEN F. A. 1984. Noncohesive critical Coulomb wedges: An exact solution. *J. Geophys. Res.*, **89**, 10,125-33.
- DAHLEN F. A. 1990. Critical Taper Model of Fold-and-Thrust Belts and Accretionary Wedges. *Annu. Rev. Earth Planet Sci.*, **18**, 55-99.
- DAVIS D., SUPPE J. & DAHLEN F. A. 1983. Mechanics of Fold-and-Thrust Belts and Accretionary Wedges, *J. Geophys. Res.*, **88**, 1153-72.
- DAVIS D. M., & VON HUENE R. 1987. Inferences on sediment strength and fault

- friction from structures at the Aleutian trench, *Geology*, **15**, 517-22.
- DE ROSA R., ZUFFA, G.G., TAIRA, A. & LEGGETT, J.K. 1986. Petrography of trench sands from the Nankai Trough, southwest Japan: implications for long-distance turbidite transportation. *Geological Magazine*, **123**, 477-86.
- DOMINGUEZ S., LALLEMAND S.E., MALAVIEILLE J. & VON HUENE R. 1998. Upper plate deformation associated with seamount subduction. *Tectonophysics*, **293**, 207-24.
- DOMINGUEZ S., MALAVIEILLE J. & LALLEMAND S.E. 2000. Deformation of accretionary wedges in response to seamount subduction: Insights from sandbox experiments, *Tectonics*, **19**, 1, 182-96.
- FERGUSON C. L. 2003. Provenance of Miocene, Pleistocene turbidite sands and sandstones, Nankai Trough, Ocean Drilling Program Leg 190. *Proceedings of the Ocean Drilling Program, Scientific Results*, **190/196**, 1-28 [online]. Available from: <http://www-odp.tamu.edu/publications/190196sr/205/205htm>
- GEOLOGICAL SURVEY OF JAPAN, 2000. *Gravity CD-ROM of Japan* [CD-ROM].
- GEOLOGICAL SURVEY OF JAPAN, 1996. *Magnetic Anomaly Map of East Asia 1:4,000,000* [CD-ROM], Ibaraki, Japan.
- GUTSCHER M. A., KUKOWSKI N., MALAVIEILLE J. & LALLEMAND S. E. 1998. Episodic imbricate thrusting and underthrusting; analog experiments and mechanical analysis applied to the Alaskan accretionary wedge. *J. Geophys. Res.*, **103(5)**, 10,161-176.
- GUTSCHER M. A., KLAESCHEN D., FLUEH E. R. & MALAVIEILLE J. 2001. Non-Coulomb wedges, wrong-way thrusting, and natural hazards in Cascadia. *Geology*, **29**, 379-82.
- HARRIS R. A. 1998. Introduction to special section: Stress triggers, stress shadows, and implications for seismic hazard, *J. Geophys. Res.*, **103**, 24,347-58.
- HIBBARD J. P. & KARIG D. E. 1990. Alternative plate model for the early Miocene evolution of the Southwest Japan margin, *Geology*, **18**, 170-74.
- HICKMAN S., SIBSON R. & BRUHN R. 1995. Introduction to Special Section - Mechanical Involvement of Fluids in Faulting: *Journal of Geophysical Research*, **100**, 12831-40.
- HORI T. 2006. Mechanisms of separation of rupture area and variation in time interval and size of great earthquakes along the Nankai Trough, southwest Japan, *J. Earth*

- Simulator*, **5**, 8–19.
- HOSHINO K. & Kato H. 2001. C.f.C.o.E. Data, Handbook of Mechanical Properties of the Japanese Rocks under High Confining Pressure, Geological Survey of Japan, AIST, 479 pp.
- ISHII T., SATO H., MACHIDA S., HARAGUCHI S., USUI S., ISHIZUKA O., TANIGUCHI H. & YAGI K. 2000. Geological and petrological studies of the Kinan and Izu-Ogasawara-backarc-echelon seamounts Chains, *Bulletin of the Geological Survey of Japan*, **51**, 615-30.
- KAIKO I RESEARCH GROUP, 1986. Topography and Structure of Trenches around Japan – Data Atlas of Franco-Japanese Kaiko Project, Phase I, Univ. of Tokyo Press, Tokyo.
- KAIZUKA S. 1975. A tectonic model for the morphology of arc-trench systems, especially for the echelon ridges and midarc faults, *Japanese Journal of Geology and Geography*, **45**, 9-28.
- KANAMORI H. & BRODSKY E. E. 2004. The physics of earthquakes, *Reports on Progress in Physics*, **67** 1429-1496, doi:10.1088/0034-4885/67/8/R03
- KARIG D. E. & INGLE, J. C. JR. 1975. *Initial Reports of the Deep Sea Drilling Project*, **31**, Washington: U.S. Government Printing Office.
- KERR B.C., SCHOLL D. W. & KLEMPERER S. L. 2005. Seismic stratigraphy of Detroit Seamount, Hawaiian-Emperor seamount chain: Post-hot-spot shield-building volcanism and deposition of the Meiji drift, *Geochemistry, Geophysics, and Geosystems*, **6**, Q07L10, doi:10.1029/2004GC000705.
- KIMURA J., STERN R. J. & YOSHIDA T. 2005. Reinitiation of subduction and magmatic responses in SW Japan during Neogene time, *Geological Society of America Bulletin*, **117**, 7-8, 969-86; doi: 10.1130/B25565.1d
- KIMURA G., KITAMURA Y., HASHIMOTO T., YAMAGUCHI A., SHIBATA T., UJIIE K. & OKAMOTO S. 2007. Transition of accretionary wedge structures around the up-dip limit of the seismogenic subduction zone, *Earth Planet.Sci.Lett.* **255**, 471-84.
- KIDO Y. & FUJIWARA T. 2004. Regional variation of magnetization of oceanic crust subducting beneath the Nankai Trough, *Geochemistry, Geophysics, and Geosystems*, **5**, Q03002, doi:10.1029/2003GC000649
- KOBAYASHI K. & NAKADA M. 1978, Magnetic anomalies and tectonic evolution of the Shikoku inter-arc basin, in Geodynamics of the Western Pacific, *Journal of*

- Physical Earth*, **26**, 391-402.
- KOBAYASHI K., CADET J.P., AUBOUIN J., BOULEGUE J., ET AL. 1987. Normal faulting of Daiichi Kashima Seamount in the Japan Trench revealed by the KAIKO I cruise, Leg 3, *Earth and Planetary Science Letters*, **83**, 257-66.
- KOBAYASHI K., KASUGA K. & OKINO K. 1995. Shikoku Basin and its Margins, In B. Taylor ed. *Backarc Basins: tectonics and magmatism*, Plenum Press, 381-405.
- KODAIRA S., TAKAHASHI N., NAKANISHI A., MIURA S. & KANEDA Y. 2000. Subducted seamount Imaged in the Rupture Zone of the 1946 Nankaido Earthquake, *Science*, **289**, 104-6.
- KODAIRA S., HORI T., ITO A., MIURA S., FUJIE G., PARK J. O., BABA T., SAKAGUCHI H., & KANEDA Y. 2006. A cause of rupture segmentation and synchronization in the Nankai trough revealed by seismic imaging and numerical simulation, *Journal of Geophysical Research*, **111**, B09301, doi:10.1029/2005JB004030.
- KOPF A. & BROWN K. M. 2003. Friction experiments on saturated sediments and their implications for the stress state of the Nankai and Barbados subduction thrusts, *Marine Geology*, **202**, 193-210.
- KOPP H. & KUKOWSKI N. 2003. Backstop geometry and accretionary mechanics of the Sunda margin, *Tectonics*, **22**(6), 1072, doi:10.1029/2002TC001420.
- KOYI H. A. & SCHOTT B. 2001. Stress estimations from fault geometries applied to sand-box accretionary wedges. *Geophys. Res. Lett.* **28**(6), 1087-1090.
- KOYI H. & VENDEVILLE B. 2003. The effect of decollement dip on geometry and kinematics of model accretionary wedges, *J. Struct. Geol.*, **25**, 1445-50.
- KUKOWSKI N., SCHILLHORN T., HUHN K., VON RAD U., HUSEN S. & FLUEH E. R. 2001. Morphotectonics and mechanics of the central Makran accretionary wedge off Pakistan, *Mar. Geol.*, **173**, 1-19.
- RUFF L. J. 1989. Do trench sediments affect great earthquake occurrence in subduction zones?, *Pure and Applied Geophysics*, **129**, 263-82.
- LALLEMAND S. & LE PICHON X. 1987. Coulomb wedge model applied to the subduction of seamounts in the Japan Trench. *Geology*, **15**, 1065-69.
- LALLEMAND S. E., P. SCHNURLE P. & MALAVIELLE J. 1994. Coulomb theory applied to accretionary and nonaccretionary wedges: Possible causes for tectonic erosion and/or frontal accretion, *J. Geophys. Res.*, **99**, 12,033-55.

- LALLEMANT S.J., CHAMOT-ROOKE N., LE PICHON X. & RANGIN C. 1989. Zenu Ridge: a deep intraoceanic thrust related to subduction, off Southwest Japan. *Tectonophysics*, **160**, 151-74.
- LE PICHON, X., IYAMA T., BOULEGUE J., CHARVET H., FAURE M., KANO K., LALLEMANT S., OKADA H., RANGIN C., TAIRA A., URABE T. & UYEDA S. 1987. Nankai trough and Zenu ridge: a deep-sea submersible survey, *Earth Planet.Sci.Lett.*, **83**, 285-99.
- LE PICHON, X., HENRY P. & LALLEMANT S. J. 1993. Accretion and erosion in subduction zones: The role of fluids, *Annu. Rev. Earth Planet. Sci.*, **21**, 307-31.
- LOHRMANN, J., KUKOWSKI N., ADAM J. & ONCKEN J. 2003. The impact of analogue material properties on the geometry, kinematics, and dynamics of convergent sand wedges, *J. Struct. Geol.* **25**, 1691-711.
- MCCANN W. R. & HABERMANN R. E. 1989. Morphologic and geologic effects of the subduction of bathymetric highs, *Pure and Applied Geophysics*, **129**, 41-69.
- MITCHELL N. C. 2003. Susceptibility of mid-ocean ridge volcanic islands and seamounts to large-scale landsliding, *Journal of Geophysical Research*, **108(B8)**, 2397, doi:10.1029/2002JB001997.
- MIYAZAKI S. & Heki K. 2001. Crustal velocity field of southwest Japan: Subduction and arc-arc collision, *J. Geophys. Res.*, **106**, 4305-326.
- MOORE, G. F., SHIPLEY T. H., STOFFA P. L., KARIG D. E., TAIRA A., KURAMOTO S., TOKUYAMA H. & SUYEHIO K. 1990. Structure of the Nankai Trough Accretionary Zone from Multichannel Seismic Reflection Data, *J. Geophys. Res.*, **95**, 8753-8765.
- MOORE G. F., TAIRA A., KLAUS A., MALTMAN A. J., ET AL. 2001a. New insights into deformation and fluid flow processes in the Nankai Trough accretionary prism: Results of Ocean Drilling Program Leg 190, *Geochemistry, Geophysics, and Geosystems*, **2**, (10), doi:10.1029/2001GC000166.
- MOORE G. F., et al. (2001b), Data report: Structural setting of the Leg, 190 Muroto transect, data report, *Proc. Ocean Drill. Program Initial Rep.* [CD-ROM], 131, 1-14.
- MOORE J. C. 1989. Tectonics and hydrogeology of accretionary prisms: Role of the décollement zone, *J. Struct. Geol.*, **11(1-2)**, 95-106.
- MOORE J.C., KLAUS A., BANGS N. L., BEKINS B., BÜKER C. J., BRÜKMANN W.,

- ERIKSON F., HANSEN O., HORTON T., IRELAND P., MAJOR C.O., MOORE G. F., PEACOCK S., SAITO S., SCRATON E. J., SHIMELD J. W., STAUFFER P.H., TAYMAZ T., TEAS P.A., TOKUNAGA T. 1998. Consolidation patterns during initiation, and evolution of a plate-boundary décollement zone: Northern Barbados accretionary prism, *Geology*, **26**, 811–14.
- MORGAN J. K., Moore G. F. & CLAGUE D. A. 2002, Slope failure and volcanic spreading along the submarine south flank of Kilauea volcano, Hawaii, *Journal of Geophysical Research*, **108(B9)**, 2415, doi:10.1029/2003JB002411.
- MUCK M.T. & UNDERWOOD M.B. 1990. Upslope flow of turbidity currents: a comparison among field observations, theory, and laboratory methods, *Geology*, **18**, 54-57.
- NAKAMURA K., SHIMAZAKI K. & YONEKURA N. 1984. Subduction, bending and education, Present and Quaternary tectonics of the northern border of the Philippine Sea plate, *Bulletin de la Societe Geologique de France*, **26**, 221-43.
- OBARA K., HIROSE H, YAMAMIZU F. & KASAHARA K. 2004. Episodic slow slip events accompanied by non-volcanic tremors in southwest Japan subduction zone, *Geophys. Res. Lett.*, **31**, L23602. doi:10.1029/2004GL020848.
- OKINO K., SHIMAKAWA Y. & NAGAOKA S. 1994. Evolution of the Shikoku Basin, *Journal of Geomagnetism and Geoelectricity*, **46**, 463-79.
- OKINO K. & KATO Y. 1995. Geomorphological study on a clastic accretionary prism: The Nankai Trough, *The Island Arc*, **4**, 182-98.
- OKINO K., OHARA Y., KASUGA S. & KATO Y. 1999. The Philippine Sea: New survey results reveal the structure and the history of the marginal basins, *Geophysical Research Letters*, **26**, 2287-90.
- PARK J.-O., TSURU T., KODAIRA S., TAKAHASHI N., KANEDA Y., KINOSHITA H. & KONO Y. 1999. A subducting seamount beneath the Nankai accretionary prism off Shikoku, southwestern Japan, *Geophys. Res. Lett.*, **26(7)**, 931-4.
- PARK J. -O., TSURU T., KODAIRA S., TAKAHASHI N., NAKANISHI A., MIURA S., KANEDA T. & KONO Y. 2000. Out-of-sequence thrust faults developed in the coseismic slip zone of the 1946 Nankai earthquake (Mw=8.2) off Shikoku, southwest Japan, *Geophys. Res. Lett.*, **27(7)**, 1033-6.
- PARK J. -O., TSURU T., TAKAHASHI N., HORI T., KODAIRA S., NAKANISHI A., MIURA S. & KANEDA Y. 2002a. A deep strong reflector of the Nankai accretionary

- wedge from multichannel seismic data: Implications for underplating and interseismic shear stress release, *J. Geophys. Res.*, **107(B4)**, 10.1029/2001JB000262.
- PARK J. -O., TSURU T., KODAIRA S., CUMMINS P. R. & KANEDA Y. 2002b. Splay fault branching along the Nankai subduction zone, *Science*, **297**, 1157-60.
- PARK J.-O, MOORE G. F., TSURU T., KODAIRA S., & KANEDA Y. 2003. A subducted oceanic ridge influencing the Nankai megathrust earthquake rupture, *Earth Planet. Sci. Lett.*, **217**, 77-84.
- PARKER, R.L. 1991. A theory of ideal bodies for seamount magnetism. *Journal of Geophysical Research*, **96**, 16101-12.
- RICCI-LUCCHI G. & CAMERLENGHI A. 1993. Upslope turbiditic sedimentation on the southeastern flank of the Mediterranean ridge. *Bollettino di Oceanologia Teorica Ed Applicata*, **11**, 3-25.
- ROGERS G. & DRAGERT H. 2003. Episodic tremor and slip on Cascadia subduction zone: The chatter of silent slip, *Science*, **300**, 1942-1943.
- SAFFER D.M. & BEKINS B.A. 2002. Hydrologic controls on the morphology and mechanics of accretionary wedges, *Geology*, **30**, 3, 271-4.
- SAFFER D. M. & BEKINS B. A. 2006. An evaluation of factors influencing pore pressure in accretionary complexes: Implications for taper angle and wedge mechanics, *Journal of Geophysical Research*, **111**, B04101, doi:10.1029/2005JB003990.
- SANDWELL D.T. & SMITH W.H.F. 1997. Marine gravity anomaly from Geosat and ERS 1 satellite altimetry, *Journal of Geophysical Research*, **102**, B5, 10039-54.
- SCHOLZ. C.H. & SMALL C. 1997. The effect of seamount subduction on seismic coupling. *Geology*, **25**, 487-490.
- SCHOTT B. & Koyi H. A. 2001. Estimating basal friction in accretionary wedges from the geometry and spacing of frontal faults. *Earth Planet. Sci. Lett.*, **194 (1-2)**, 221-7.
- SCREATON E. 2006. Excess pore pressures within subducting sediments: Does the proportion of accreted versus subducted sediments matter?, *Geophys. Res. Lett.*, **33**, L10304, doi:10.1029/2006GL025737.
- SOH W., PICKERING K. T., TAIRA A. & TOKUYAMA H. 1991. Basin evolution in the arc-arc Izu collision zone, Mio-Pliocene Miura Group, central Japan. *Journal of the Geological Society*, (London, U.K.), **148**, 317-30.

- SENO T., STEIN S. & GRIPP A. E. 1993. A model for motion of the Philippine Sea plate consistent with NUVEL-1 and geological data, *Journal of Geophysical Research*, **89**, 17,941-8.
- SHIPBOARD SCIENTIFIC PARTY, 1986. Site 582. In Kagami, H., Karig, D.E., Coulbourn, W.T., et al., Init. Repts. *DSDP, 87*: Washington (U.S. Govt. Printing Office), 35-122
- SONG T.-R.A. & SIMONS M. 2003. Large Trench-Parallel Gravity Variations Predict Seismogenic Behavior in Subduction Zones, *Science*, **301**, 630-3.
- SPINELLI G., & UNDERWOOD M. 2004. Character of sediments entering the Costa Rica subduction zone: Implications for partitioning of water along the plate interface, *Island Arc*, **13**, 432-451.
- TAIRA A. 2001. Tectonic evolution of the Japanese island arc system. *Annual Review of Earth and Planetary Sciences*, **29**, 109-34.
- TAIRA A., HILL I., FIRTH J.V., ET AL. 1991. *Proceedings of the Ocean Drilling Program, Initial Reports*, **131**, College Station, Texas.
- TAIRA A. & NIITSUMA N. 1986. Turbidite sedimentation in the Nankai Trough as interpreted from magnetic fabric, grain size, and detrital modal analyses. In Kagami, H., Karig, D.E., Coulbourn, W.T., ET AL. *Initial Reports of the Deep Sea Drilling Project, 87*: Washington (U.S. Govt Printing Office), 611-32.
- TAIRA A., & CUREWITZ D. 2005. *CDEX Technical Report, Volume 1*: Nankai Trough Seismogenic Zone Site Survey: Kumano Basin Seismic Survey, Philippine Sea, Offshore Kii Peninsula, Japan [online]. Available from: <http://sio7.jamstec.go.jp/publication>.
- TANIOKA Y., RUFF L. & SATAKE K. 1997. What controls the lateral variation of large earthquake occurrence along the Japan Trench?, *The Island Arc*, **6**, 261-6.
- TAYLOR F. W., MANN P., BEVIS M.G., ET AL. 2005. Rapid forearc uplift and subsidence caused by impinging bathymetric features: Examples from the New Hebrides and Solomon arcs, *Tectonics*, **24**, TC6005, doi:10.1029/2004TC001650.
- TOBIN H. J. & KINOSHITA M. 2006. NanTroSEIZE Project: Investigations of seismogenesis at the Nankai Trough, Japan. IODP Project Sci. Prosp, NanTroSEIZE Stage doi:10.2204/iodp.sp.nantroseize1.2006.
- YOSHIOKA S. & ITO Y. 2001. Lateral variations of effective elastic thickness of the subducting Philippine Sea plate along the Nankai trough, *Earth, Planets and Space*, **53**, 261-73.

- UNDERWOOD M.B., ORR R., PICKERING K. & TAIRA A. 1993. Provenance and dispersal patterns of sediments in the turbidite wedge of Nankai Trough, in Hill, I.A., Taira, A., Firth, J.V., ET AL. *Proceedings of the Ocean Drilling Program, Scientific Results*, **131**: College Station, Texas, Ocean Drilling Program, 15-34.
- UNDERWOOD M.B. 2002. Strike-parallel variations in clay minerals and fault vergence in the Cascadia subduction zone, *Geology*, **30(2)**, 155–8.
- UNDERWOOD M.B. 2007. Sediment inputs to subduction zones: Why lithostratigraphy and clay mineralogy matter, in *The Seismogenic Zone of Subduction Thrust Faults*, edited by T. Dixon et al., Columbia Univ. Press, New York.
- VON HUENE R., RANERO C. R., WEINREBE W. & HINZ K. 2000. Quaternary convergent margin tectonics of Costa Rica, segmentation of the Cocos plate, and Central American volcanism, *Tectonics*, **19**, 314-34.
- WANG K. & Hu Y. 2006. Accretionary prisms in subduction earthquake cycles: The Theory of dynamic Coulomb wedge. *J. Geophys. Res.*, **111(B6)**, B06410, doi:10.1029/2005JB004094.
- WESSEL P. & SMITH W. H. F. 1995. New version of Generic Mapping Tools released, *Eos Transactions, American Geophysical Union*, **76**, 329.
- WDOWINSKI, S. 1992, Dynamically supported trench topography, , *Journal of Geophysical Research*, **97**, B12, 17,651–17,656.
- YAMAZAKI T. & OKAMURA Y. 1989. Subducting seamounts and deformation of overriding forearc wedges around Japan, *Tectonophysics*, **160**, 1-4, 207-17, doi:10.1016/0040-1951(89)90392-2.
- ZANG S.X., CHEN Q. Y., NING J. Y., SHEN Z. K., LIU Y. G. 2002. Motion of the Philippine Sea plate consistent with the NUVEL-1A model, *Geophys. J. Int.*, **150(3)**, 809-19.